DOE/ER/40141--8

DE91 000929

Annual Report for the High Energy Physics Program at The University of Alabama

DOE Grant No. DE-FG05-84ER40141, Task B

Report for the following period
April 1, 1990 to September 30, 1990

Prepared by

D. D. DiBitonto
J. K. Busenitz
L. Baksay

Department of Physics and Astronomy
The University of Alabama
Tuscaloosa, Alabama 35487

Submitted by

Office for Sponsored Programs
The University of Alabama
Tuscaloosa, Alabama 35487

September 1990

Table of Contents

I. Introduction	1.
The High Energy Physics Program at Alabama	1.
Faculty and Staff	2.
Research Facilities	3.
II. The L3 Experiment at CERN	8.
Study of Z^0 Decays	11.
QCD	19.
New Particles	19.
Higgs	24.
III. The L★ Experiment at SSCL	26.
Physics Motivation	26.
Forward Hadron Calorimeter System	29.
IV. The Van de Graaff Institute	39.
V. Research Plans for L3	43.
References	63.
Tables	66.
Appendicies	73.

Summary

During the past year our group has experienced a significant growth in the number of full-time faculty and research staff and has reached new milestones in our various research initiatives. The most noteable was the successful completion of the first major data taking run of the CERN L3 experiment at LEP in the summer of 1990. This run produced an integrated luminosity of 7 pb^{-1} at a center-of-mass energy of 91 GeV from which approximately 140,000 Z^0 events were recorded in L3. High precision tests of the Standard Model and searches for new physics beyond the Standard Model are now underway, with significantly higher statistics expected in the spring run of 1991. In addition to these activities, our group has also been preparing for its anticipated role in the L★ experiment at SSCL with electronic design and testing of a prototype forward hadron calorimeter for this detector. The University, in turn, is also planning a major expansion of its research facilities for high energy physics in support of this program.

In the accompanying report we will present the details of these and other accomplishments which we were able to achieve this year and outline our group's plan for its continued participation in these research programs for the coming twelve month period (April 1, 1991 - March 31, 1992).

I. Introduction

The University of Alabama is developing a comprehensive program in experimental high energy physics which parallels and complements the existing program in theoretical elementary particle physics. Although only one year old, this program already includes active participation in a world-class international experiment studying e^+e^- physics at the world's highest center of mass energy. More recently, this group has also been given a major responsibility in the design and construction of a subsystem in one of the world's largest scientific experiments at the Superconducting Super Collider (SSC). Thanks to the generous support of the University Administration, this group is able .o provide modern analysis and laboratory facilities for high energy physics research and development, both for existing experiments and those planned for the SSC. These facilities will enable us to train the next generation of scientists and engineers in this field, a mission which we feel is vital to the national interest and uniquely suited to the university.

During the next 3-5 years, the University plans a significant expansion in the high energy physics program, which will include substantial growth in its tenured and tenure-track faculty. Expanded laboratory and machine shop facilities are also planned for the experimental program in anticipation of its future role in a major SSC experiment. We view this proposal as a long-term partnership with the Department of Energy and describe below our program and plans for high energy physics research here at The University of Alabama.

The High Energy Physics Program at Alabama

Present research activities within the group include participation in the CERN L3 experiment, which is currently studying e^+e^- collider physics around the Z^0 pole. Since July, 1977, the Alabama group has been a member of the L3 Collaboration (see Appendix I) and has since then been contributing primarily to the analysis and simulation of data. Approximately 140,000 Z^0 events have been recorded by the L3 experiment to date. During the upcoming run in March of

1991, the LEP Collider will remain at the Z^0 pole to be able to raise, hopefully, the total statistical sample to 1-2 million events. Definitive high precision tests of the Standard Model will then be possible, in addition to searches for new physics signatures beyond the Standard Model. The status of these and other physics programs within L3 is detailed in Section II.

The Alabama group is also preparing to study proton-proton collisions at $\sqrt{s}$ = 40 TeV at the SSC. This group is a member of the L★ Collaboration and is also represented on the L★ Executive Committee (D. DiBitonto). We are collaborating with the First Physics Institute, RWTH, Aachen, Germany, and the Tata Institute for Fundamental Research (T.I.T.R.), Bombay, India, to develop fast forward hadron calorimetry for this future SSC experiment. Much of this work has been driven by the generic detector R&D and subsystem work already supported by the SSC Laboratory. Alabama's principal role in this research has been directed towards the development of fast warm liquid calorimetry for the forward region, which is detailed in Section III.

Faculty and Staff

The experimental high energy physics group presently consists of three faculty members (Drs. Daryl DiBitonto, Laszlo Baksay, and Jerome Busenitz), a research scientist (Dr. Raul Muñoz), and a postdoctoral research associate (Dr. Panos Razis). Two technical staff are also part of the high energy physics group: Dr. Surendra Pal Singh, specializing in electronics design and engineering, and Mr. Tad Pennington, research technician and systems manager for the HP/Apollo computers (see next section). In addition to the principal research faculty and staff, the group also supports 3 graduate students who are working on the analysis of L3 data for their theses. The University also provides half-time secretarial support for the group.

The principal activities and the percentage time in Full Time Equivalents (FTE) units are given below for members of the high energy physics group. Involvement in the L3 experimental program continues to be the group's major

research activity, although additional manpower and resources for the L★ program will be required as this program continues to grow.

Activity (% FTE)

Researcher	L3	L★
D. DiBitonto, Associate Professor	90	10
L. Baksay, Associate Professor	100	0
J. Busenitz, Assistant Professor	100	0
R. Muñoz, Research Scientist	20	80
P. Razis, Postdoc. Research Associate	100	0

Research Facilities

Analysis

Analysis facilities within the high energy physics group include an Apollo DN10000 and DN3500, as well as the University's IBM 3090 and access to the Alabama CRAY XMP24 supercomputer. A Micro-VAX II within the Department is also available for analysis. The DN10000 is presently configured with 1.4 Gigabytes of hard disk and approximately 15 mips of CPU computing power and serves as the group's principal physics analysis machine.

Principal simulation and analysis codes for L3 now running on the Apollo system include the Lund Monte Carlo, principal generator for e^+e^- physics in this experiment, as well as the GEANT detector simulation code for the experimental apparatus. ISAJET and PYTHIA simulation codes for general physics and pp collisions at SSC energies in particular will be implemented shortly.

The Alabama group is linked to the L3 analysis network, LEP3NET, via a high speed (56 KBaud) leased line. This link is necessary to update large analysis programs and releases, calibration data files for production (soon to be implemented at Alabama), as well as transfer of large simulation data files generated

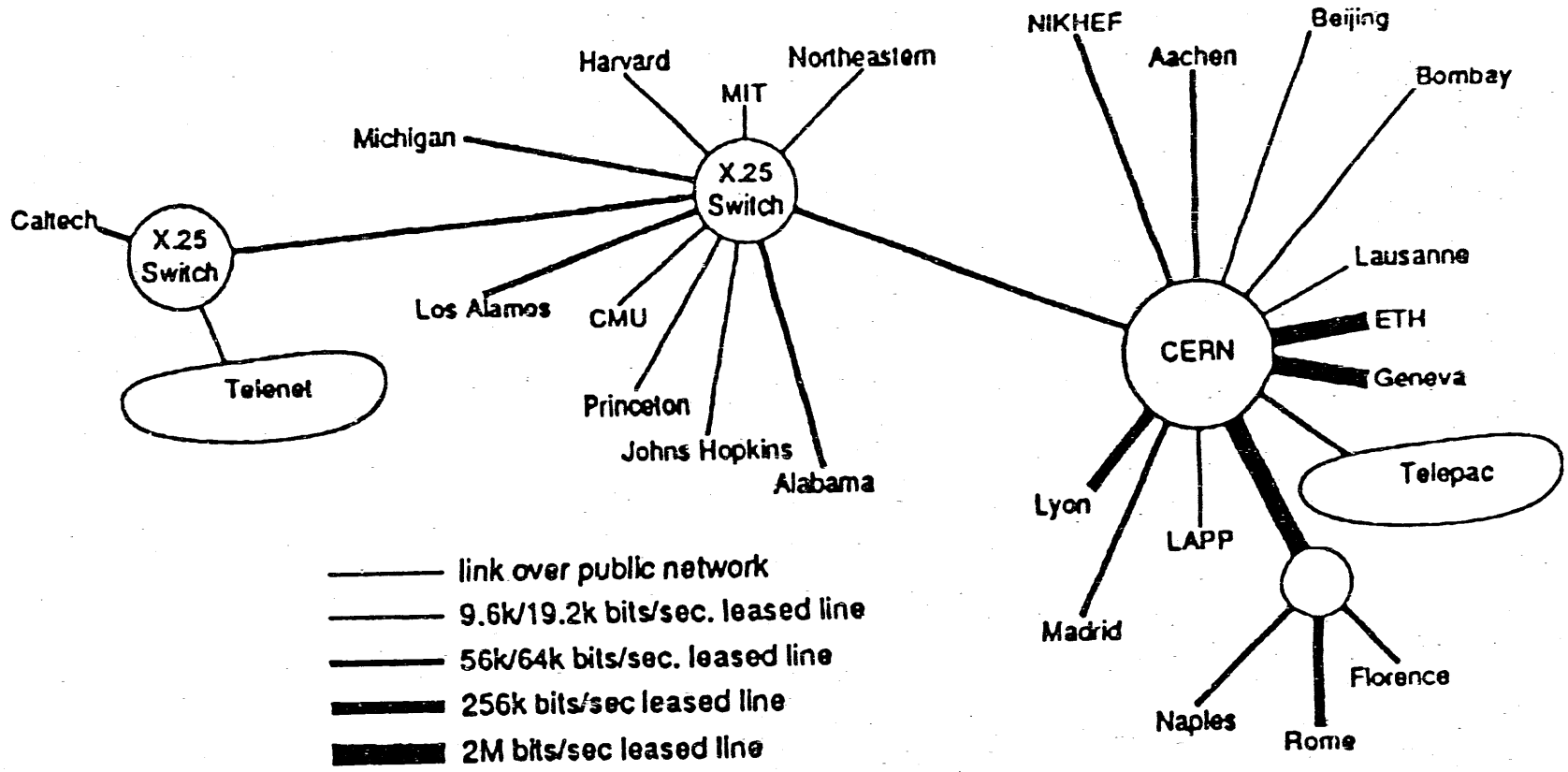

Figure I.1. Network lines serving L3.

at Alabama and analyzed now at CERN. This extensive worldwide network will also serve as the principal communications link for the L★ experiment, whereby engineering data files can be exchanged with collaborators as far away as Bombay, India (T.I.T.R.) and Beijing, P.R.C. (see Figure I.1).

The Apollo DN 3500 is principally used to support the group's electronic circuit simulation program, MENTOR GRAPHICS. This $150,000 software system was donated to the group through the Educational Gifts Program of the MENTOR GRAPHICS Corp. and is used in designing fast, monolithic electronics for detector research within the group. This software system includes the analog design program MSPICE, as well as monolithic circuit layout and simulation, routing, packaging, and digital simulation routines. The close collaboration between U.S. semiconductor industry (Harris Corp., and Texas Instruments) and this group has resulted in state of the art electronics applicable to the SSC.

Measurement

Experimental facilities within the high energy group are located in the newly completed Materials Science and Energy Resource Building of The University of Alabama. This 145,000 square foot complex houses analytical facilities for surface science evaluation such as a Hitachi transmission electron microscope, a Digital Instruments scanning tunneling microscope, and two general purpose clean rooms each 600 square feet, one class 100 and the other class 1000. These facilities are ideally suited to the group's detector R&D program in warm liquid calorimetry for the SSC which requires strict chemical control and evaluation for the ionizing liquid media. Plans are presently underway to add two new wings onto this facility of approximately 50,000 square feet which will include a high bay area for detector staging, machine shops, and additional space for laboratories and offices for the high energy physics program (see Section IV).

The group's instrumentational support consists of a 3-dimensional CAD system for engineering design (see Figure I.2) and a VLSI evaluation laboratory (see Figure I.3). Each system is separately driven by its own HP 9000 workstation,

THE UNIVERSITY OF ALABAMA

HIGH-ENERGY PHYSICS LAB

COMPUTER AIDED DESIGN SYSTEM

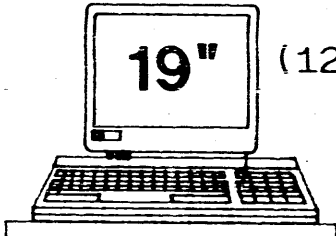

(1280 x 1024)

16 MB — **370CHX**

5 1/4" DISK DRIVE — **9127A**

323 MBYTE — **7959S**

323 MBYTE — **7959S**

APPLICATIONS:
HP-UX
C, FORTRAN, HP-BASIC/UX
3-D MECHANICAL DESIGN

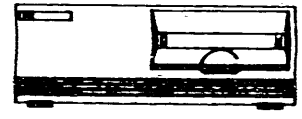

9145A
1/4" TAPE DRIVE

LASERJET II

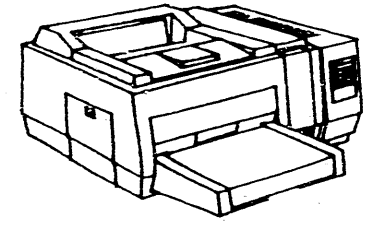

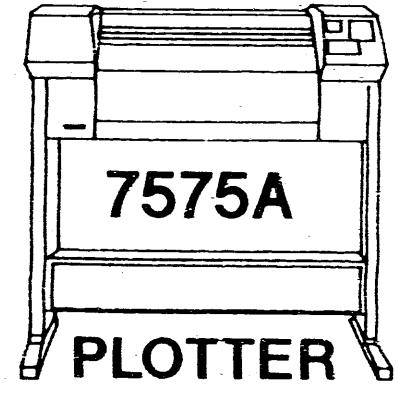

PLOTTER

HEWLETT PACKARD

THE UNIVERSITY OF ALABAMA

HIGH-ENERGY PHYSICS LAB

VLSI EVALUATION SYSTEM

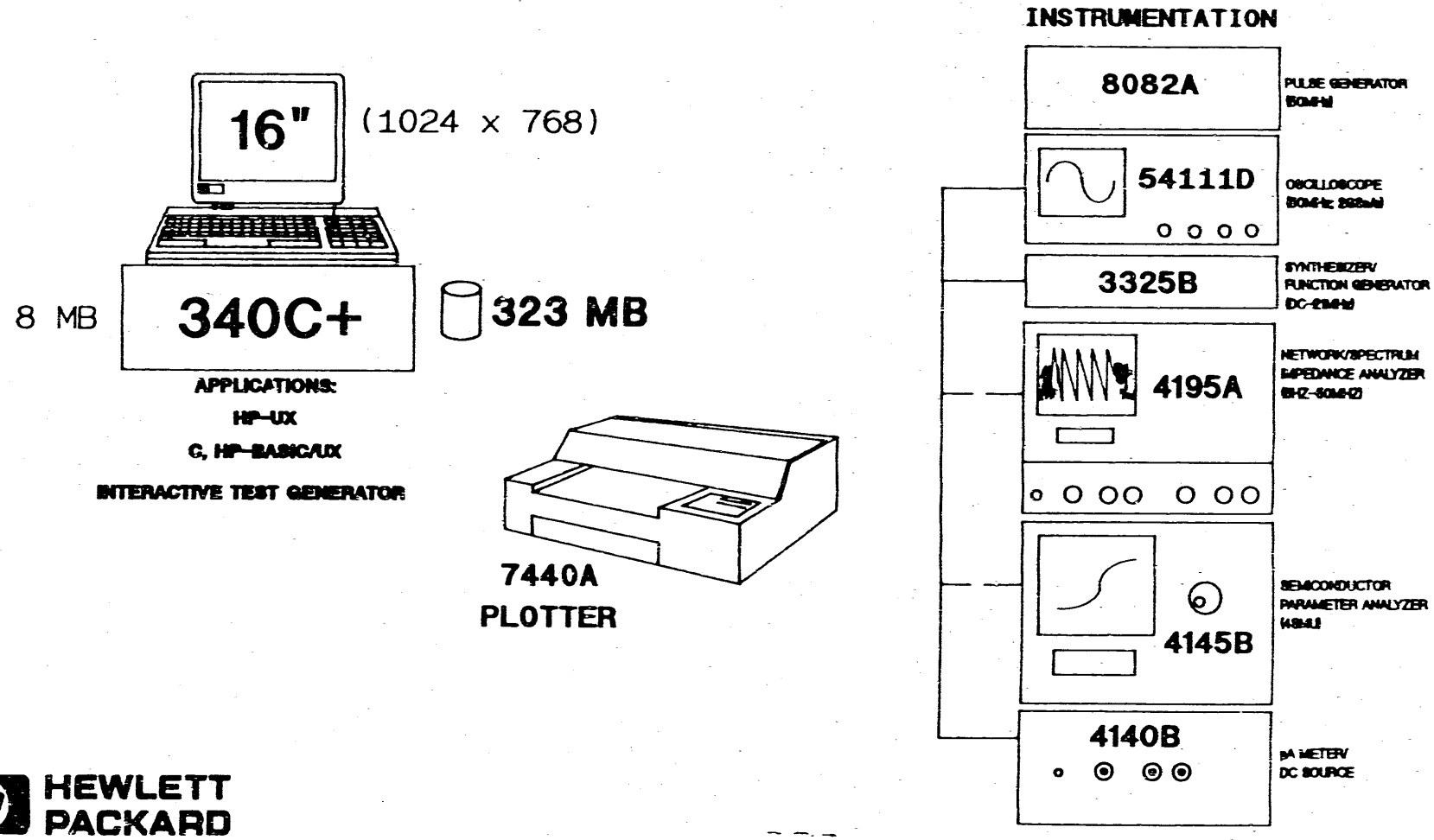

HEWLETT PACKARD

Figure I.3. VLSI Evaluation Laboratory of The University of Alabama.

which together have nearly 1 Gigabyte of hard disk storage. The VLSI evaluation laboratory is used primarily to test fast, radiation-hard charge preamplifiers designed for warm liquid calorimetry. This equipment includes a 1 GHz digitizing oscilloscope, model HP54111D, function generators, picoammeters, and a logic state analyzer. Online programs from the HP 9000 can provide instantaneous fast Fourier analysis of these data as they are taken.

Other research facilities within the group include an SX-200 quadrupole mass spectrometer (VG Instruments) for partial pressure trace detection down to 10^{-14} Torr, ultrahigh vacuum equipment, and general surface science characterization available within the Materials Science Program. The group is presently designing and constructing a purification and filling station for the warm liquid TMS in preparation of the R&D requirements for the L★ forward calorimeter.

II. The L3 Experiment at CERN

The L3 detector [1] is a high precision spectrometer for electrons, photons, and muons designed to study e^+e^- collisions between $M_Z \leq \sqrt{s} \leq 160$ GeV (see Figure 1). The principal physics program in this experiment includes high precision tests of the Standard Model, searches for new physics within the Standard Model (top, Higgs), QCD, and searches for signatures of new physics (supersymmetry and other new particles). We describe below the present status of this physics program [2], based on a subsample of approximately 100,000 of the 140,000 $e^+e^- \rightarrow Z^0$ events recorded in this experiment.

General properties of the L3 spectrometer are summarized in Table I. At the Z^0 mass, this spectrometer's mass resolution, $\Delta M/M$, is approximately 1% for electrons and muons, and roughly 10% for hadrons. Although the determination of the Z^0 mass is largely defined by the energy resolution of the LEP beams (σ_E = 30 MeV), high precision reconstruction of leptonically decaying Z^0's is crucial in missing mass searches for new (Higgs) particles far off the Z^0 pole. Determination of the Z^0 width, which involves important tests of the Standard Model, depends critically on the intrinsic mass resolution of the Z^0.

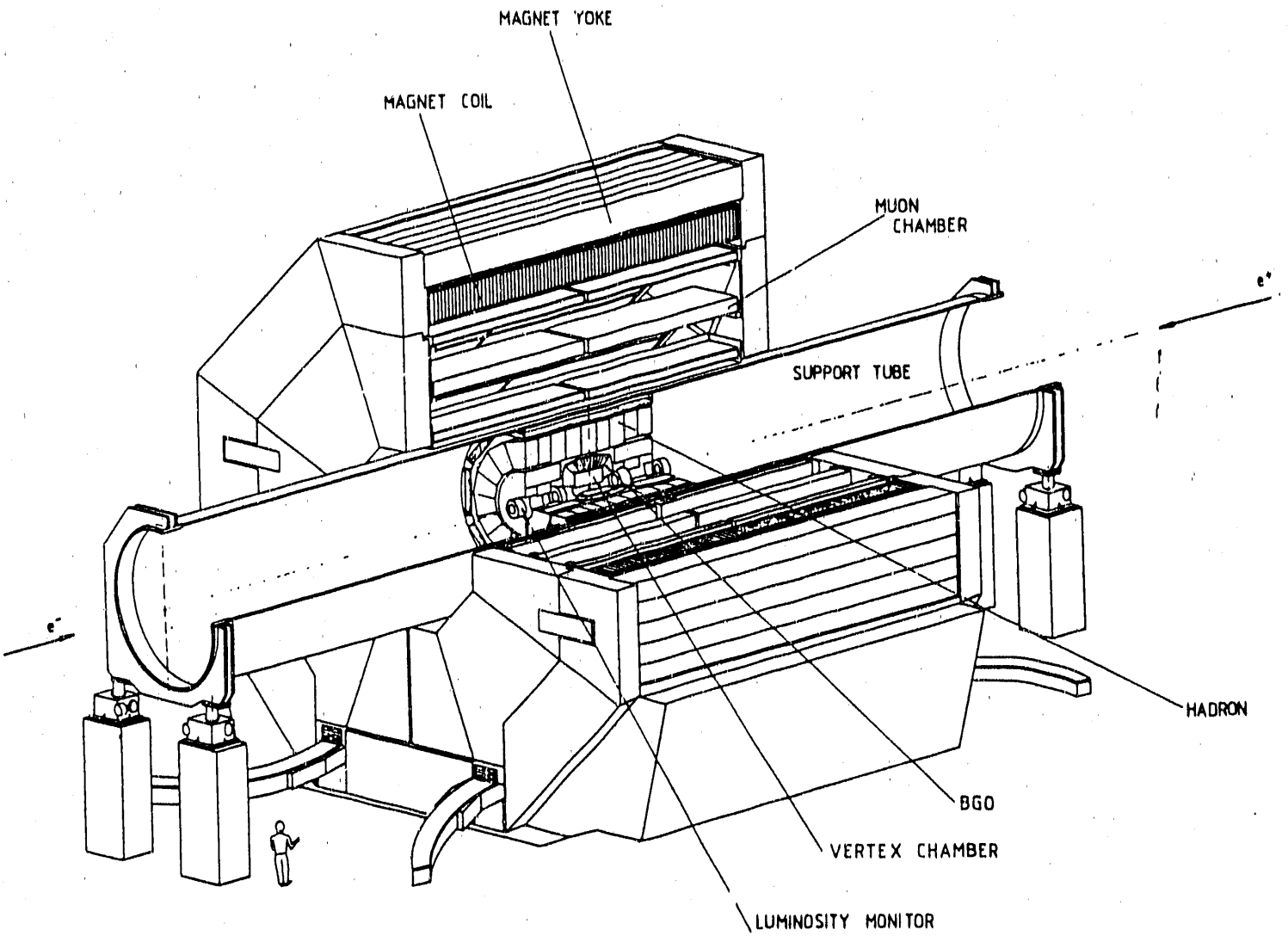

Figure II.1. Schematic view of the L3 spectrometer.

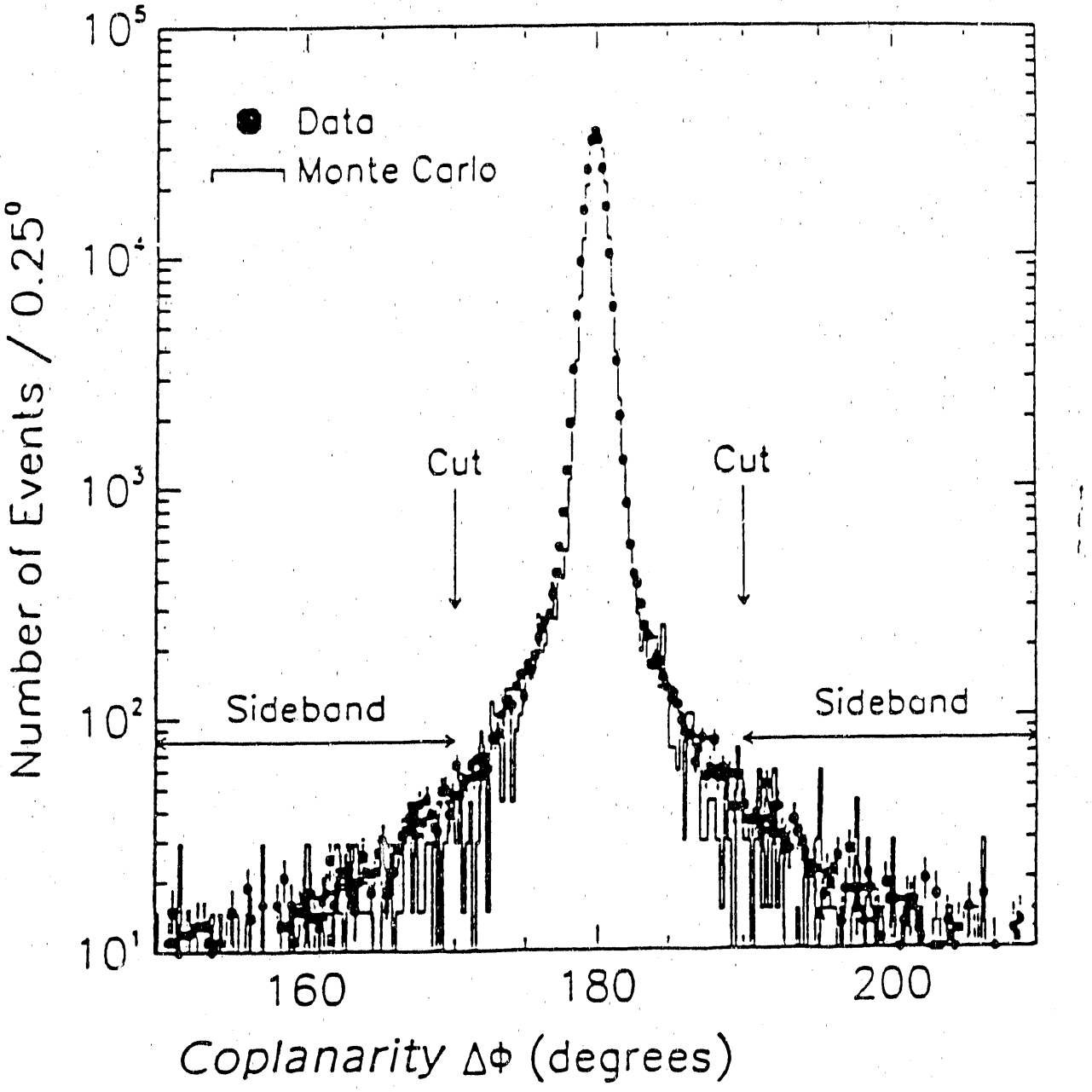

Figure II.2. Bhabha scattering events recorded in the L3 spectrometer.

Cross section measurements are all normalized to luminosity measurements of Bhabha scattering events, detected typically between 30 and 65 mrad from the LEP beams. Data taken with the luminosity monitor is compared with Monte Carlo predictions in Figure II.2. Both data and simulation are in excellent agreement. The total systematic error on this luminosity measurement is 1.3%, with equal contributions coming from Monte Carlo statistics, detector geometry, event selection, and higher order terms in the Monte Carlo cross section.

Study of Z^0 decays

A plot of the number of events for the process $e^+e^- \rightarrow$ hadrons on the Z^0 pole is shown in Figure II.3, along with a comparison to Monte Carlo simulation. This data has been fit within the Standard Model framework [3,4,5]:

$$\sigma_h(s) = \frac{12\pi s \Gamma_{ee}\Gamma_h}{M_Z^2(s-M_Z^2)^2 + s^2\frac{\Gamma_Z^2}{M_Z^2}}\,(1+\delta_{QED}(s))$$

with the following parameters for the Z^0 mass and neutrino width:

$$M_Z = 91.164 \pm 0.013 \pm 0.030 \text{ (LEP) GeV/c}^2$$
$$\Gamma_{inv} = 0.502 \pm 0.018 \text{ GeV.}$$

The fit quality is a $\chi^2/DF = 13.2/15$. From this fit we infer that the number of neutrino species in the universe, according to the Standard Model [6], is therefore:

$$N_\nu = 3.01 \pm 0.11$$

The differential cross section for the processes $e^+e^- \rightarrow Z^0 \rightarrow e^+e^-$, $\mu^+\mu^-$, $\tau^+\tau^-$ gives information on the electroweak coupling constants, g_A and g_V:

$$\frac{d\sigma}{d\Omega} = \frac{\alpha^2}{4\pi}\,[\{1+2g_V^2 Re(\chi)+(g_V^2+g_A^2)^2|\chi|^2\}\cdot(1+cos^2\theta)$$
$$+\{2g_A^2 Re(\chi)+4g_V^2 g_A^2|\chi|^2\}\cdot 2cos\theta],$$

with

$$\chi = \frac{G_\mu M_Z^2}{2\sqrt{2}\pi\alpha}\,\frac{s}{(s-M_Z^2)+iM_Z\Gamma_Z}.$$

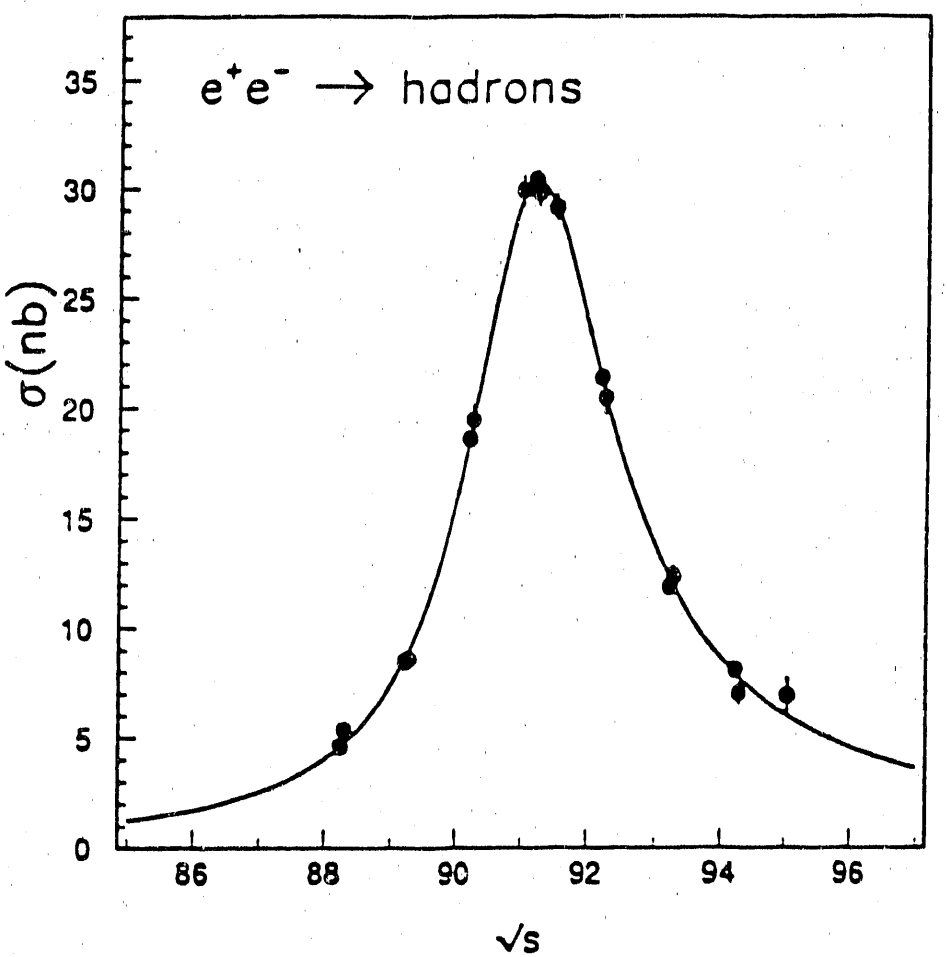

Figure II.3. Absolute cross section for $e^+e^- \rightarrow$ hadrons in L3.

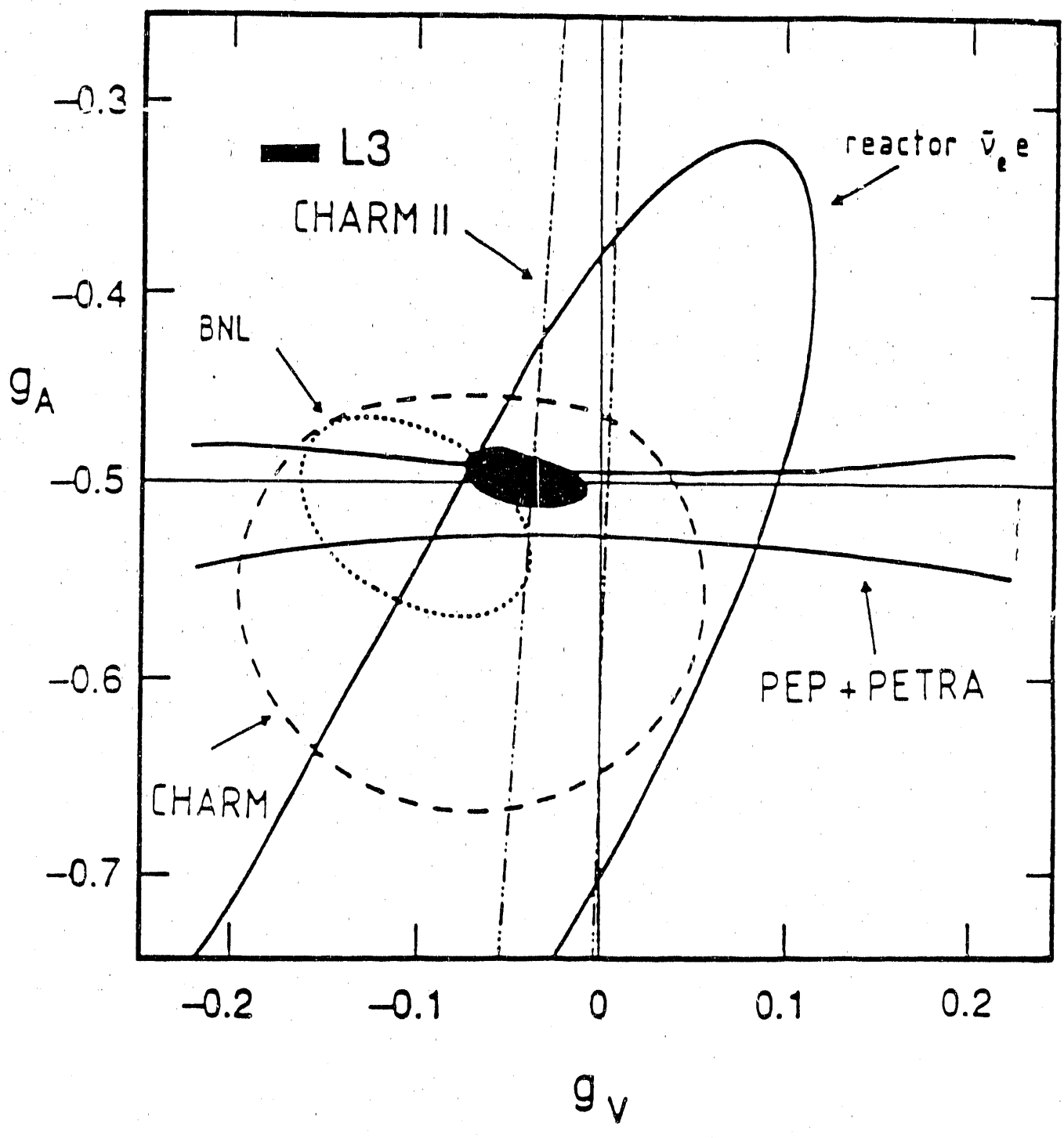

Figure II.4. Comparison of g_A versus g_V for various experiments.

For each of the three lepton species $l = e^{\pm}, \mu^{\pm}, \tau^{\pm}$, the total cross section for Z^0 decay, $\sigma(e^+e^- \rightarrow Z^0 \rightarrow l^+l^-)$, is fit with the Z^0 mass and width, as measured from the hadron data taken in L3. By defining the forward-backward asymmetry parameter for each of the three lepton species,

$$A_{FB} = \frac{N_F - N_B}{N_F + N_B},$$

where $N_{F(B)}$ is the number of leptons (l^-) detected with $\theta \leq (\geq) 90^0$, the coupling constants g_A and g_V have been determined [7, 8] and are summarized in Table II. Assuming μ-e-τ universality, we find the following values of the electroweak parameters:

$$\Gamma_{ll} = 83.7 \pm 0.9 \text{ (stat.)} \pm 0.8 \text{ (sys.) MeV}$$

$$g_A = 0.499 \pm 0.0004$$
$$g_V = 0.062^{+0.016}_{-0.013}$$

A comparison of g_A and g_V is shown in Figure II.4 for various experiments. Data from the LEP Collider provides the most stringent limits on the values of the axial and vector weak coupling constants and electroweak parameters [9] to date.

Searches for Z^0 decay into new particles which, in turn, decay into purely neutral electromagnetic final states have resulted only in an upper limit for these exotic processes.

$\underline{Z^0 \rightarrow b\bar{b}}$

Inclusive muon and electron events have been used to tag $b\bar{b}$ events from Z^0 decay [10]. Distinguishing kinematic features of this decay channel are the large momentum and relative transverse momentum these events possess, thus allowing for a cleaner event selection from $c\bar{c}$ decays. For $b\bar{b}$ decays, $p_T^{\mu} \approx M_b/4$.

A data sample of 3198 inclusive muon events were used in this analysis, which also includes 130 dimuon events. A cut in the muon momentum of 4 GeV/c was made to reduce the background from u,d,s, and c decays. The result-

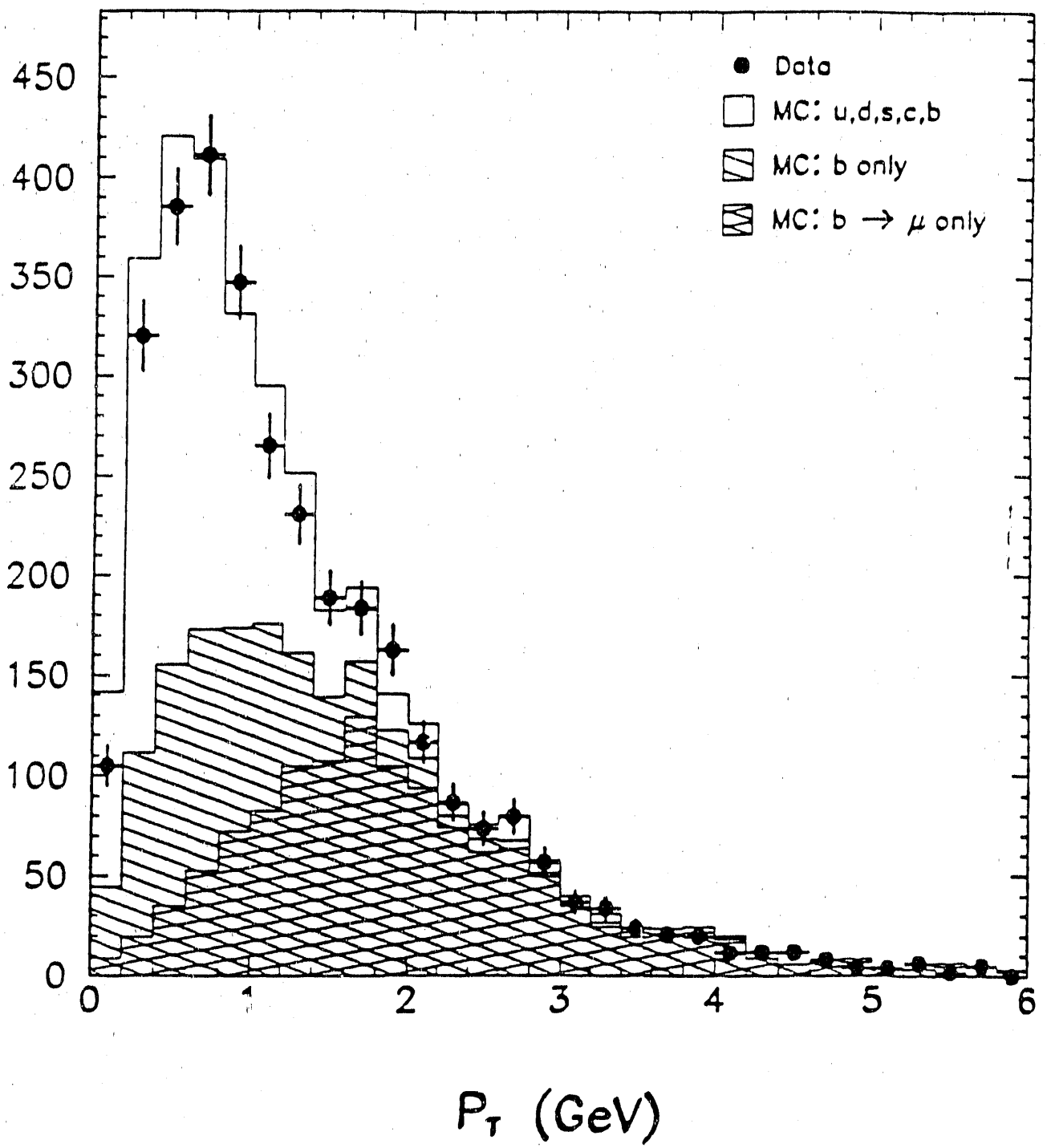

Figure II.5. Relative muon transverse momentum to nearest jet for inclusive muon events.

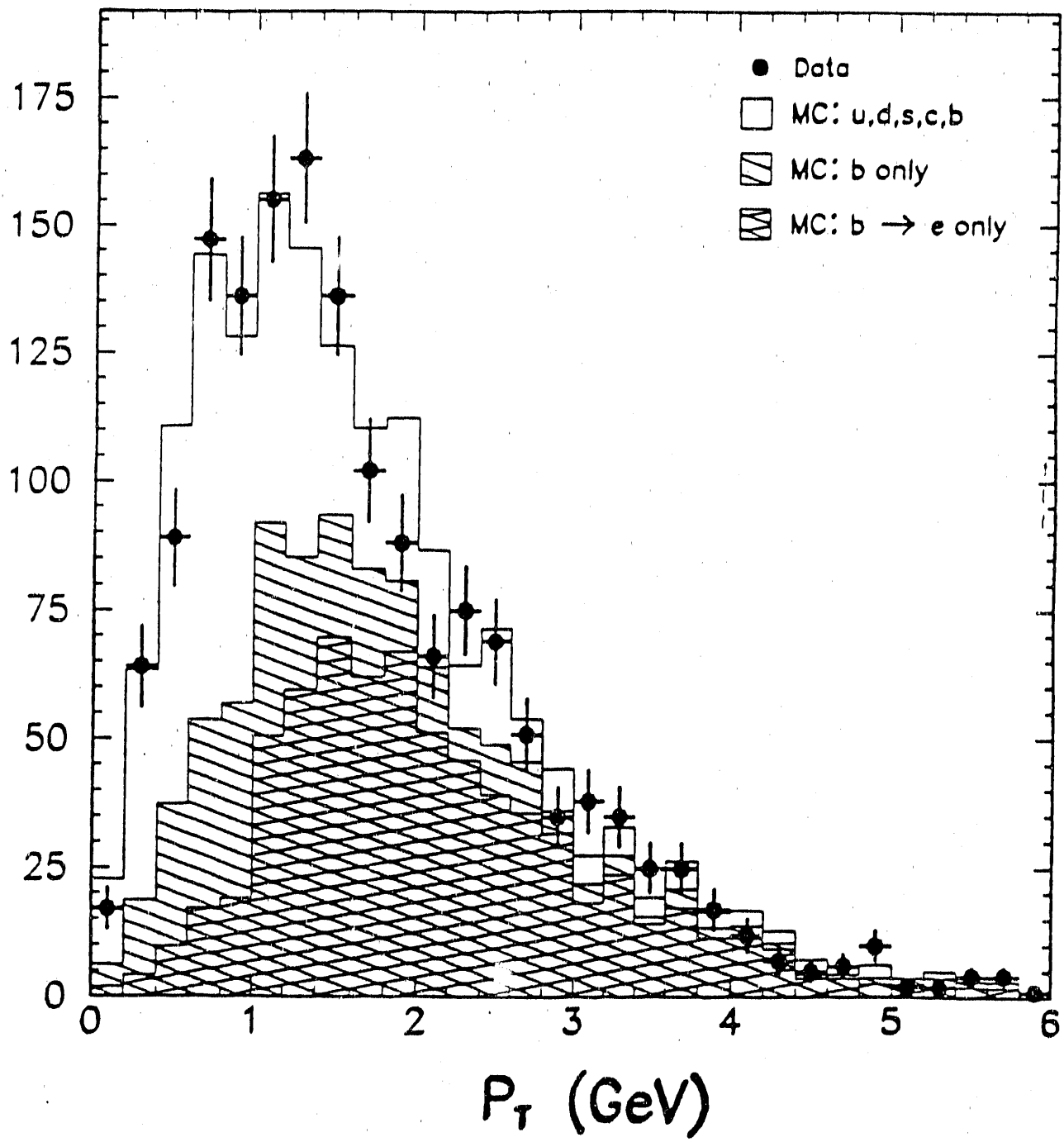

Figure II.6. Relative electron transverse momentum to nearest jet for inclusive electron events.

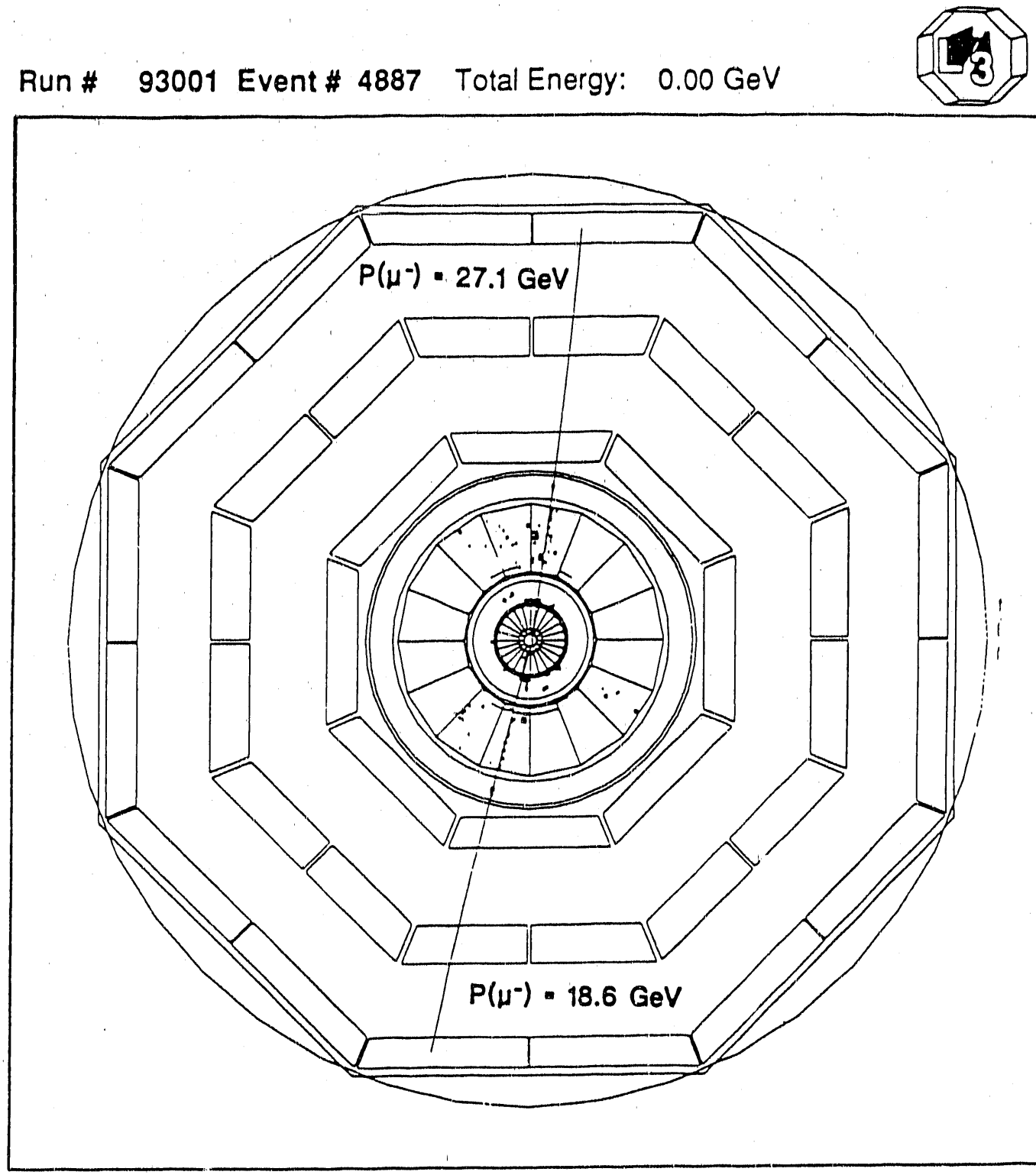

Figure II.7. Like-sign dimuon event recorded in L3.

ing distribution of the muon relative transverse momentum to the nearest jet is shown in Figure II.5, along with a comparison of Monte Carlo expectation from the Standard Model. The following parameters were fit to this data:

$$\Gamma_{b\bar{b}} = 367 \pm 12 \text{ (stat.)} \pm 18 \text{ (sys.)} \pm 33 \text{ (BR) MeV}$$

$$\langle x_\epsilon \rangle \equiv \frac{2E_B}{\sqrt{s}} = 0.66 \pm 0.01 \pm 0.02,$$

where $\langle x_\epsilon \rangle$ is the fraction of longitudinal energy carried by the b-quark with respect to the total available beam energy. Assuming $\Gamma_{b\bar{b}} = 378$ MeV from the Standard Model, we find a semileptonic $b\bar{b}$ branching ratio prediction of:

$$\text{BR}(B \rightarrow \mu, \text{ prompt}) = 11.6\% \pm 0.4\% \text{ (stat.)} \pm 0.4\% \text{ (sys.)}$$

Inclusive electron and muon events have also been used to measure the $b\bar{b}$ forward-backward asymmetry, $A'_{b\bar{b}}$. From a combined sample with $p_T^\mu \geq 4$ GeV/c and $p_T^e \geq 3$ GeV/c (see Figure II.6), the measured asymmetry (with no correction for $B^0\bar{B}^0$ mixing) is:

$$A'_{b\bar{b}} = 8.4\% \pm 3.3\% \text{ (stat.)}$$

A limited number of like-sign dimuon events have been observed in this year's data, consistent with the kinematics of $B^0\bar{B}^0$ mixing (see Figure II.7). A determination of the $B^0\bar{B}^0$ mixing fraction, χ_B, from the dimuon sample yields:

$$\chi_B = 0.11^{+0.08}_{-0.06},$$

which represents a 2.9 σ deviation from no mixing at all ($\chi_B = 0$). From a simultaneous fit to the data, the value for $A_{b\bar{b}}$ corrected for mixing then becomes:

$$A_{b\bar{b}} = 10.9\% \pm 4.4\% \text{ (stat.)}.$$

Higher statistics in next year's run will allow for more precise measurements of the asymmetry and mixing in $b\bar{b}$ systems.

QCD

Tests of QCD have been performed by comparing the 2-, 3-, and 4-jet production rate from e^+e^- coupling to gluons and subsequent hadronic decay [11]. Specifically, the 3-jet process, or hard gluon process, is directly proportional to the strong coupling constant, α_s. This coupling constant, in turn, is a function of the available center of mass energy (multi-jet invariant mass) μ:

$$\alpha_s^{-1} \propto ln(\mu^2/\Lambda^2),$$

where Λ is the QCD parameter necessary for renormalization of the theory. A comparison of the 3-jet fraction of events as a function of energy is shown in Figure II.8 for a number of e^+e^- experiments. A fit to these data, including that of L3, is consistent with the internal fit to L3 data for Λ:

$$\Lambda = 190^{+60}_{-50}(\text{exp.})^{+170}_{-90}(\text{theor.})\ \text{MeV}$$

over the range $\mu^2/s = 0.001$ to 1.

4-jet events have been used to test the nonabelian structure of QCD [12]. In its present form QCD is nonabelian, thus allowing gluon self-coupling. In a hypothetical alternative abelian model, only double bremsstrahlung diagrams would contribute to the $e^+e^- \rightarrow q\bar{q}gg$ process. Comparison of the 4-jet fraction as a function of the Nachtmann-Reiter angle excludes an abelian model in the L3 data (see Figure II.9).

New Particles

Negative searches for excited leptons [13,14] (composite structure), sequential heavy leptons, scalar leptons [15], and heavy neutrinos have all been reported by the L3 Collaboration with lower limits for the masses of these hypothetical particles. We summarize below these limits for the respective searches.

Excited leptons: $e^+e^- \rightarrow l^+l^* \rightarrow ll\gamma$

Events characterized by two tracks with large electromagnetic showers back

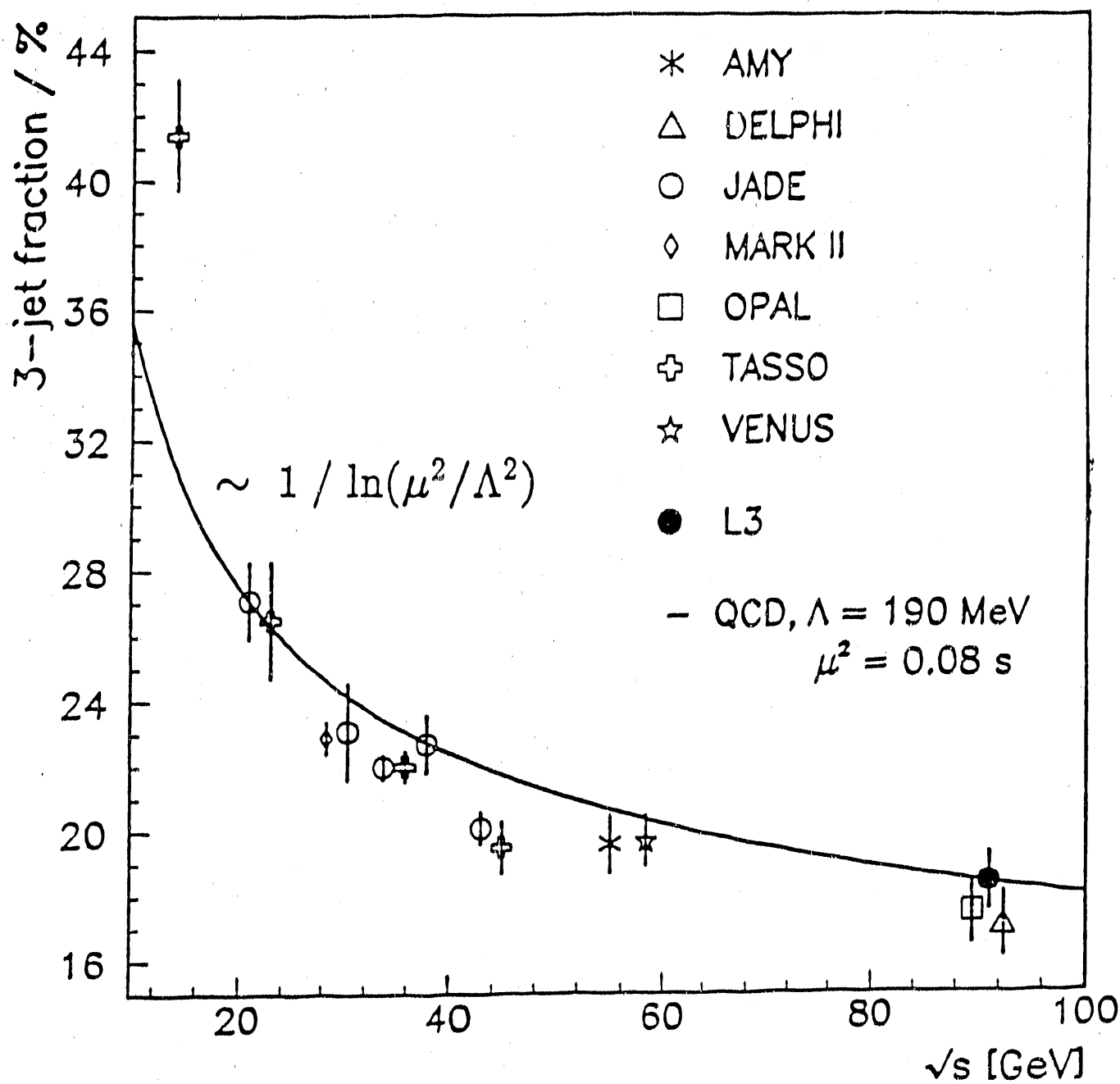

Figure II.8. Energy dependence of 3-jet fraction.

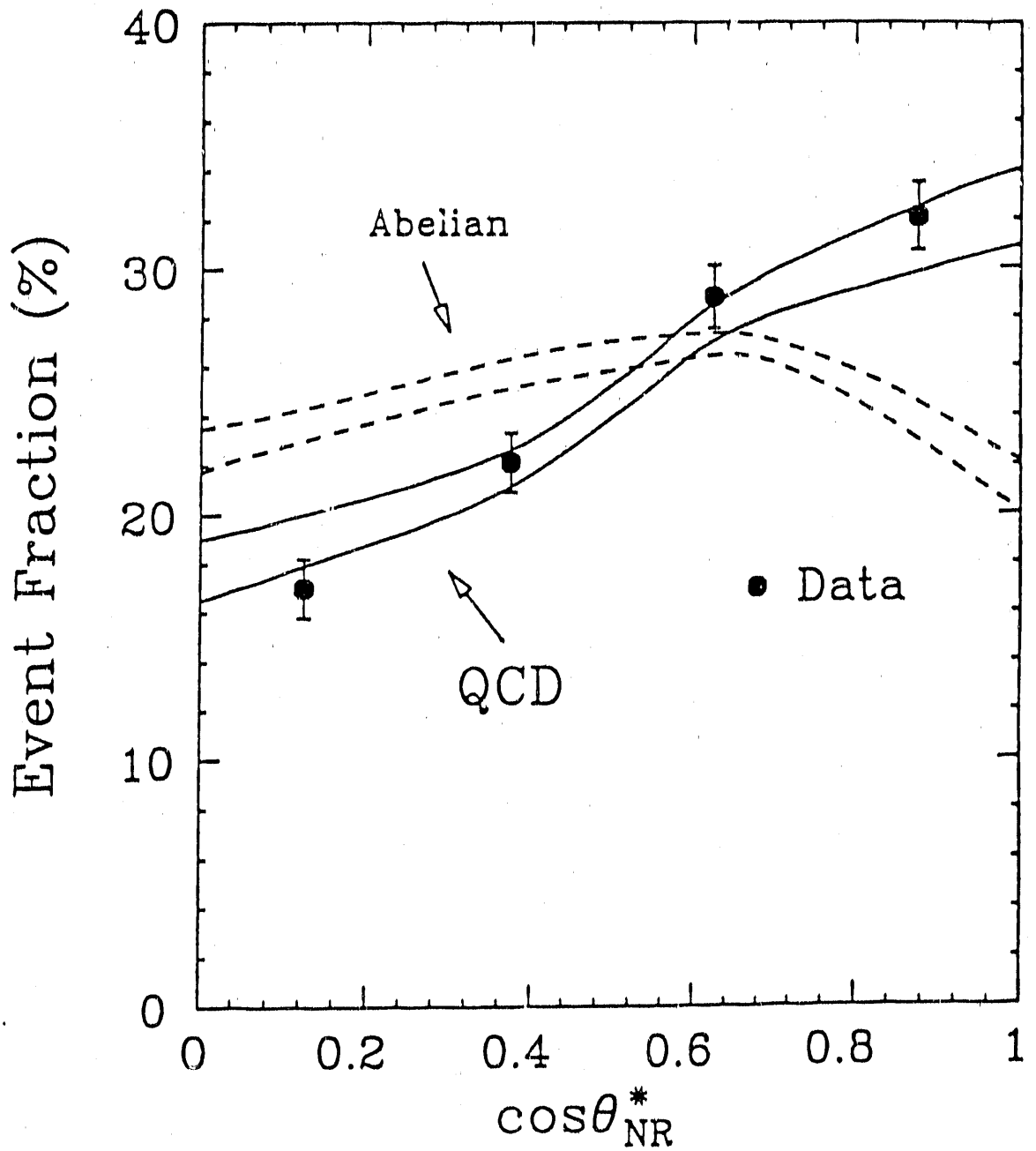

Figure II.9. 4-jet event fraction versus $\cos\theta^*_{NR}$.

to back in ϕ, a large angle angle between the lepton (e,μ,τ) and photon, accompanied by a large photon energy were analyzed for structure in the invariant ($l\gamma$) invariant mass. Assuming a coupling constant at the ($ll^*\gamma$) vertex with the same strength as α ($\lambda = 1$), the following 95% CL lower limits for the masses of these excited states were obtained:

$$m_e^* \geq 88 \text{ GeV}/c^2$$
$$m_\tau^* \geq 89 \text{ GeV}/c^2$$
$$m_\mu^* \geq 85 \text{ GeV}/c^2$$

Sequential heavy leptons: $e^+e^- \rightarrow L^+L^-$

Searches for heavy stable charged leptons decaying sequentially into electrons and muons have resulted in a lower mass limit of 38 GeV/c^2, as determined by the cutoff in energy and subsequent detection within the L3 apparatus.

Heavy neutrinos: $e^+e^- \rightarrow Z^0 \rightarrow \nu_4\overline{\nu_4}$

Mass limits for heavy neutrinos within the Dirac and Majorana theoretical framework have been derived from the measured widths Γ_Z and Γ_{inv} of the Z^0 pole. The current structure for these heavy neutrinos predicts a partial width given by:

$$\Gamma_{\nu 4} = \frac{G_F M_Z^3}{12\sqrt{2}\pi} \times \left\{ \begin{array}{ll} \frac{1}{4}\beta(3+\beta^2) & Dirac \\ \beta^3 & Majorana \end{array} \right\}.$$

The subsequent decay width into final state leptons is given by:

$$\Gamma(\nu 4 \rightarrow l + X) = 9|V_{\nu 4,l}|^2 \left(\frac{G_F^2 M_{\nu 4}^5}{192\pi^3}\right),$$

where $V_{\nu 4,l}$ is the matrix element determining the coupling between $\nu 4$ and l. The experimental signatures in this decay channel are hadronic events with isolated leptons, and multi-lepton events.

Lower limits for the heavy neutrino mass have thus been determined by the measurement constraints that $\Gamma_Z = 2.492 \pm 0.025$ GeV and $\Gamma_{inv} = 502 \pm 18$ MeV

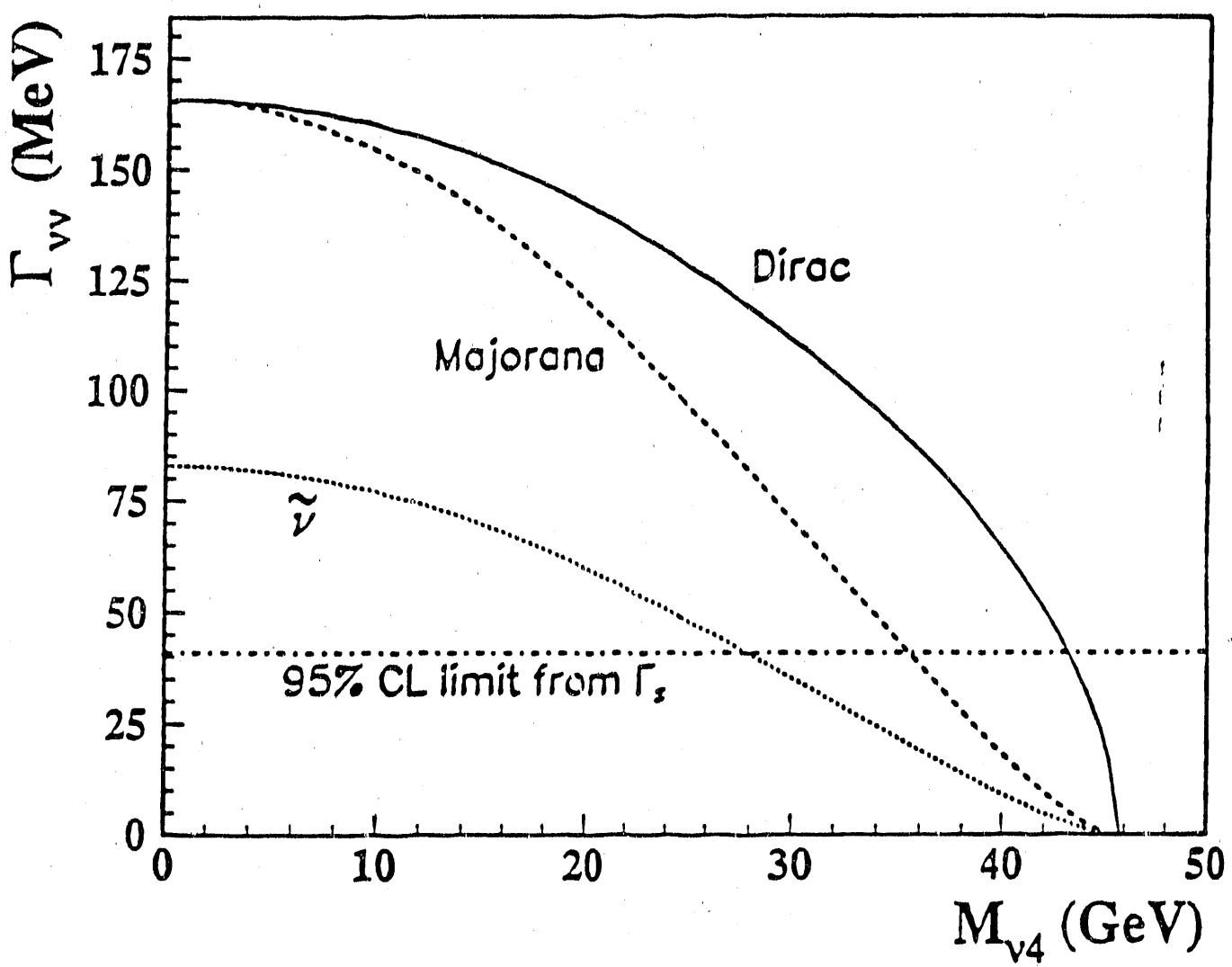

Figure II.10. Γ_{ll} width versus $M_{\nu 4}$ for Dirac, Majorana, and scalar neutrinos.

separately. A plot of the Γ_{ll} width as a function of M_{ν_4} is shown in Figure II.10 for Dirac, Majorana, and scalar neutrino masses. From the 95% CL limit for the values of Γ_{inv} and Γ_Z (shown in Figure II.10), lower limits for the masses of these heavy neutrinos can be obtained (see Table III). Lower mass limits for heavy neutrinos have also been obtained from searches for isolated electrons, muons, and taus in the data (see Table III).

Supersymmetry: $e^+e^- \rightarrow Z^0 \rightarrow A_0h_0$

Searches for supersymmetric particles in the minimal supersymmetric Standard Model have focused on the $(b\bar{b}b\bar{b})$, $(b\bar{b}\tau\bar{\tau})$, and $(\tau\bar{\tau}\tau\bar{\tau})$ decay channels. These final states are characterized by a 4-jet topology, with potentially high rates in the $(b\bar{b}b\bar{b})$ channel. Results of these searches exclude masses for h_0 up to 41 GeV/c^2. Tables IV and V summarize the search for supersymmetric particles deduced from the hadronic and neutrino widths of the Z^0. A determination of the top quark mass from the L3 values of M_Z and Γ_Z, combined with νN and $\bar{p}p$ data yield:

$$M_{top} = 134^{+36}_{-41}\ GeV/c^2.$$

Higgs: $e^+e^- \rightarrow H^0\nu\nu$

Searches for the minimal Standard Model Higgs [16] and minimal supersymmetric Standard Model Higgs [17] have been performed on events selected with large missing energy and large energy imbalance. $q\bar{q}$, $\tau^+\tau^-$, and 2 photon backgrounds have been rejected by excluding events with back to back topologies and events with low energy and low multiplicity. A plot of the expected kinematic properties of these selected events along with simulated distributions for a 40 GeV/c^2 Higgs mass is shown in Figure II.11. On the basis of these distributions, a mimal Higgs mass is excluded in the following kinematic range:

$$2 \leq M_H \leq 36.2\ GeV/c^2.$$

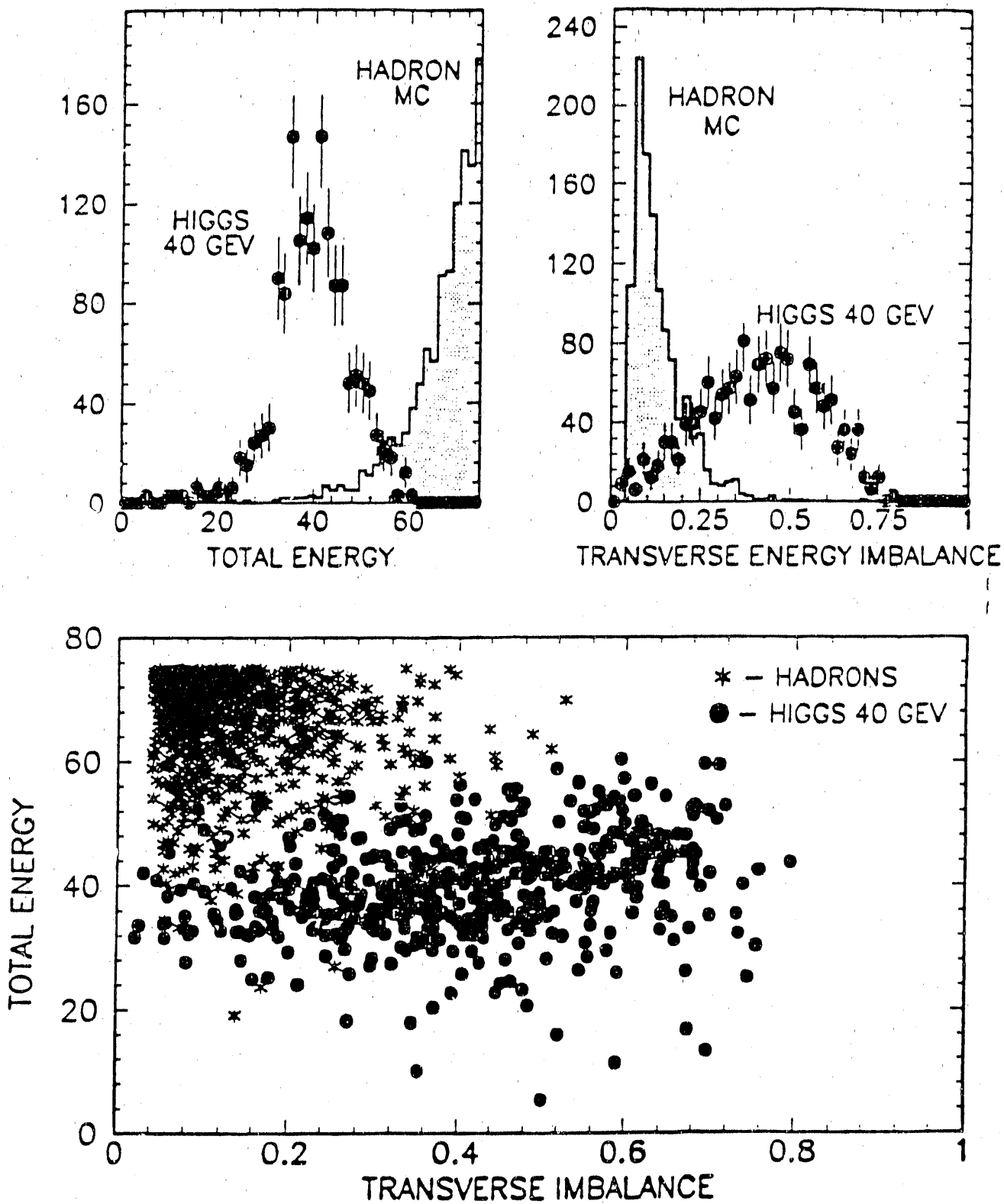

Figure II.11. Energy distributions of events selected for minimal Higgs search.

III. The L★ Experiment at SSCL

The Alabama group is also preparing to study pp collisions at $\sqrt{s}$ = 40 TeV. This group is a member of the L★ Collaboration which has recently submitted an expression of interest to the SSC Laboratory for experimental research [18]. The L★ detector, shown in Figure III.1, is a high precision spectrometer designed to measure leptons and photons with a hadron rejection ratio $\frac{lepton}{hadron} \approx 10^{-4}$ for $p_T \geq 0.1$ TeV and measure lepton pairs with a mass resolution $\frac{\Delta m}{m} \approx 1\%$ at a mass of 1 TeV. Searches for the Higgs particle and new and unpredicted phenomena are the principal physics objectives of this experimental program.

In this proposal Alabama will be responsible for the forward hadron calorimeter subsystem of this detector, in close collaboration with the First Physics Institute, RWTH, Aachen, Germany, and with the Tata Institute for Fundamental Research (TITR), Bombay, India. Members of the L★ Executive Committee are listed in Table VI and include representation from the University of Alabama. The physics programs and detector issues for the L★ forward region are outlined below. A general description of this calorimetry is given in Appendix II.

Physics Motivations

For many interesting production processes in the central region at the SSC, the forward region ($|\eta| \geq 3$) plays an important role in improving the overall acceptance phase space and energy resolution in their measurement. In particular, searches for intermediate mass Higgs boson production and decay depend largely on acceptance in the forward region. In searches for new vector bosons, pp $\rightarrow$ W', Z' + X, the production cross section for these new states is enhanced in the forward region, where antiquarks from the sea are found at higher values of Feynman x. Searches for supersymmetric states, in turn, rely mainly on the ability to accurately measure missing transverse energy, which can be significantly affected by energy flow into the forward region. Here, the calorimeter response to jets and other energy is an important factor. The ability to measure energy flow accurately in the forward region will ultimately define this hermeticity.

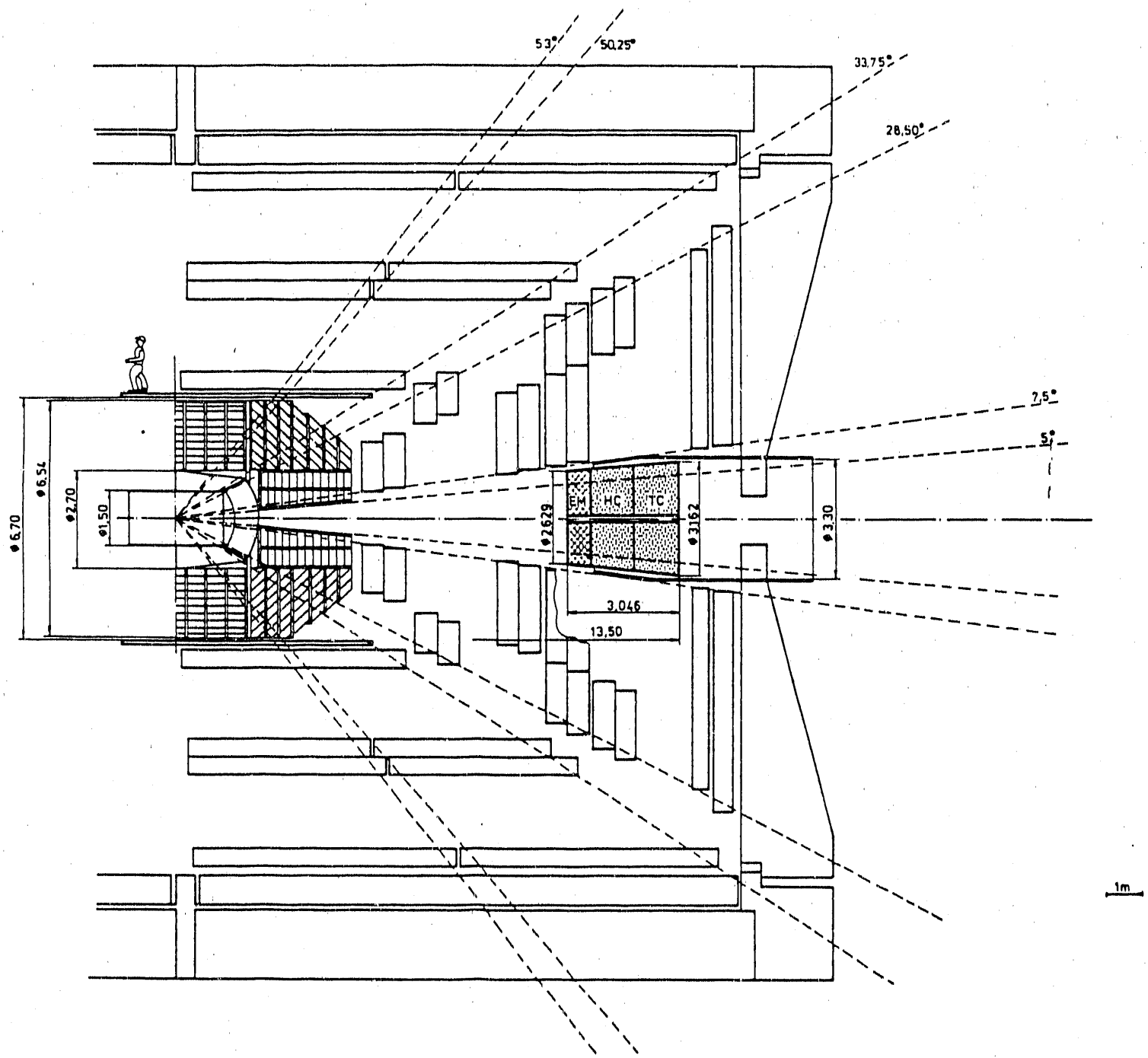

Figure III.1. Side view of the L★ detector with central and forward calorimeters.

The search for an intermediate mass Higgs particle in the mass range between 80 GeV and $2M_Z$ is an important test of supersymmetric theories. Minimal supersymmetric extensions of the Standard Model require that $M_H \leq M_Z$, whereas nonminimal supersymmetric theories require $M_H \leq 200$ GeV. If $M_H \geq 200$ GeV, then SUSY is ruled out. For masses between 140 GeV and $2M_Z$, the best signal for Higgs detection is in the four lepton channel via the Z^0Z^* intermediate state, $H \rightarrow Z^0Z^* \rightarrow l^+l^-l^+l^-$. Rapidity distributions of the largest rapidity lepton from either Z^0 or Z^* decay have recently been studied for a 140 GeV Higgs mass [19]. On the basis of these calculations, lepton acceptance must extend to five units of rapidity to keep most of the signal events. With coverage below $|\eta| \leq 3$, this acceptance is only 58%.

Intermediate vector boson production at the SSC extends out to $|\eta| \leq 6$ and is nearly flat over this entire pseudorapidity interval [20]. For higher mass vector boson states, W′ and Z′, the edge of the corresponding production plateau will diminish approximately as $\ln(M_{W',Z'})$. Detection of these states will therefore require instrumentation in the forward region, with the ability to accurately measure missing transverse and longitudinal energy for purely leptonic decays.

Missing transverse energy measurements can be affected by the hermeticity and resolution of jet energy. At 2^0 a 1 TeV jet can already contribute 35 GeV to missing E_T measurements. With sufficient transverse segmentation, an angular precision of 2 mrad for the jet direction can be expected on the basis of similar results already attained in current collider experiments. For a hadron calorimeter with $(50/\sqrt{E} + 4)\%$ energy resolution (expected in most calorimeters with high longitudinal segmentation), the energy and angular resolution will contribute equally to the jet transverse momentum resolution at 2^0. Further down the angular resolution is dominating. These measurements implicitly assume, however, that the jet energy is entirely contained in the forward calorimeter, i.e., no leakage through uninstrumented regions. Additional energy resolution can be achieved if the calorimeter responds equally to electromagnetic and hadronic energy.

Detector response is crucial in preserving any intrinsic calorimeter resolution from smearing effects due to pileup [21]. Ideally the calorimeter should respond with a bandwidth matched to the SSC beam crossing time, 16 nsec. Not only does this requirement affect the calorimeter's energy response to jets, but also its ability to observe directly and therefore correct for gammas radiated off by muons observed in a forward spectrometer in the presence of high particle rates [18].

Forward Hadron Calorimeter System

Forward calorimetry extending down to the beampipe can double the overall acceptance of an SSC detector beyond most central calorimetry. For detectors with multi-leptonic detection capability down to very small angles [18], forward calorimetry is necessary to match this acceptance. Forward calorimetry down to $\eta = 5.95$ (corresponding to 0.3^0 as imposed by the outer diameter of the beampipe [50 mm]) improves the overall hermeticity of the experiment, particularly in measurements of (missing) longitudinal and transverse energy of inclusive states produced at small angles. In this region a small change in angular coverage $\Delta\theta$ corresponds to a much improved coverage in pseudorapidity, $\Delta\eta = \frac{\Delta\theta}{\theta}$. Arguments for the specific layout of the forward calorimeter system are explained below. These design considerations include radiation hardness, speed, resolution, and segmentation. Fast detector response, in turn, depends largely on the ability of the readout electronics to respond with a bandwidth and sensitivity matched to the SSC beam crossing time. Detector specifications are given in Table VII.

The anticipated high radiation environment in the forward region places severe constraints on the choice of detector technology. At a distance of 10.5 m from the primary interaction vertex, the expected neutron fluency at 2^0 ($\eta = 4.05$) is 10^4 neutrons/cm^2/year while the corresponding gamma dose at the same position is 10 Mrad [22]. This ensures operation at radiation levels comparable or less than in the endcap region of most central calorimetry [18]. Below this angular region, these radiation levels rise rapidly and can seriously reduce the operational lifetime of most detector technologies, such as BaF_2, or silicon. These rates are plotted in Figure III.2 as a function of radial distance.

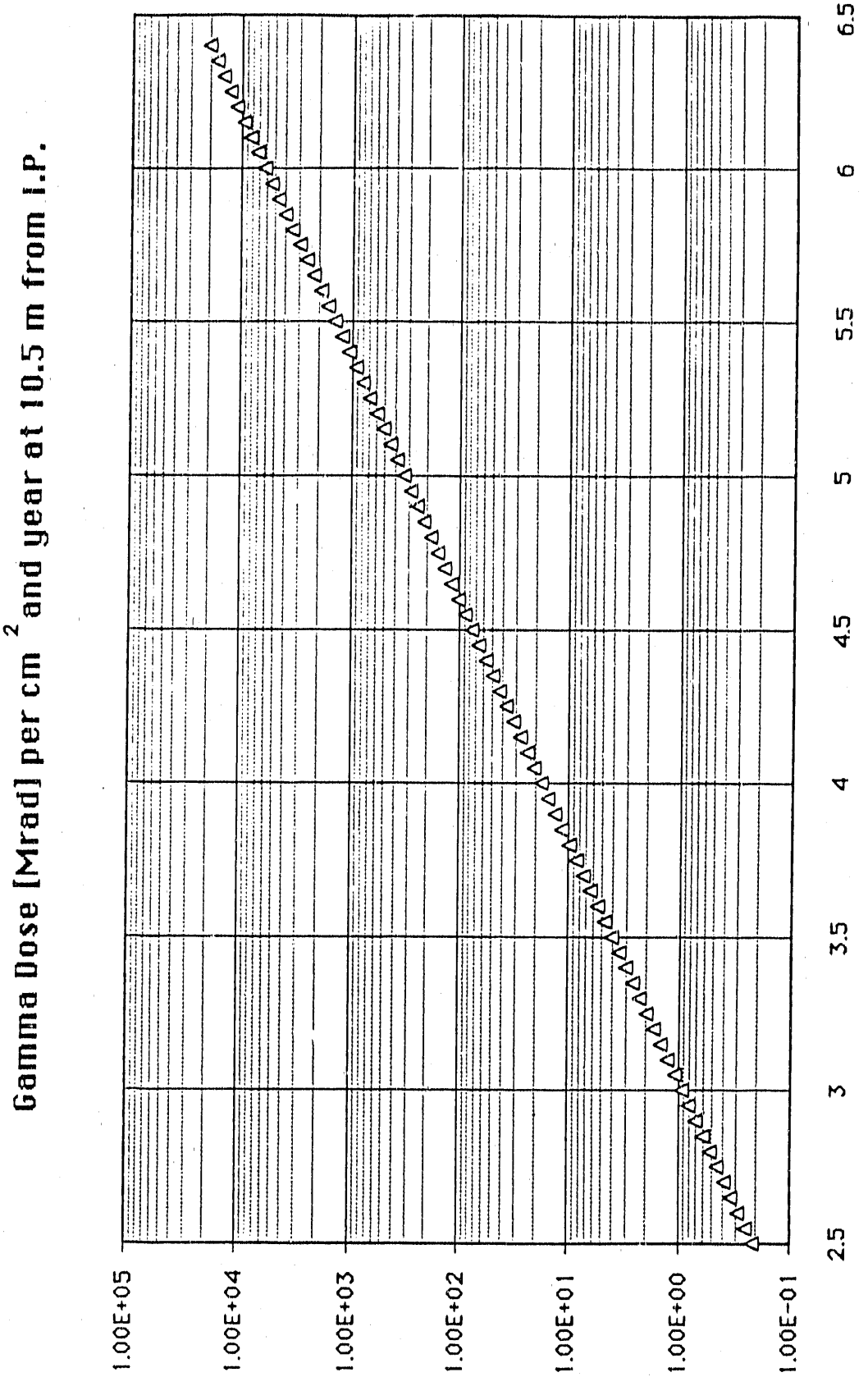

Figure III.2. Gamma ray dose (Mrad cm^{-2} $year^{-1}$) at 10.5 m from the interaction point.

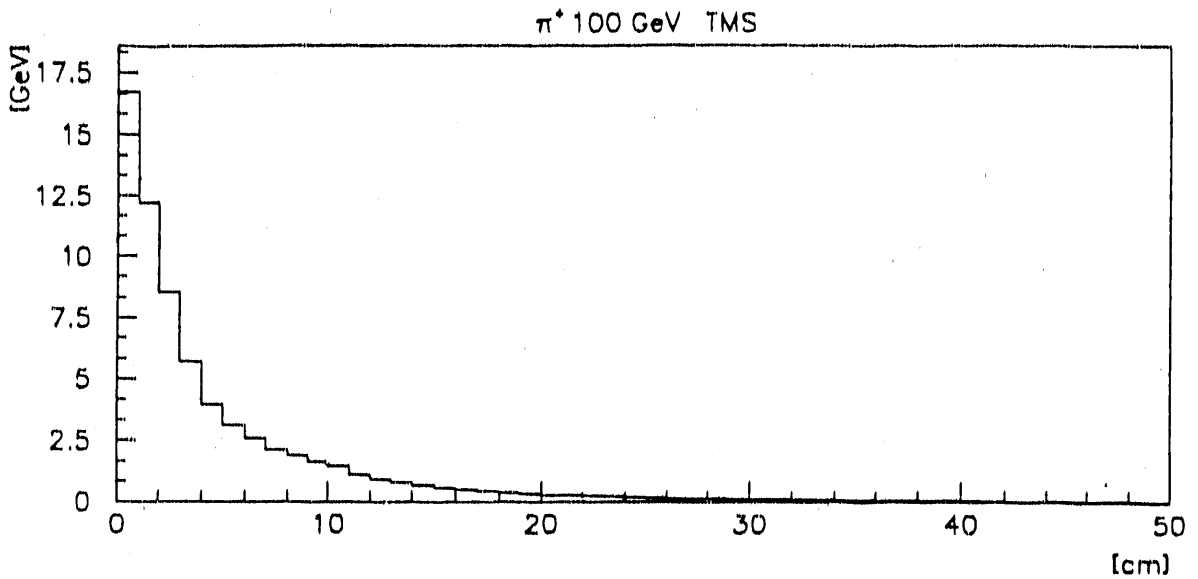

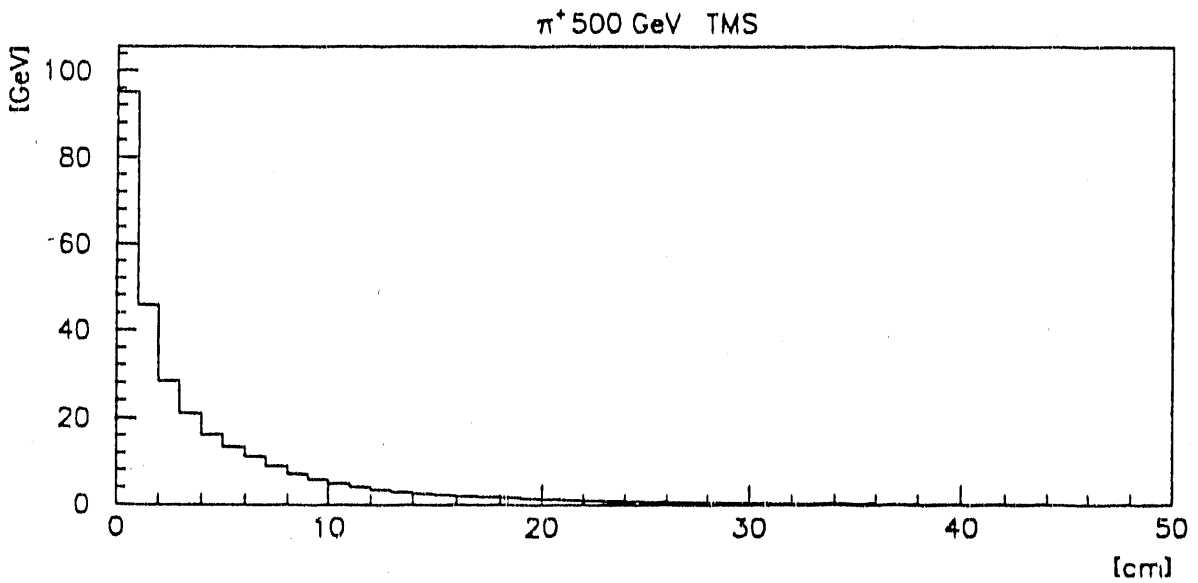

Figure III.3. Maximum transverse shower profile for a) 100 GeV, b) 500 GeV π in Fe-TMS..

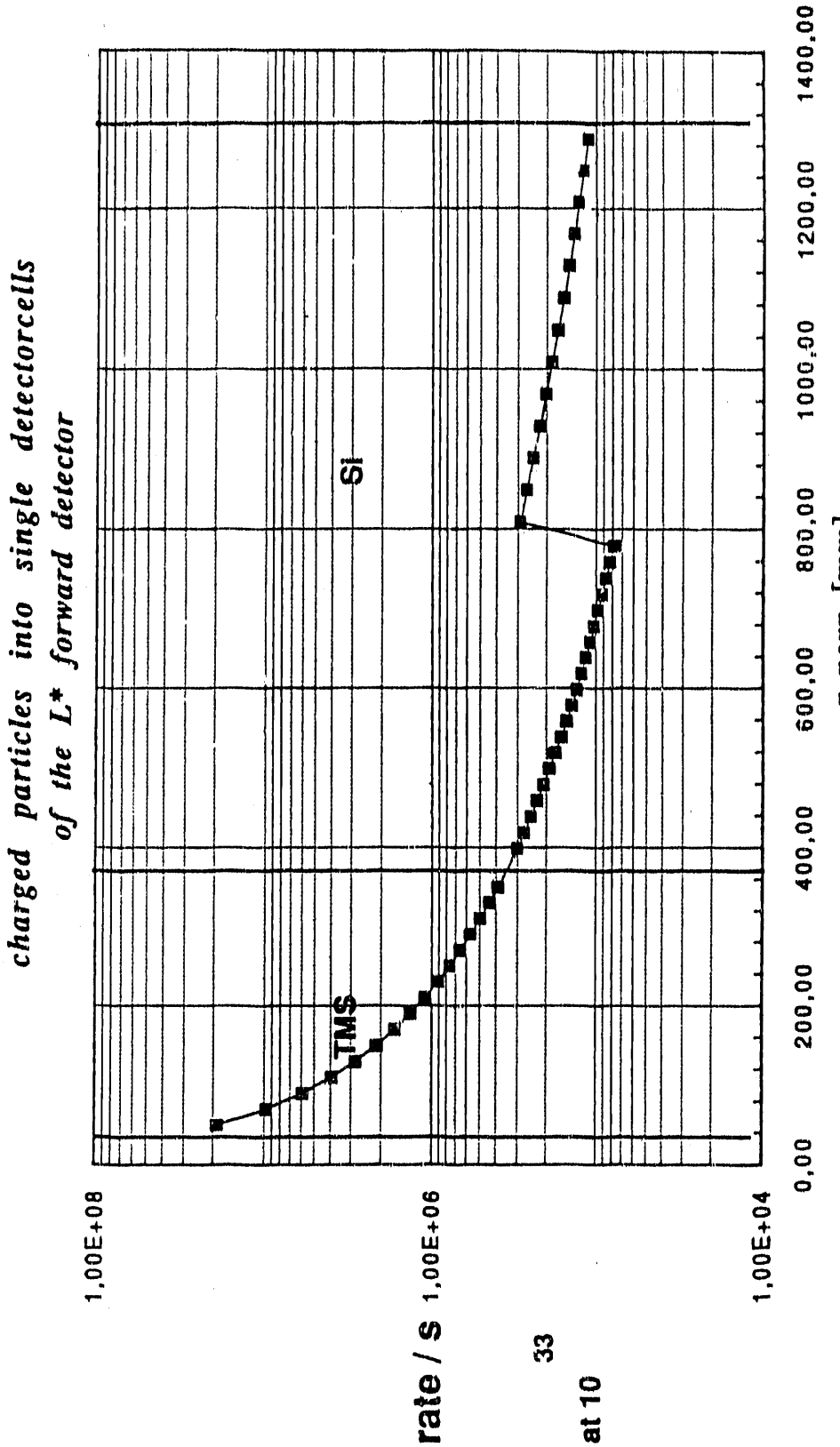

Figure III.4. Charged particle rate per pad versus radial distance at 10.5 m.

Lateral segmentation has been determined on the basis of pion response within the calorimeter. Monte Carlo studies of the maximum transverse shower size for 100 and 500 GeV pions have been performed using the GEANT simulation code for a fine sampling Fe-TMS calorimeter, with specifications given in Table VII. On the basis of these calculations, shown in Figures III.3 a) and III.3 b), a 20 mm pad size is sufficient to sample the maximum hadronic shower core and still distinguish a purely electromagnetic shower. At 2^0 a jet lying within a cone of $\Delta R = 0.3$ will span 4 pads. We take this 4 cm^2 area as the basic pad size within the calorimeter. The corresponding number of charged particles traversing each detector cell is shown in Figure III.4 at a luminosity of 10^{33} $cm^{-2}sec^{-1}$, assuming a total inelastic cross section of 100 mb. The proposed lateral segmentation is hence sufficient for keeping pileup below the 1% level at this design luminosity.

Experience with the L3 hadron calorimeter at LEP suggests that approximately 100 longitudinal energy samples are required to achieve an energy resolution of $50\%/\sqrt{E}$ with a (statistical) baseline level of 4%. The corresponding longitudinal depth of this calorimeter should also be sufficient to absorb at least 99% of a 1 TeV jet, or 14 λ. Ideally the sampling fraction should be identical with the central calorimetry and overlap with the endcap of the central calorimetry at least 1.5 λ for uniform detector response. In the absence of a dedicated electromagnetic calorimeter before this detector, a warm liquid (TMS) calorimeter can also be compensating, with sufficient segmentation at the front for electromagnetic identification.

The proposed forward hadron calorimeter is shown in Figure III.5. Above 2^0 the outer calorimetry consists of a fine sampling Pb-Fe-Si calorimeter and front BaF_2 electromagnetic calorimeter similar to the central and endcap region. Below 2^0 we choose warm liquid technology, which can be recirculated and also regenerated under the high radiation conditions foreseen in this region. Warm liquids are also the first alternative technology choice for silicon and BaF_2.

Mechanical and physical specifications of the inner warm liquid calorimeter are listed in Table VII. A side view of this calorimeter is shown in Figure III.6,

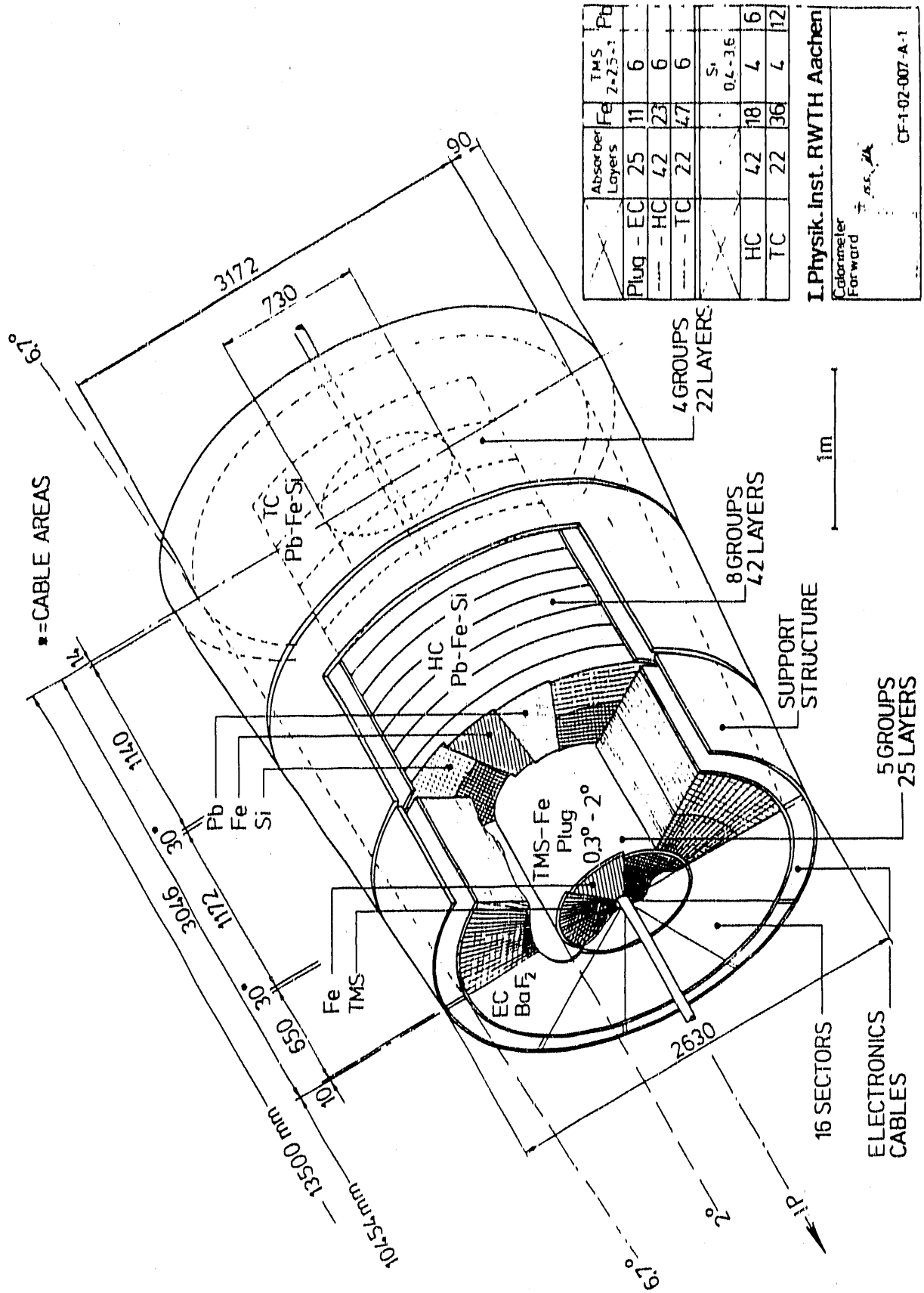

Figure III.5. Proposed Forward Hadron Calorimeter with inner warm liquid detector.

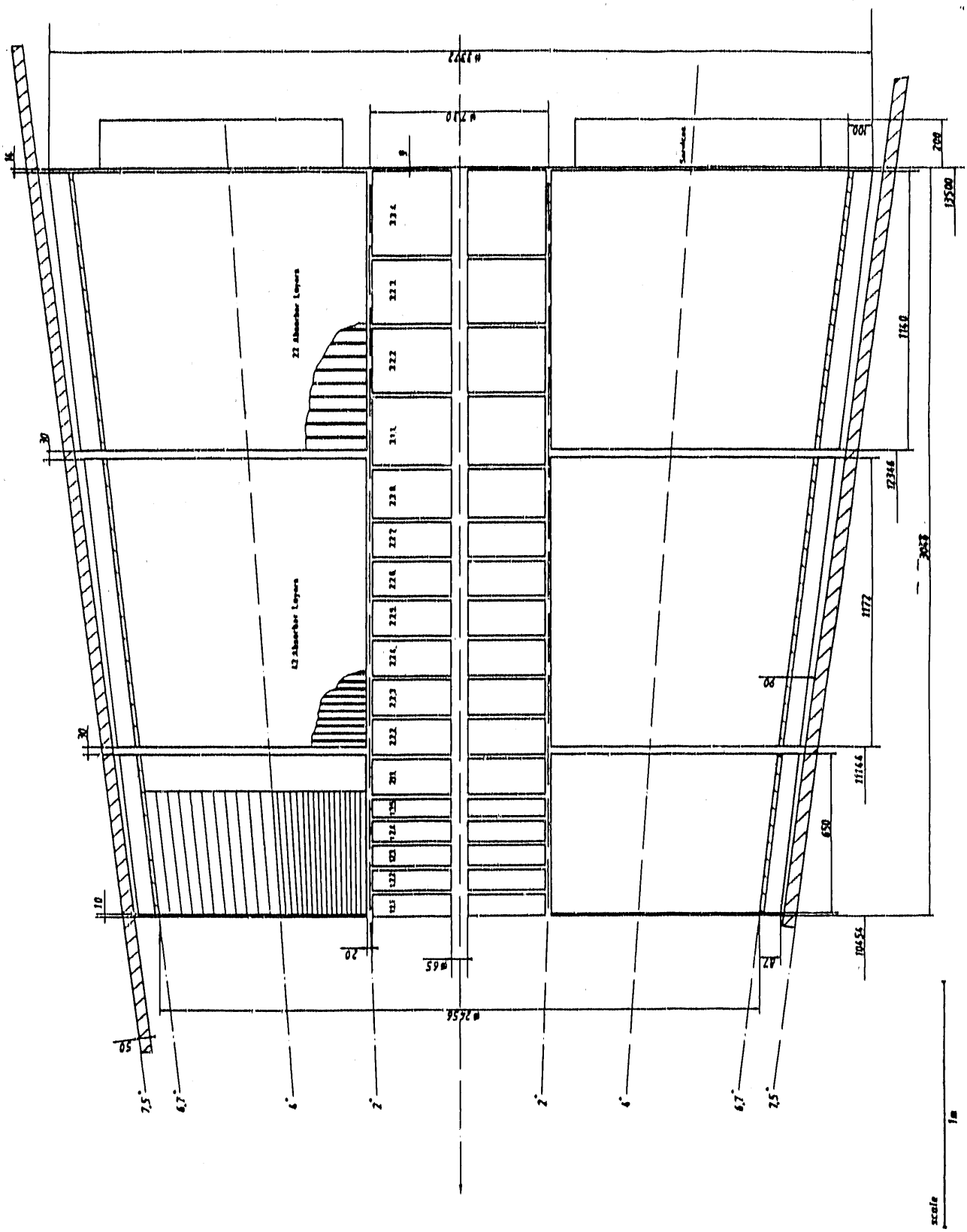

Figure III.6. Side view of forward hadron calorimeter showing supermodule structure.

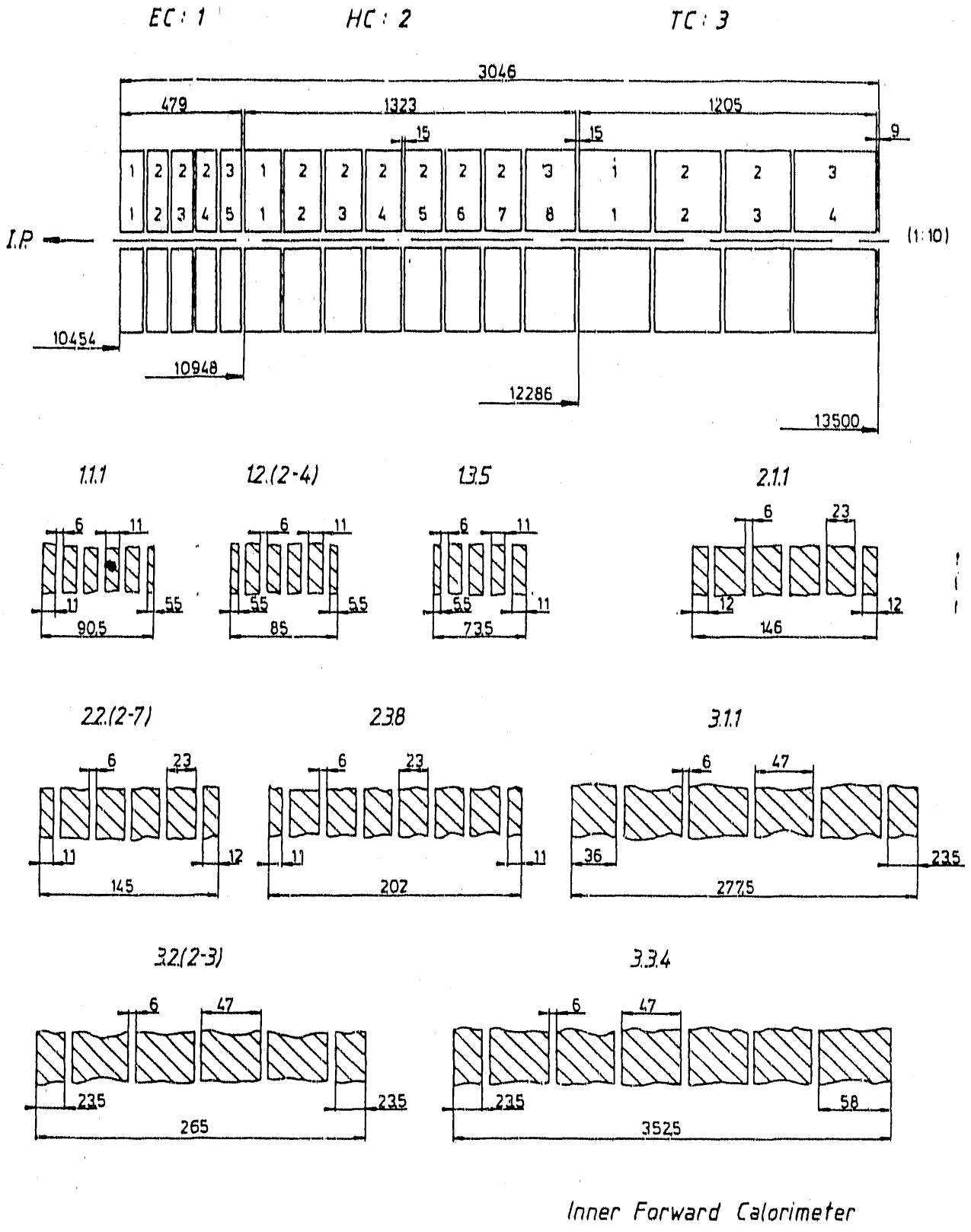

Figure III.7. Detail within each supermodule of the inner calorimeter with detector gaps.

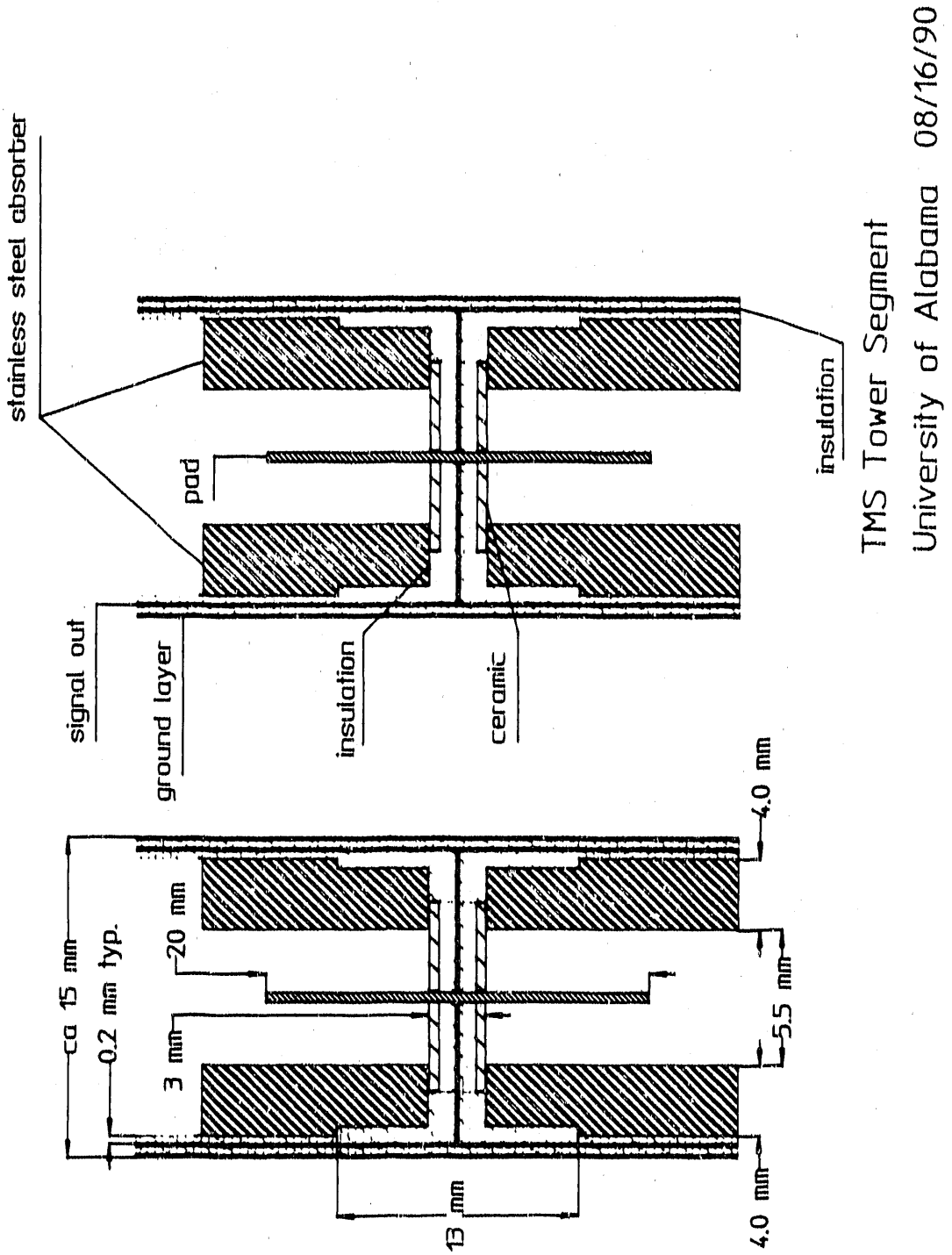

Figure III.8. Engineering detail of metallic anode tile and feedthrough system.

where the longitudinal sampling segments have been grouped into larger supermodules for ease of assembly and installation. A detail within each of the individual supermodules is shown in Figure III.7 along with the 89 individual dual 2.5 mm liquid ionization gaps sandwiched between the iron absorber material. Each supermodule is an unbroken, azimuthally continuous cylinder to guarantee complete hermeticity around the beampipe. The supermodules, in turn, are grouped into three larger sections: a finely layered electromagnetic section with 25 layers each 11 mm thick, a hadronic central region with 42 layers each 23 mm thick, and finally a tail catcher section of 22 layers each 47 mm thick. The total thickness represents a calorimeter 14 absorption lengths deep with a transverse pad size of 20×20 mm^2.

Designs for a specific pad arrangement are presently underway at the University of Alabama and Aachen which either incorporate the absorber material within the warm liquid volume or isolate the liquid and electrode as a separate assembly. Preliminary indications of material incompatibility with warm liquids suggest that a separate can containing this liquid may be a safer approach, thereby allowing more flexibility in the choice of detector material. To handle the corresponding high channel density per container, innovative techniques with metalized ceramic electrodes are presently being pursued [23]. One possible pad configuration is shown in Figure III.8 in which each electrode is supported as an individual metallic tile. Charge collecting anodes are connected through insulating seals for external routing to nearby signal electronics and high voltage biasing. Designs for the outer silicon detector are identical to those for the central hadron calorimeter in L★ [18].

With the development of fast, radiation-hard charge preamplifiers for warm liquid calorimetry [24], fast detector response is possible despite the relatively slow drift velocities in these liquids. In response to the repetition rate of the SSC (16 nsec) only the very front spike of the ionization signal will be used. To maintain the intrinsically fast response of the front-end electronics (less than 10 nsec), the preamplifiers must be mounted directly on the detector. Detector capacitance, in turn, must kept as low as possible [25].

IV. The Van de Graaff Institute

This chapter describes a proposed institute for high energy physics research, to be established at The University of Alabama and named for one of its most illustrious alumni, Dr. Robert J. Van de Graaff. The institute would support a major effort in research on the fundamental structure of matter, and would build on the experimental and theoretical high energy physics groups already active at this university. In the following paragraphs we describe why it is appropriate and timely to establish an institute in honor of Dr. Van de Graaff. We then describe the structure of the institute as we envision it.

Dr. Van de Graaff was a native of Tuscaloosa, Alabama, and is linked to many of the prominent families in the history of the city. He received his B.S. degree and later his M.S. degree from The University of Alabama in 1923. After earning his Ph.D. in physics at Oxford in 1928, he went to Princeton and MIT, where he built the first of the very successful high voltage generators which bear his name. These Van de Graaff generators, and the particle accelerators which bear the same name, were among the first tools used by physicists to explore the structure of the nucleus. Although the search for the fundamental structure of the matter has led physicists to develop other, higher-energy machines, the Van de Graaff accelerators continue to play a vital role, both as injectors for the new machines and for continuing research in nuclear and other areas of physics. Robert Van de Graaff is certainly the most distinguished scientist to have graduated from the University of Alabama in its 150 year history and perhaps the most distinguised to have emerged from the entire Southeast United States. One cannot overestimate the importance of his work as a source of pride to the citizens of the state and as a potential role model for future students of science. It is for this reason that we feel it is appropriate to establish an institute in honor of Dr. Van de Graaff and the role he played in the development of high energy physics.

The time is especially auspicious for the establishment of a new high energy physics institute because the United States is constructing an accelerator that will greatly surpass all existing machines in size and capabilities. For physi-

cists, the SSC is necessary to answer a number of crucial questions regarding the fundamental particles and their interactions. It will also assuredly uncover new, unanticipated phenomena which will present challenges to our current theories, and lead to further refinement in our understanding of the structure of nature, but will also certainly lead to spin-off technologies which can have significant economic impact regionally. Areas that have reaped the benefits of technology from high energy physics include medical technology, ion implantation, food disinfestation, energy storage, materials science, and national defense. Several recent government and private reports have pointed out the desirability of a greatly increased participation in high energy physics by the southeastern states. The highly industrialized states and those that attract the lion's share of new high technology industry have, relative to Alabama, a much higher share of their state supported physics faculties working in the area of nuclear and particle physics. For example California, Illinois, New York, and Massachusetts have an average of 41% of their state supported physics faculty working in these areas of subatomic physics whereas the state of Alabama has only 12%. The University of Alabama is home to the only sizeable effort in high energy physics in the state and is the natural location for a strong, concentrated, and non-duplicated program.

Description of Budget of the Proposed Institute

The proposed Van de Graaff Institute for high energy physics would house physicists, technical support personnel, and students. Building on the existing high energy groups, the professional staff would include University faculty, non-tenure track research physicists, visiting scholars, and post-doctoral research associates. The institute would have offices, conference rooms, a dedicated machine shop and electronics shop with computational facilities, a research library, and housing facilities for visitors to support the experimental and theortical activities conducted there. The institute will have a high bay area of several thousand square feet for the construction of very large detectors to be used in future SSC experiments. A building of approximately 25,000 is presently being planned as an additional wing onto the existing Material Science and Energy Resource building, specifically for high energy physics research. Graduate students from the

institute would travel to the SSC and other leading accelerator laboratories for direct involvement in the construction of sophisticated particle detectors and in the aquisition and analysis of data. Other graduate students would work with the theoreticians to analyze the implications of the data and to develop more fundamental mathematical models for the underlying structure of matter. Undergraduate students would also be involved in research and development of detector components.

In order to establish a quality high energy physics program of international stature, the total particle physics faculty should be at least twenty, not including the director, with about 2/3 of these having tenure track appointments in the department of physics and the remaining 1/3 having adjunct appointments that would be indefinitely renewable or permanent within the lifetime of the institute. Salaries for these personnel should be at a nationally competitive level in order to attract top quality personnel. To provide sufficient funds for a director's salary to attract a high energy physicist on the National Academy of Science and perhaps one of Nobel calibre, a chair with an endowment of $2,000,000 should be established.

We list in Table VIII the proposed personnel requirements and an estimated budget. Much of this data has been developed after consultation with several eminent experimental and theoretical physicists and after study of the high energy physics facilities of major institutions. It is expected that a large amount of support would be forthcoming from the U.S. Department of Energy. The DOE recognizes the need to spread high energy physics support more evenly throughout the country in order to more efficiently tap the nation's scientific and intellectual potential. Indeed, high energy experimental groups cannot function without this support. In order to enter the ranks of the major research universities, the University of Alabama needs to engage much more heavily in federally funded research activities. High energy physics is one of the most heavily supported scientific activities of the federal government. The annual federal budget for high energy physics research in universities exceeds $100M, most of which comes through the Energy and Water Development subcommittee.

The budget of Table VIII lists expenses that the University of Alabama would bear, as well as those that DOE would support. One-time expenditures for the construction of a new building and for major equipment in the machine and electronics shops are also listed which would be funded largely by matching state funds.

The personnel listed in the budget include the 20 faculty positions plus the director already referred to. Allowance is also made in the budget for a number of visitors to attend annually. These would be established physicists who would come for limited periods of time to collaborate with the permanent faculty, to lecture, and to interact in less formal ways with the institute participants. In addition, post-doctoral research associates are provided for, at the rate of one per two faculty. These positions are an important stepping-stone for the new Ph.D., and are vital to the productivity of the institute. Finally, because the institute can be expected to attract a large number of graduate students, support for these students is also included. Education will, of course, be a major function of the institute. The remaining personnel, who will not be physicists but will play an essential role in the activities of the institute, include research engineers (for electronics and computers), machinists, technicians, and secretaries.

V. Research Plans for L3

A. Introduction

The physics program which can be pursued at LEP, both near the Z^0 pole and eventually above the W^+W^- production threshold, is rich and diverse. An important part of this program, which capitalizes on the superior photon detection capabilities of the L3 detector, is single-photon physics. The remainder of this chapter is devoted to a discussion of the physics motivation for the analysis of single-photon events, a review of the current experimental situation and prospects for single-photon physics, and a summary of the University of Alabama's participation, both current and anticipated, in the study of single-photon data taken with the L3 detector. Although the focus of this chapter is single-photon physics, it is very important to note that with expansion of the group, including Dr. Razis and several graduate students, the active participation of the Alabama group will extend into other research activities as well.

B. Physics Motivation

The process $e^+e^- \rightarrow \gamma(X)$, where we use the notation (X) to represent neutral weakly interacting particles, receives contributions from primarily two mechanisms. The first is radiative production, in which bremsstrahlung from the initial-state electron or positron is followed by annihilation of the electron and positron into undetected particles. The standard example [26,27] from the Standard Model of a process occuring by such a mechanism is $e^+e^- \rightarrow Z^0\gamma$, $Z^0 \rightarrow \nu\bar{\nu}$. The other important mechanism leading to $\gamma(X)$ is radiative decay into a weakly interacting particle. For example, within the context of supersymmetry an allowed scenario [28] is the decay $Z^0 \rightarrow \chi'\chi$ followed by $\chi' \rightarrow \chi\gamma$ where the χ is weakly interacting. (The neutralinos χ and χ' are superpositions of the supersymmetric partners of the Standard Model photon, Z^0, and Higgs.) In the following paragraphs we review the range of physics which can be profitably addressed by analyses of one-photon events at LEP.

At center-of-mass energies on or slightly above the Z^0 pole, the process $e^+e^- \rightarrow \gamma(X)$ provides a means of measuring the partial decay width Γ_{inv} of the Z^0 into weakly interacting particles [29,30]. Γ_{inv} receives contributions from the decay of the Z^0 into neutrinos as well as from any New Physics in which weakly interacting particles pairs ($m < m_Z/2$) couple to the Z^0. For photons emitted at least a few degrees away from the beam line and with energy above a few hundred MeV, the Standard Model contribution to the single-photon sample can be predicted-and implemented in Monte Carlo event generators-with a precision better than 1% [29,31]. If the observed single-photon spectrum agrees well in shape with the predicted spectrum but differs in normalization, this would indicate the existence of additional "light" weakly interacting particles into which the Z^0 decays.

In discussing the utility of single-photon events for measuring Γ_{inv} it is important to point out that the single-photon measurement complements well the determination of Γ_{inv} from the lineshapes of the Z^0 decays into hadrons and charged leptons. This complementarity is threefold: First, except for a small contribution at the percent level from W-exchange, the number number of single-photon events observed depends only on Γ_{inv}; whereas the other method arrives at a result for the invisible width by subtracting, in the most model-independent approach, the measured hadronic and charged leptonic partial widths from the measured total width. Second, the single-photon measurement is less sensitive to the uncertainties in the top mass, Higgs mass, and the strong coupling constant. Third, the experimental techniques and analysis cuts used to obtain the single-photon sample differ greatly from those used to obtain the hadronic and leptonic samples.

The measurement of the radiative production of weakly interacting particles is also important at higher energies up to the maximum achieved by LEP2 [30]. The crossing of a threshold for the production of a massive weakly interacting pair will be accompanied by an increase, relative to Standard Model expectations, in the number of single-photon events. This is true, no matter what the mechanism is (Z-exchange in the s-channel, wino-exchange in the t-channel, etc.) by which

the production occurs. Such an increase will be more difficult to detect, however, owing to the smaller cross sections away from the Z^0 pole and the backgrounds which are proportionately larger in consequence.

To indicate roughly the single-photon cross sections expected from the Standard Model with three generations and for reference by discussions given below, Figure V.1 shows the differential single-photon cross sections as a function of photon energy for two center-of-mass energies, $\sqrt{s}$=M_Z and $\sqrt{s}$=M_Z + 4 GeV, with the requirement that the single photon be emitted into the region $45 < \theta_\gamma < 135$ degrees. The cross sections are calculated in the Born approximation with the further approximation $M_W \rightarrow \infty$, but nonetheless they are a good indication of how the cross section depends on energy. On the pole, the cross section falls monotonically, crossing through about 40 pb/GeV at 1 GeV and falling below a few pb/GeV by a photon energy of 4 GeV. At 4 GeV above the pole, the reflection of the resonance is clearly visible and the cross section peaks at around 25 pb/GeV near a photon energy of 4 GeV. Using finite M_W, adding weak and electromagnetic corrections, and integrating over photon energies from 1 GeV upwards with the same angular cut as above, a cross section of 34 pb is obtained for the on-resonance case and 84 pb for the center-of mass energy 4 GeV above the Z^0 mass [29]. For an integrated luminosity of 50 pb^{-1} at each center-of-mass energy, this corresponds to some 1700 and 4200 events, respectively.

Given the large sample of Z^0 decays that will be obtained at LEP1, it is attractive to search for evidence of New Physics via observation of decays to γ(X). The radiative production of neutrino pairs according to the Standard Model contributes a genuine single-photon background in this case, but the effects of this background could be minimized by taking into acccount not only the number of decays expected but also their distribution in energy and angle. From the curve shown in Figure 1 for $\sqrt{s} = M_Z$, extensions to the Standard Model which contribute Z^0 decays to γ(X) with $E_\gamma > 10$ GeV do not suffer much from the Standard Model background since most of the bremsstrahlung photons have energy less than 5 GeV. Examples of New Physics which can be searched for via radiative decays are as follows.

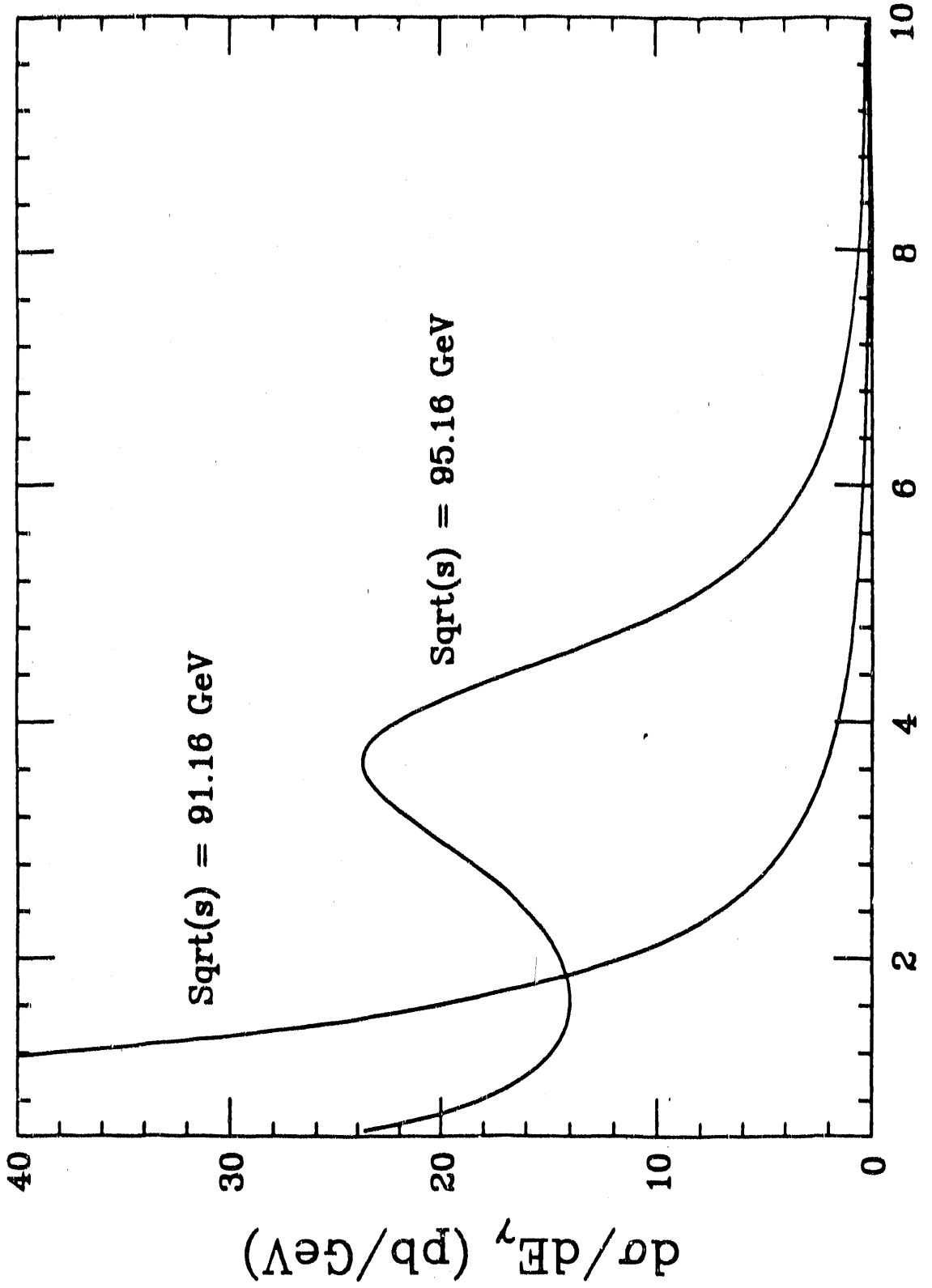

Figure V.1. $d\sigma(e^+e^- \to \gamma\nu\bar{\nu})/dE_\gamma$ in the Born approximation for $N_\nu = 3$ and $|\cos\theta_\gamma| < 0.707$.

A segment of the supersymmetric particle spectrum consists of the so-called neutralinos, which are superpositions of the neutral gauge fermions (photino, zino) and the higgs-fermions. In the minimal supersymmetric model (MSM), there are four such particles ($\chi, \chi', \chi'', \chi'''$) and the χ is a good candidate for being the lightest supersymmetric particle (LSP), which is usually assumed to be weakly interacting [28]. Assuming the χ to be LSP with mass low enough to be produced in pairs at LEP, its presence could be detected through a deviation of the invisible width from Standard Model expectations. Alternatively, due to the mixing of the neutral gauginos and higgsinos, large off-diagonal elements in the coupling of the neutralinos to the Z are induced, leading to decays of the form $Z^0 \rightarrow \chi\chi'$ followed by the de-excitation decay $\chi' \rightarrow \chi X$. If the MSM Higgs and charginos are too heavy, X will be either a charged fermion pair or a photon. The decay $12\chi' \rightarrow \chi\gamma$ would give an excess of single-photon events. For a03 broad range of m_χ and $m_{\chi'}$, the requirement that the photon energy be greater than 5–10 GeV retains most of the photons from χ' decay but heavily suppresses the background from radiative production of neutrinos. In the case an excess is not observed, limits can be set on $\Gamma(Z^0 \rightarrow \chi\chi') \times BR(\chi' \rightarrow \chi\gamma)$ as a function of the χ and χ' masses. These limits in turn may be combined with those obtained on $\Gamma(Z^0 \rightarrow \chi\chi') \times BR(\chi' \rightarrow \chi f^+ f^-)$ to derive upper limits on $\Gamma(Z^0 \rightarrow \chi\chi')$ and the neutralino mixing factors as a function of the neutralino masses.

A second example of an extension to the Standard Model which leads to a decay process whose experimental signature is a single photon is the excited neutrino ν^* [32]. An excited neutrino is expected in the context of composite models for the fermionic sector. Transitions between the excited neutrino and the ordinary light fermions are described in an SU(2) × U(1) invariant form by the following effective Lagrangian

$$L = \frac{g_W f}{\Lambda}\left(\bar{L}^* \sigma_{\mu\nu} \frac{1}{2}\tau l_L + h.c.\right) i\partial^\nu W^\mu$$

$$+\frac{g_Y f'}{\Lambda}\left(-\frac{1}{2}\bar{L}^* \sigma_{\mu\nu} l_L + h.c.\right) i\partial^\nu B^\mu$$

where g_W and g_Y are the usual weak couplings, τ denotes the Pauli matrices, L^* and l_L are the excited and ordinary lepton doublets, respectively, and Λ is the

compositeness scale. The coupling constants f and f′ are introduced in order to allow for differences in the relative couplings to the charged and neutral gauge fields beyond those due to the difference between g_W and g_γ In the case that (f – f′) is nonvanishing, the transition $\nu^* \rightarrow \nu\gamma$ is allowed. The search for excited neutrinos as a first sign of compositeness complements the search for excited charged leptons since, taking the electron mode as an example, the decay $e^* \rightarrow e\gamma$ probes the sum (f + f′). For m_{ν^*} less than m_W and (f – f′) not small, the $\nu\gamma$ decay mode will dominate the νZ and eW modes. If one assumes that the Z couples to $\nu^*\overline{\nu^*}$ with the same strength as to $\nu\overline{\nu}$, measurements of the invisible width already carried out at LEP constrain m_{ν^*} to be greater than about 40 GeV. In this case the excited neutrino is produced almost at rest and thus the energy of the photon is $m_{\nu^*}/2$. (For the full range of $(f - f')/\Lambda$ likely to be probed at LEP, the excited neutrino is short-lived so that the photon appears to come from the primary vertex.) Finally, assuming that $\gamma\nu$ decay mode is dominant, Figure V.2 plots the branching ratio for $Z^0 \rightarrow \nu^*\nu, \nu^* \rightarrow \nu\gamma$ as a function of excited neutrino masses for several different values of f_Z/Λ where $f_Z = f\cot(\theta_W) + f'\tan(\theta_W)$.

Composite models for the Z predict a contribution to the electric dipole transition $Z^0 \rightarrow Z^*\gamma$ where the Z^* indicates a virtual Z [33,34]. The single-photon topology is obtained for the decay of the virtual Z into neutrinos. For $\sqrt{s} = M_Z$ and massless neutrinos, the amplitude for the electric dipole transition is proportional to

$$e f_1 \epsilon^{\alpha\beta\mu\nu} e_\alpha e_\beta \epsilon_\mu k_\nu$$

where e_α, e_β, and ϵ_μ are the polarization vectors for the initial Z, final Z, and photon, respectively, and k_ν is the photon momentum. The form factor f_1 can be approximately expressed as $\beta(s'/M_Z^2 - 1)$. The Standard Model predicts that $\beta \sim 4 \times 10^{-5}$, but composite models of the Z investigated so far predict values for β as large as 0.05. In Figure V.3, the differential cross section $d\sigma(e^+e^- \rightarrow \nu\nu\gamma)/dx$, where x is the photon energy scaled by beam energy, is plotted as a function of x for the Standard Model, for β=1 and for β=0.5. The contribution to the electric dipole transition due to compositeness grows with increasing x so that for values of $x > 0.5$, the contribution of large-x single photons to the sample from

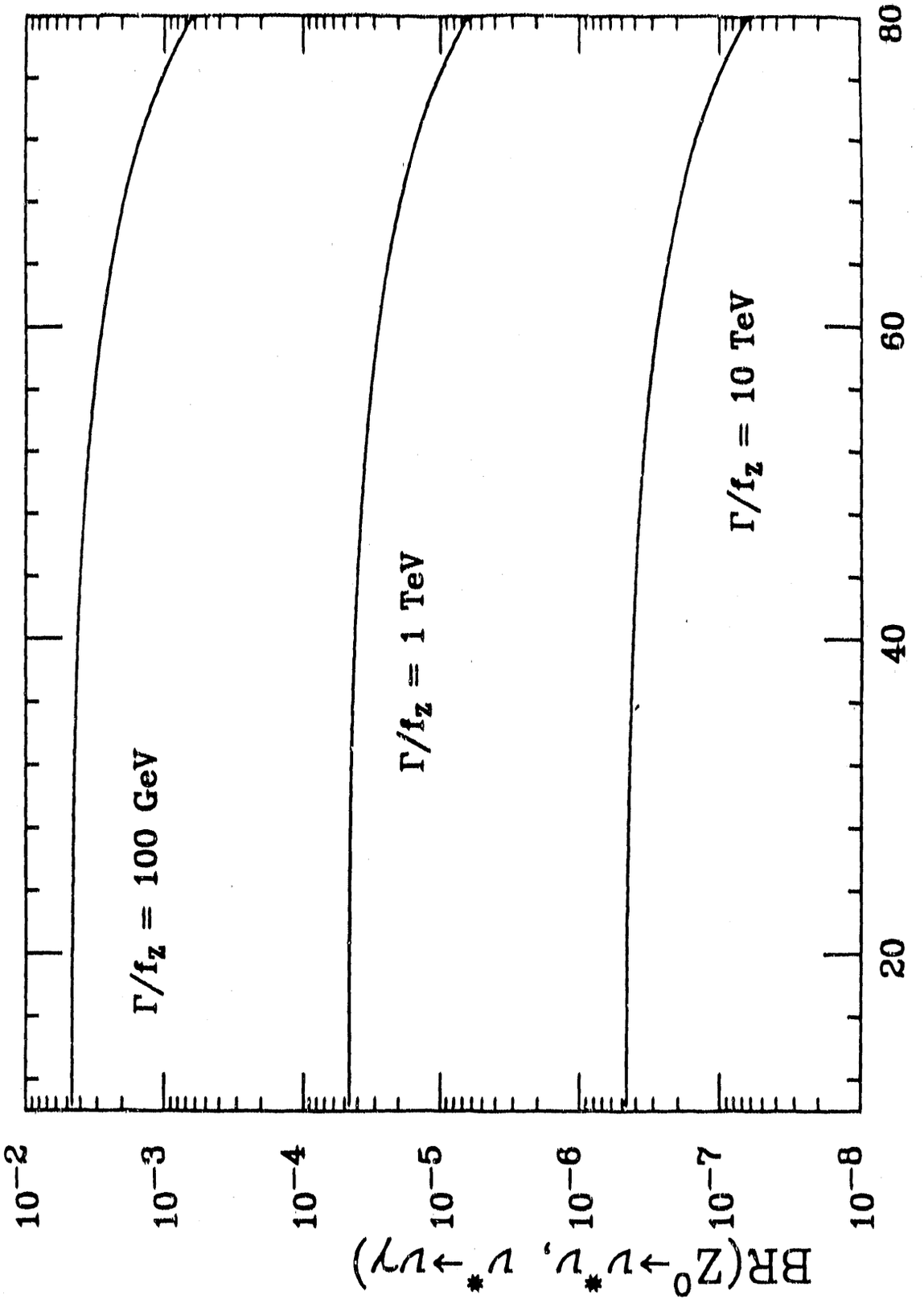

Figure V.2 Branching ratio for $Z^0 \to \nu^* \nu, \nu^* \to \nu\gamma$ versus ν^* mass.

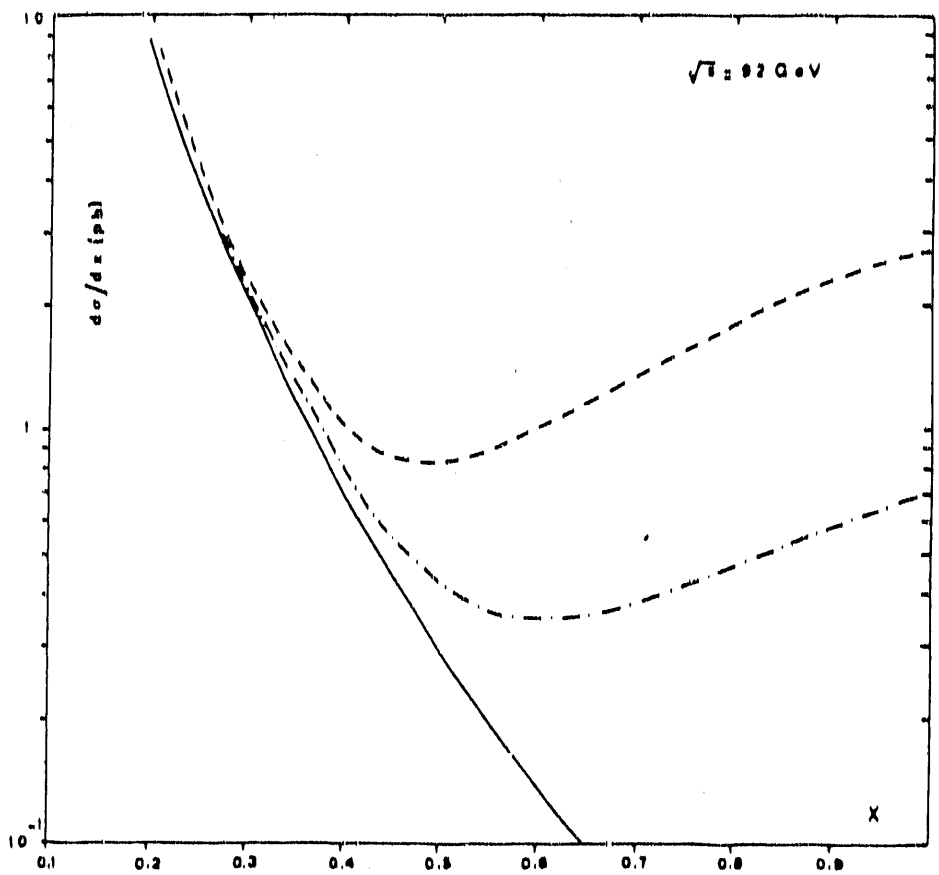

Fig. 3 $d\sigma/dx$ as a function of x, for $\beta = 1$ (dashed curve), $\beta = 0.5$ (dash-dotted curve) and standard model (solid line).

Figure V.3 $d\sigma(e^+e^- \rightarrow \gamma\nu\overline{\nu})/dx$ versus x (from Reference 34).

compositeness dominates those from the Standard Model.

The final example we review is the decay $Z^0 \rightarrow a\gamma$ where a is a variant axion [35]. Variant axions were first proposed [36,37] several years ago in connection with the narrow e^+e^- peak observed at the Darmstadt GSI experiment but have since been ruled out by beam dump experiments. It is possible, however, to circumvent the beam dump limits by embedding the axions in a model in which no coupling is allowed between the axion and electron. Within such models, a Z^0–γ–a coupling is induced at the one-loop level through the chiral anomaly. The strength of the coupling goes as $C_{aZ\gamma}/F_a$ where $C_{aZ\gamma}$ is calculable from the Weinberg angle and the masses of the light quarks while F_a is a free parameter of the Lagragian. For the experimentally allowed values of F_a, the axion decays outside the detector, in which case the event is characterized by a single photon with energy equal to $m_Z/2$. The branching ratio for $Z^0 \rightarrow a\gamma$ is plotted as a function of F_a in Figure V.4. The value $C_{aZ\gamma} = 1$ is shown for reference while $C_{aZ\gamma} = -0.43$ is characteristic of the specific model discussed in Reference 35.

C. Experimental Situation and Prospects

1. LEP Luminosity and Energy

With one year of operation completed, LEP has delivered about 7 pb^{-1} of integrated luminosity in the Z^0 resonance region. Significant improvements in the luminosity were realized in the latter part of the 1990 run as compensations for the effects of the experimental solenoids were implemenented and careful beam tuning succeeded in positioning the minimum of the β^* function at the experimental interaction points. In the last few weeks of the run, luminosities achieved were typically $5 \times 10^{30}/cm^2$–s with the record luminosity being $7 \times 10^{30}/cm^2$–s. Further increases in the luminosity will be achieved by increasing the injection currents, further minimizing effects of beam-beam interactions, and improving monitoring of the beams. The integrated luminosity will also be increased by reducing the time between fills and solving problems which lead to beam aborts. For the 1991 run, one can realistically anticipate that typical luminosities will

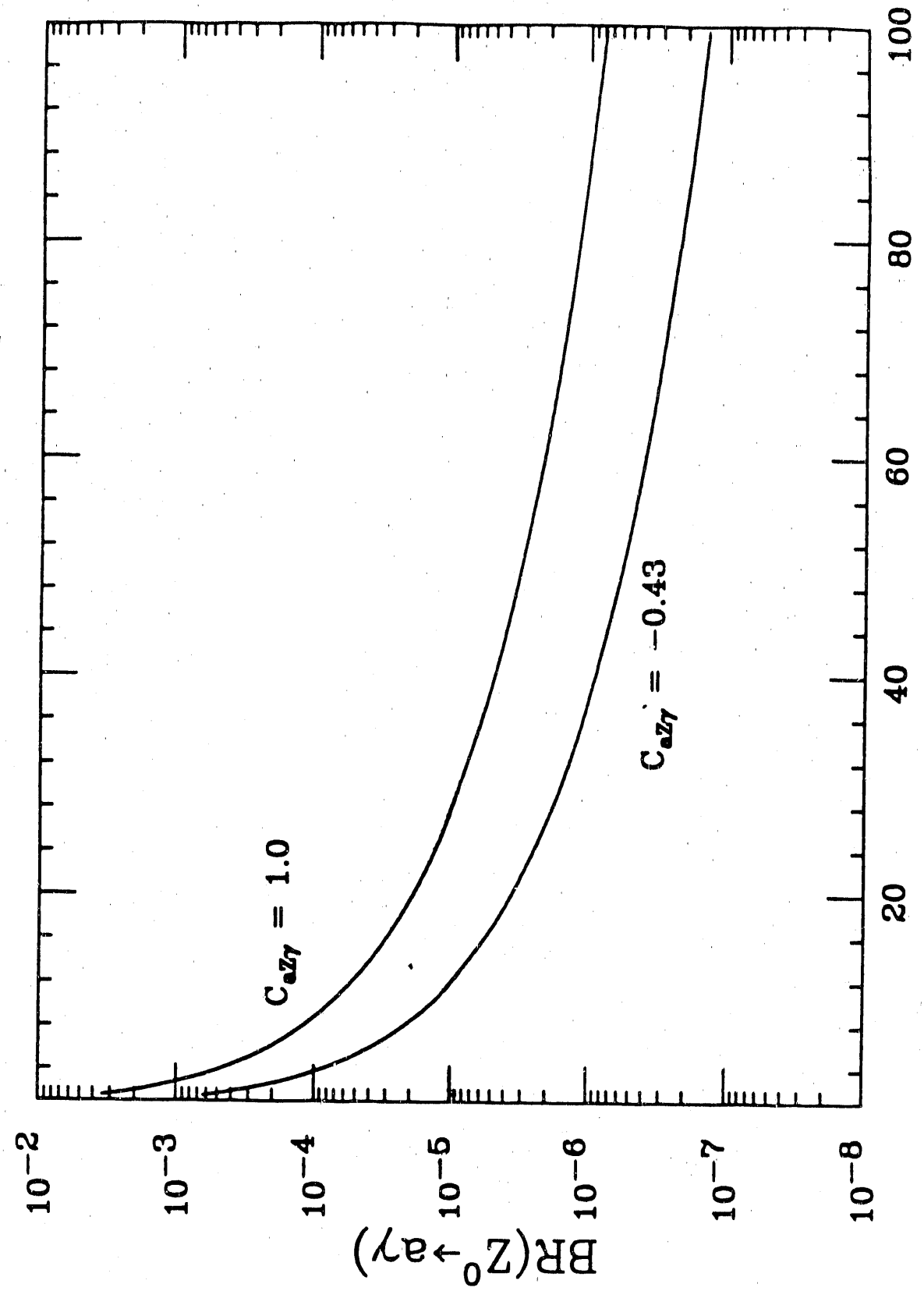

Figure V.4 Branching ratio for $Z^0 \rightarrow a\gamma$ versus scale F_a

approach 1 $\times$ $10^{31}cm^2$–s and that the integrated luminosity will be about 50 pb^{-1} or larger. In subsequent runs, significantly larger integrated luminosities can be expected, as LEP realizes its design luminosity of 2 $\times$ $10^{31}cm^2$–s. A further significant increase in luminosity will also be realized within the next few years if the proposal, currently under consideration, for increasing the number of bunches is implemented.

In the 1989-1990 runs emphasis was given to scanning in energy across the Z^0 pole in order to accurately measure the Z^0 mass, the total width of the Z^0, and the partial decay widths into hadrons and leptons. In the next run greater emphasis will probably be given to running on the pole in order to maximize the statistics needed for Higgs searches, heavy flavor physics, measurements of forward-backward asymmetries, etc. It is also likely that the majority of the LEP experiments will request some running at 4-5 GeV above the pole in order to optimize the counting of single photons. It also has to be kept in mind that LEP will eventually begin raising the energy to make the transition from LEP1 to LEP2. Assuming a successful 1991 run, this transition may commence in earnest sometime during the 1992 run.

With respect to single-photon physics, plans to emphasize $\sqrt{s}=M_Z$ in the next run will clearly benefit the study of Z decays to $\gamma(X)$. Assuming that L3 is able to achieve a stable single-photon trigger which is efficient above 1 GeV, the data taken at the pole can be used to make a precision measurement of Γ_{inv}. Any running done at 4-5 GeV above the pole will clearly benefit measurement of the invisible width since that is the most favorable energy for carrying out such a measurement with single photons.

2. L3 Detector

As has already been mentioned in the general introduction to L3 made earlier, the experiment has been designed for the the precision measurement of photons and leptons. Using BGO crystal calorimetry, L3 has achieved an energy resolution for photons which is about 2% at 1 GeV. The superior energy resolution around

1 GeV is especially crucial to direct measurements of the invisible width made on the pole because the single-photon spectrum falls off sharply with increasing energy and the backgrounds also vary rapidly with energy in the same region. For the 1989 and 1990 runs, the BGO calorimeter covered the angular region 42 to 138 degrees, and with the installation of the BGO endcaps during the 1990 shutdown, the coverage in future runs will extend down to within 10 degrees of the beamline. An important complement to the BGO endcaps, also being installed during the 1990 shutdown, are the Forward Tracking Chambers (FTC) which will be used to flag showers in the endcaps due to electrons. Thus the entire BGO calorimeter can be used to detect single photons.

At present the L3 detector has uninstrumented holes in the endcap regions between about 4.5 and 6 degrees from the beamline. A proposal to fill these gaps with small lead-scintillating-fiber calorimeter modules is now receiving serious consideration. If approved, these modules will be installed in time for the 1991 run and will further reduce the number of background events in the energy region important to the measurement of the invisible width. (A fuller discussion of the backgrounds is given below in the section on analysis.)

During the 1990 run L3 implemented a stable single-photon trigger with a nominal threshold of about 1.2 GeV. The nominal threshold corresponding to a trigger which is efficient above 1 GeV is about 750 MeV. Based on the experience gained during the last run, this can be achieved by further reducing the Level 1 BGO trigger electronics noise. Toward this end, the Level 1 BGO trigger modules are being overhauled during the 1990 shutdown with emphasis on improving grounding and isolation between channels.

3. Analysis

Critical to the task of measuring the invisible width is an accurate determination of the single-photon trigger efficiency. This measurement must be as detailed as possible not only because the energy spectrum of the produced photons falls off rapidly but also because the relative contributions of backgrounds are sensi-

tive to the energy dependence of the efficiency. Adding to the challenge of this measurement is that in the this energy range (below 4 GeV approximately), the method of using redundant triggers (luminosity trigger from a radiative Bhabha event, muon trigger from $Z^0 \rightarrow \mu^+\mu^-\gamma$, etc.) to measure the single-photon trigger efficiency is limited statistically. The L3 analysis is pursuing the efficiency measurement along three lines.

First, despite limited statistics, the sample of $\mu^+\mu^-\gamma$ events, taken independently by the muon trigger, is being analyzed to obtain a result which can be used to roughly cross-check results of other methods. Included in this analysis is a detailed study of the trigger information for the cases where the single-photon trigger did not fire. What is learned from these cases will yield additional insight into single-photon trigger inefficiencies.

The second approach is a hybrid approach utilizing real data and simulation: Taking into account dead channels, the energy resolution of the Level 1 trigger, the sharing of the shower between BGO "superblocks" (each "superblock" contributes an analog sum over 30 crystals to the Level 1 trigger), etc., a simulated photon shower is superimposed on the analog sums from a real beam gate event. (There were about 500 beam gate triggers taken per hour in the last run.) The resulting sums are passed to a simulation of the on-line trigger logic which determines whether or not the single-photon trigger fired.

Finally, the criteria used to select single-photon candidates from the production output were made loose enough to accept events from other processes having potential utility for measuring the efficiency. One subset of events selected consists of a single electron or positron track pointing into the BGO barrel with a single tag in the luminosity monitor. These events are primarily radiative Bhabha events with also some contribution from two-photon production of e^+e^- pairs where one member of the pair does not go into the BGO. As far as the single-photon trigger is concerned, these events are identical to single-photon events. First studies have shown that number of such events is about 10 times the number of genuine single-photon events we expect to be produced, and as would

be expected, the energy and angular distribution of the electron tracks is very similar to that of the bremsstrahlung photons. Single-tag radiative Bhabha and two-photon production of dileptons can be reliably simulated, hence by comparing the generated distributions against the measured distributions and taking into account the total luminosity and effects of selection cuts, another measurement of the trigger efficiency can be obtained.

In addition to determining the trigger efficiency and minimizing the systematic errors in its determination, a second major challenge to the analysis is the estimation of backgrounds. Owing to holes in the L3 detector, namely the beampipe, which restricts angular coverage to within 1.5 degrees of the beamline, and also–for the 1989 and 1990 runs–the hole in polar angle between 4.5 degrees and 6 degrees from the beamline, a number of processes are able to mimic single-photon events. The significant ones are

$$e^+e^- \rightarrow (e^+e^-)\gamma$$

$$e^+e^- \rightarrow (e^+e^-)R,\ R \rightarrow \gamma(X)$$

$$e^+e^- \rightarrow \gamma(\gamma\gamma)$$

$$e^+e^- \rightarrow \gamma(e^+e^-l^+l^-)$$

where R is a resonance (π^0, η, etc.), l stands for e or μ, and the particles enclosed in parentheses are undetected. For an idealized detector with a hole only below 1.5 degrees and applying cuts for detection of a single photon with $45 < \theta_\gamma < 135$ degrees and $E_\gamma > 1.0$ GeV, the resulting cross sections for the above processes are estimated to be 6 pb, 1.1 pb, 0.6 pb, and 2 pb, respectively [29]. The corresponding cross section for radiative production of the Z followed by decay into neutrinos is about 34 pb at $\sqrt{s} = M_Z$, hence the backgrounds have to be carefully taken into account. Estimation of the backgrounds from the above processes for the L3 case is underway. Generators exist for all the above processes and with the exception of the generator for two-photon production of resonances, they have

been interfaced to the L3 detector simulation program.

Another background to one-photon events is showers in the BGO by cosmic muons. These events can be largely removed by requiring that the shape of the shower be consistent with a photon coming from the interaction point and making use of timing information.

Selection of single-photon event candidates has been carried out for the 1989 and 1990 data in three steps. (This selection has been carried out independently by two groups. The selection sketched here is the one carried out by the group to which the University of Alabama belongs.) In the first step, carried out at the production stage after the event has been fully reconstructed, cuts are applied to reject Z^0 decays into hadrons or charged leptons, beam gas events, and events which show unambiguous evidence of being due to cosmics. Additional cuts are applied to reject events triggered by noise in the BGO and events in which there are no "good" showers or too many (> 5) "good" showers. Care is taken in the first step to accept certain topologies from radiative Bhabha and two-photon interactions which could be useful for trigger efficiency measurement. In the second step, events are accepted only if there is a single "good" shower in the BGO with energy greater than 1 GeV and the activity in the remainder of the detector is consistent with noise. Tight cuts are also applied to the shower shape to further reject cosmics. For the 1990 run, the number of events left after the second step is roughly 200 and the selection efficiency of the first two steps is above 95%. The third step consists of scanning the events and electronically analyzing them in detail in order to identify a final sample of single-photon event candidates.

Figure V.5a shows the beam's eye view of the complete detector for a candidate single-photon event surviving the first two steps of the selection process. Except for a few noise hits in the tracking chamber, the only visible signal is a single shower in the BGO, represented by the radial pulse height projection in the BGO region. A closeup of the shower as seen looking down on the detector is shown in Figure V.5b.

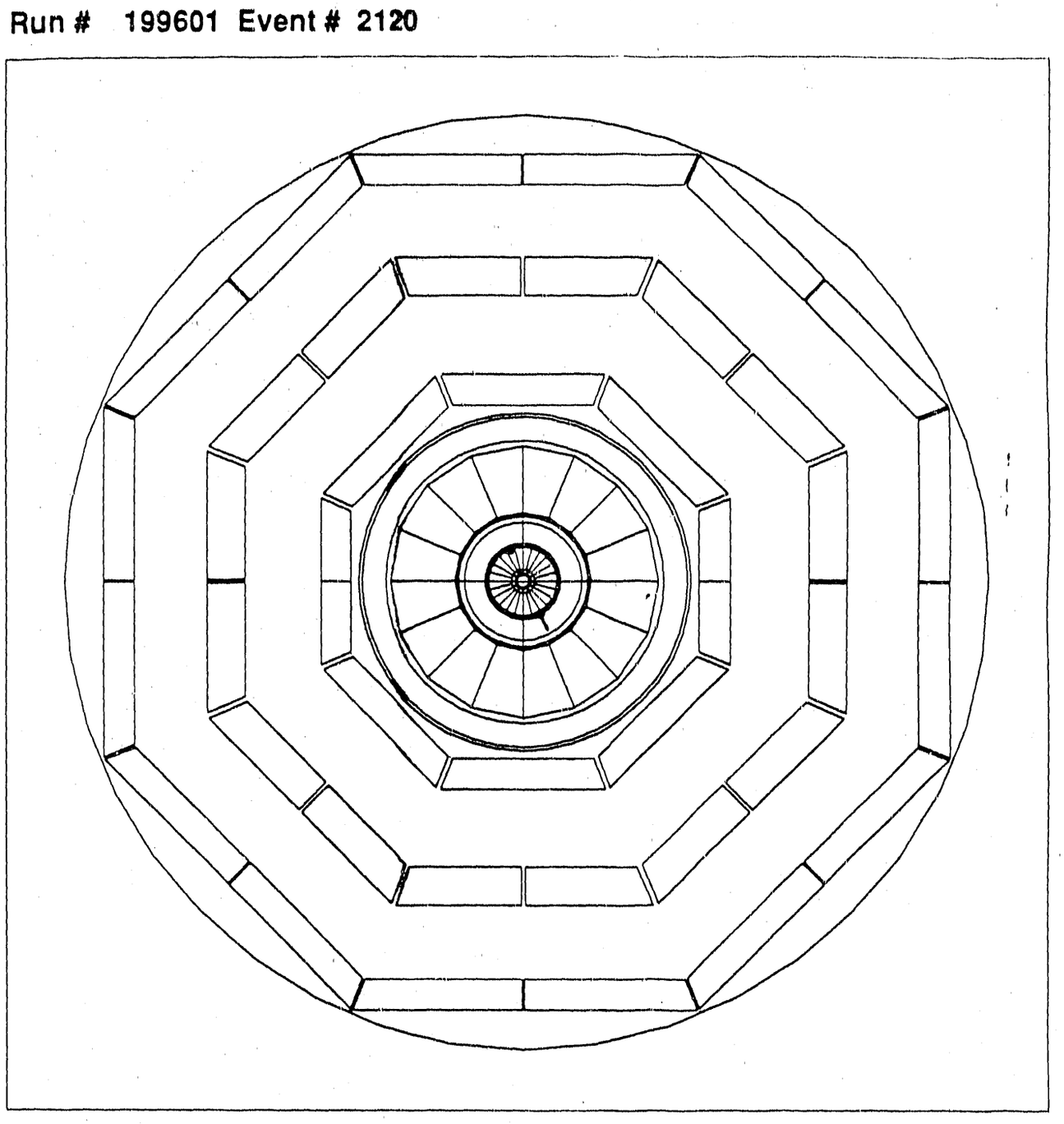

Figure V.5a Single-photon event candidate in the L3 detector. Beam's eye view.

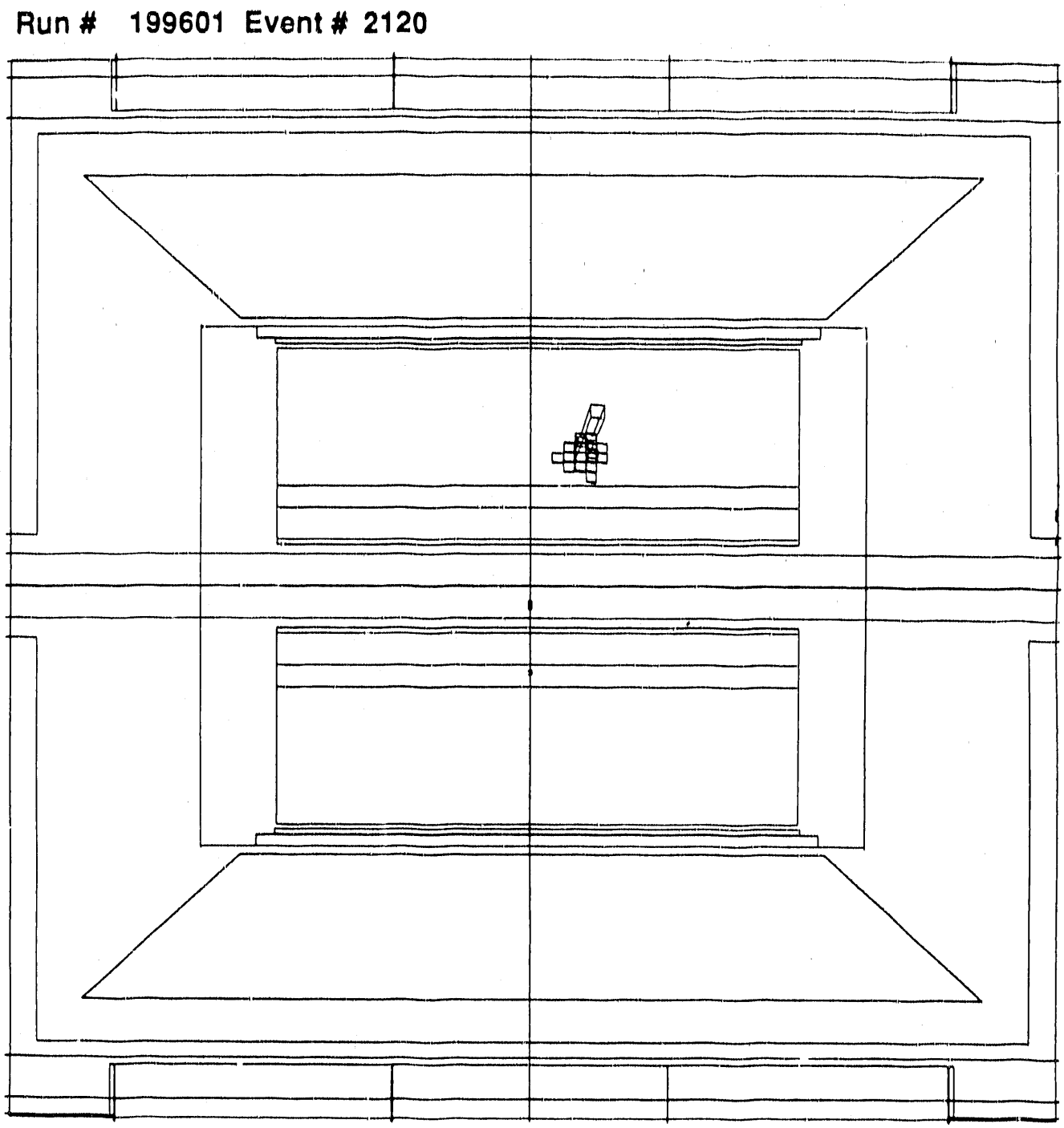

Figure V.5b Single-photon event candidate in the L3 detector. Close-up view from below.

A direct measurement of Γ_{inv} based on the 1989-90 data will probably reach a precision of 10-20%. Although a rough measurement compared to the potential of what L3 will be able to achieve at LEP over the next 1–2 years, it is nonetheless important to carry out because the experience of carrying out the full analysis is valuable to understanding what is most critical to such an analysis and what the limitations of the single-photon measurement are. A good experimental understanding of the single-photon contributions from radiative production of neutrinos and processes such as $e^+e^- \rightarrow (e^+e^-)\gamma$ is also important when looking for evidence of $Z^0 \rightarrow \gamma(X)$ decays.

The search for evidence of decays $Z^0 \rightarrow \gamma(X)$ due to New Physics benefits from the fact that the photon energy range most likely to be populated lies well above the plateau of the single-photon trigger and, in some cases, even above the thresholds of the other L3 energy triggers. With a data sample equivalent to about about 10^5 Z^0 hadronic decays and assuming no excess events are observed, upper limits on $BR(Z^0 \rightarrow \gamma(X))$ of $O(10^{-4})$ at 95% confidence level will be obtained. In terms of the search for evidence of a composite Z boson, for example, no observation of single photons with energy above 25 GeV will reduce the current upper limit on β from about 50 to approximately 2.

Finally, we briefly discuss what sensitivity can be achieved in one-photon physics over the next 2 years. We assume that in this period at least 100 pb^{-1} is obtained on or near the peak, that the single-photon trigger is implemented which is efficient above 1 GeV, and that the detector is fully instrumented above 1.5 degrees.

With 100 pb^{-1} at the pole, we estimate that the statistical precision, including the effects of background subtraction, on the direct measurement of the invisible width will be about 2%. Systematic uncertainties will arise from background subtractions, from measurement of trigger efficiency, from luminosity, etc. For indirect measurement of the hadronic width from Z decays into hadrons and leptons, the statistical precision achieved should be 1% or better. Estimates of the systematic theoretical uncertainty for "model-independent" fits vary from 2-4%.

There is additional systematic uncertainty due to luminosity but that is common to the single-photon measurement as well. For the single-photon measurement to be competitive with the indirect method then requires that the total systematic error be controlled to the 1–2 percent level. Whether or not systematics can be controlled at this level can only be known by actually carrying through the analysis. It should be noted that, for the same luminosity, roughly a factor of two or more in precision is achieved by carrying out the single-photon measurement 4 GeV above the peak because (a) the cross section is larger, (b) the relative contribution from the backgrounds is smaller, and (c) the measurement is less sensitive to to the systematics of the trigger threshold (see Figure 1).

With a luminosity of 100 pb^{-1}, the rare decay searches will be sensitive to branching ratios as small as a few times 10^{-6}. In the case of the excited neutrino with an assumed mass of 50 GeV, this translates into a sensitivity to values of Λ/f_Z up to about 5 TeV, almost two orders of magnitude larger than pre-LEP limits. Taking the composite Z scenario as another example, a value of β=0.35 would give a 5σ excess above the Standard Model for photon energies greater 20 GeV.

D. Participation by the University of Alabama group

J. Busenitz joined the L3 single-photon physics group after coming to the University of Alabama in January 1990. Having been released from teaching duties for the Spring semester, he worked at CERN from Febuary through May. In addition to becoming familiar with the technical aspects of the L3 analysis and with the L3 experiment in general, he helped define the selection criteria used to skim single-photon candidate events from the production output and played an important role in identifying a new single-photon trigger scheme which, relative to the original scheme, is much more robust against the dominant types of BGO electronics noise. This scheme was implemented by the experiment in June 1990.

After taking Summer 1990 to concentrate on completing an analysis of semileptonic charm decays using data taken by Fermilab experiment E-687, Busenitz is ac-

tively participating in the L3 single-photon analysis effort. Following a two-week visit to CERN in the first part of September, the University of Alabama has major responsibility in two projects to be carried out over the next few months. The first is to interface an existing generator for two-photon production of hadronic final states to the L3 simulation program so that the contribution from

$$e^+e^- \rightarrow (e^+e^-)R,\ R \rightarrow \gamma(X)$$

to the single-photon background can be estimated for the L3. The participation of the University of Alabama in this project is made feasible by the direct connections within the group to the LEP3Net and Internet networks. The second project consists of carrying out, in cooperation with a University of Rome group, the final selection of the single-photon event candidates from the 1990 data to be used for measurement of Γ_{inv} and search for γ(X) decays from New Physics. (A parallel selection is being carried out independently by groups from the University of Lyon and the University of Florence.) The selection process requires the transfer of data sets to Alabama for scanning and electronic analysis. These data sets, which have an average size of several megabytes, are transferred easily and quickly over LEP3Net.

The addition of Dr. Razis to the Alabama group is significant for the single-photon effort in the future, as well as for the ongoing research interests in inclusive photon interactions and Z^0 decays into hadrons, dimuons, and possible 4^{th} generation down quarks. His presence at CERN and close communication with the Alabama group will facilitate the efforts made to contribute to the L3 effort from Alabama. J. Busenitz plans to spend Summer 1991 and the Fall 1991 semester at CERN. This time is critical to the L3 single-photon physics assuming a successful 1991 run.

References

1. B. Adeva et al., "Construction of the L3 Experiment," Nucl. Instr. and Meth. **A289**, 35 (1990).

2. S.C.C. Ting, "Recent Results from L3 Collaboration," invited talk, 25th International Conference on High Energy Physics, Singapore, July 30, 1990.

3. B. Adeva et al., "A Determination of the Properties of the Neutral Intermediate Vector Boson Z^0," Phys. Lett **B231**, 509 (1989).

4. B. Adeva et al., "Measurement of Z^0 Decays to Hadrons, and a Precise Determination of the Number of Neutrino Species," Phys. Lett **B237**, 136 (1990).

5. B. Adeva et al., "A Determination of Electroweak Parameters from $Z^0 \rightarrow \mu^+\mu^-(\gamma)$," to be published in Phys. Lett. B.

6. B. Adeva et al., "A Precision Measurement of the Number of Neutrino Species," to be published in Phys. Lett. B.

7. B. Adeva et al., "Measurement of g_A and g_V, the Neutral Current Coupling Constants to Leptons," Phys. Lett. **B236**, 109 (1989).

8. B. Adeva et al., "A Measurement of the Z^0 Leptonic Partial Widths and the Vector and Axial Vector Coupling Constants," Phys. Lett. **B238**, 122 (1990).

9. B. Adeva et al., "A Determination of Elecroweak Parameters from Z^0 Decays into Charged Leptons," to be published in Phys. Lett. B.

10. B. Adeva et al., "Measurement of $Z^0 \rightarrow b\bar{b}$ Decay Properties," Phys. Lett. **B241**, 416 (1990).

11. B. Adeva et al., "Determination of α_s from Jet Multiplicities Measured on the Z^0 Resonance," to be published in Phys. Lett. B.

12. B. Adeva et al., "A Test of QCD based on 4-Jet Events from Z^0 Decays," to be published in Phys. Lett. B.

13. B. Adeva et al., "Mass Limits for Excited Electrons and Muons from Z^0 Decay," to be published in Phys. Lett. B.

14. B. Adeva et al., "Search for Excited Taus from Z^0 Decay," to be published in Phys. Lett. B.

15. B. Adeva et al., "Mass Limits for Scalar Muons, Scalar Electrons, and Winos from e^+e^- Collisions near $\sqrt{s}$ = 91 GeV," Phys. Lett. **B233**, 530 (1989).

16. B. Adeva et al., "Search for the Neutral Higgs Boson in Z^0 Decay," to be published in Phys. Lett. B.

17. B. Adeva et al., "Search of the Neutral Higgs Boson of the Minimal Supersymmetric Standard Model," to be published in Phys. Lett. B.

18. L★ Collaboration, "Expression of Interest to the Superconducting Super Collider Laboratory," submitted to the SSC Laboratory (May 1990).

19. A. Bay et al., "Higgs → Four Leptons at the SSC," Proceedings of the Summer Study on High Energy Physics in the 1990s, June 27 - July 15, 1988, Snowmass, CO, p. 109 (World Scentific, publ.).

20. E. Eichten, I. Hinchliffe, K. Lane, and C. Quigg, "Supercollider Physics," Rev. Mod. Phys. **56**, 579 (1984).

21. F.E. Paige and E.M. Wang, "Pileup at the SSC," Proceedings of the Workshop on Calorimetry for the Supercollider, March 13-17, 1989, Tuscaloosa, AL, p. 113 (World Scientific publ.).

22. D. Groom, "Radiation Levels in SSC Detectors," Proceedings of the Summer Study on High Energy Physics in the 1990s, June 27 - July 15, 1988, Snowmass, CO, p. 109 (World Scentific, publ.).

23. D. DiBitonto et al., "Integrated Ceramic Electrode for Warm Liquid Calorimetry," Proceedings of the Workshop on Calorimetry for the Supercollider, March 13-17, 1989, Tuscaloosa, AL, p. 313 (World Scientific publ.).

24. D. DiBitonto et al., "Fast, Radiation-Hard Charge Preamplifiers for Warm Liquid Calorimetry," Proceedings of the Workshop on Calorimetry for the Supercollider, March 13-17, 1989, Tuscaloosa, AL, p. 583 (World Scientific publ.).

25. D. DiBitonto et al., "Advanced Forward Calorimetry for the SSC and TeVatron Colliders," Nucl. Instr. and Meth. **A279**, 100 (1989).

26. E. Ma and J. Okada, "How Many Neutrinos?" Phys. Rev. Lett **41**, 287, 1759 (1978).

27. G. Barbiellini et al., "Radiative Z^0 Production: A Method for Neutrino Counting in e^+e^- Collisions," Phys. Lett. **B106**, 414 (1981).

28. R. Barbieri et al., "Supersymmetry Searches," CERN-EP/89-08, Vol. 2, 121 (1989).

29. L. Trentadue et al., "Neutrino Counting," CERN-EP/89-08, Vol. 1, 129 (1989).

30. M. Chen et al., "Signals from Non-Strongly Interacting Supersymmetric Particles at LEP Energies," Phys. Rep. **C159**, 203 (1988).

31. R. Miquel et al., "Higher order corrections to the process $e^+e^- \rightarrow \nu\bar{\nu}\gamma$," Universitat Autònoma de Barcelona preprint UAB-LFAE 90-94 (1990).

32. F. Boudjema et al., "Looking for the LEP at LEP. The Excited Neutrino Scenario," Phys. Lett. **B240**, 485 (1990).

33. D.W. Dusedeau and J. Wudka, "Rare Z Decays in Composite Models," Phys. Lett. **B180**, 290 (1986).

34. A. Barroso et al., "Neutrino Counting and a Composite Z-Boson," Phys. Lett. **B196**, 547 (1987).

35. J.E. Kim and U.W. Lee, "Z^0 Decay to Photon and Variant Axion," Phys. Lett. **B233**, 496 (1989).

36. L. Krauss and F. Wilzcek, "A Short-Lived Axion Variant," Phys. Lett **B173**, 189 (1986).

37. R.D. Peccei et al, "A Viable Axion Model," Phys. Lett. **B172**, 435 (1986).

Table I

General Properties of the L3 spectrometer

Tracking		
	Outer: (muons)	Drift Chambers
		Resolution: $\delta(p)/p = 2\%$ at 50 GeV/c
	Inner:	Time Expansion Chamber
		Resolution: $\delta(R\Phi) = 50\ \mu m$
		$\Delta z = 2$ cm (charge division)
Calorimetry		
	E.M.:	Bismuth germanium oxide (BGO), 26.9 X_0
		Resolution: $\sigma(E)/E = (1.3/\sqrt{E} + 0.5)\%$
	Hadron:	Uranium, 5.3 - 6.5 λ (sampling proportional chambers)
		Resolution: $\sigma(E)/E = (60/\sqrt{E} + 4)\%$

Table II

Properties of the Z^0 from L3

M_Z	91.164 ± 0.013 ± 0.030 (LEP) GeV/c^2
N_ν	3.01 ± 0.11
Γ_{had}	1.748 ± 0.035 GeV
Γ_{inv}	0.502 ± 0.018 GeV
$\Gamma_{\mu\mu}$	83.3 ± 1.3 ± 0.9 MeV
Γ_{ee}	84.3 ± 1.3 ± 1.0 MeV
$\Gamma_{\tau\tau}$	84.2 ± 1.4 ± 1.4 MeV
Γ_Z	2.492 ± 0.025 GeV

Coupling	$\mu^+\mu^-$	e^+e^-
g_A	$-0.497^{+0.005}_{-0.005}$	-0.501 ± 0.0006
g_V	$-0.062^{+0.020}_{-0.015}$	-0.057 ± 0.0027

Table III

Lower Mass Limits for Stable Neutrinos from L3
95% C.L. Lower Mass Limits (GeV/c^2)

From:	Dirac	Majorana	Scalar
Γ_Z	43.2	35.4	27.8
Γ_{inv}	44.2	37.6	31.9
μ	45.5	45.2	-
e	45.5	45.1	-
τ	45.5	44.8	-

Table IV

L3 Mass Limits from Γ_{had}, Γ_{inv}, and $\Gamma_{\mu\mu}$
95% C.L. Lower Mass Limits (GeV/c^2)

Particle	Lower Limit (GeV/c^2)	From
4^{th} Family Quark	46.0	Γ_{had}
4^{th} Dirac ν	44.2	Γ_{inv}
Majorana ν	37.6	Γ_{inv}
Sneutrino $\tilde{\nu}$	31.9	Γ_{inv}
Up-Squark $\tilde{u}$	39.4	Γ_{inv}
Down-Squark $\tilde{d}$	33.2	Γ_{inv}
Stable Lepton	27	$\Gamma_{\mu\mu}$

Table V

L3 Direct New Particle Searches
95% C.L. Lower Mass Limits (GeV/c^2)

New Charged Leptons	
M_{e^*} (Excited e)	45.0; 88 ($\lambda = 1$)
M_{μ^*} (Excited μ)	45.3; 85 ($\lambda = 1$)
M_{τ^*} (Excited τ)	45.5; 89 ($\lambda = 1$)
$M_{L^\pm}$ (Sequential)	43.9
$M_{L^\pm}$ (Stable)	38
Fourth Family Neutrinos	
$M_{\nu 4}(\nu 4 \rightarrow \mu W^*)$	45.5
$M_{\nu 4}(\nu 4 \rightarrow eW^*)$	45.5
$M_{\nu 4}(\nu 4 \rightarrow \tau W^*)$	45.5
Supersymmetry	
$M_{\tilde{\mu}}$ (Smuon)	44
$M_{\tilde{W}}$ (Wino)	44
$M_{\tilde{e}}$ (Selectron)	41
$M_{\tilde{q}}$ (Squark)	45.4
Higgs	
M_{H^0} (MSM Higgs)	36.2
M_{h^0} (MSSM Higgs)	41
M_{A^0} (MSSM Higgs)	26 ($\tan\beta \approx 1$)
M_{A^0} (MSSM Higgs)	40 ($\tan\beta \gg 1$)
$M_{H^\pm}$ ($\rightarrow \tau$'s)	42.5
$M_{H^\pm}$ ($\rightarrow$ jets)	37.5
New Family: FCNC	
$M_{b'}$ (b' $\rightarrow$ b + gluon)	45.5
$M_{b'}$ (b' $\rightarrow$ b + γ)	45.5

Table VI

Partial List of Members of the L★ Executive Committee

Nations	Members
United States	U. Becker, J. Branson, W. Bugg, D. DiBitonto, A. Engler, O. Fackler, R. Heinz, H. Newman, A. Pevsner, P. Piroue, F. Plasil, J. Reidy, J. Rohlf, G. Sanders, & others
Soviet Union	Y. Galaktionov, A. Lebedev, I. Savin, N. Tchernoplekov, and others
Europe	B. Borgia, M. Bourquin, K. Lübelsmeyer, G. Rancoita, C. Sciacca, and others
Asia	S.X. Fang, Z.W. Yin, A Gurtu, Y.Y. Lee, D. Son, and others

Table VII

L★ Forward Hadron Calorimeter Specifications

Angular Coverage:	$0.03^0 \leq \Theta, (\pi - \Theta) \leq 6.7^0$ $5.95 \geq \lvert\eta\rvert \geq 2.84$
Distance from Interaction Point:	10.45 m
Outer Diameter:	3172 mm
Weight (one side):	140 tons
Absorber:	Fe/Pb, Fe (14 λ)
Detecting Medium:	Silicon (outer); Tetramethylsilane, dual 2.5 mm gap
Segmentation:	
Transverse	40×40 mm^2 (Silicon); 20×20 mm^2 ($\Delta\eta$ min/max = 0.06/0.4, $\Delta\phi = \Delta\eta$)
Longitudinal	
Front Electromagnetic:	25 layers, 15.6 X_0, 1.6 λ
Hadronic Center:	42 layers, 5.8 λ
Tail Catcher:	22 layers, 6.2 λ
Total samples:	89 layers
Energy Resolution	σ/E = 50%/$\sqrt{E}$ + 4%

Table VIII

Estimated Annual Budget for the Van de Graaff Institute

University of Alabama Contributions

Positions	Number	Salary
Director (9 mo)	1	$100,000
Faculty (9 mo)	13	$650,000
Staff Physicists (9 mo)	7	$210,000
Technical Staff (12 mo)	4	$110,000
Secretary (12 mo)	1	$15,000
Fringe Benefits		$289,800
		$1,374,800
One-time Capital Expenditures		
Building (25,000 sq. ft.)		$7,500,000
Machine Shop		$2,500,000
Electronics Shop		$2,000,000
Computer Facility		$800,000
		$12,800,000

DOE Contributions

Positions	Number	Salary
Director, Faculty (3 mo)	14	$250,000
Staff Physicists (3 mo)	7	$70,000
Postdocs (12 mo)	10	$250,000
Graduate Students (12 mo)	20	$240,000
Visitors (12 mo)	3	$180,000
Technical Staff (12 mo)	4	$120,000
Secretary (12 mo)	2	$30,000
Fringe Benefits		$189,800
Operating Costs		$250,000
Capital Equipment		$600,000
Overhead (@ 47%)		$742,506
		$2,922,306

Appendicies

I. Letter of Invitation to Alabama from the L3 Collaboration.

II. Expression of Interest to the Superconducting Super Collider Laboratory by the L★ Collaboration, May, 1990.

ORGANISATION EUROPÉENNE POUR LA RECHERCHE NUCLÉAIRE
EUROPEAN ORGANIZATION FOR NUCLEAR RESEARCH

Laboratoire Européen pour la Physique des Particules
European Laboratory for Particle Physics

GENÈVE, SUISSE
GENEVA, SWITZERLAND

Adresse postale/Mailing address:

CERN
CH-1211 GENÈVE 23

Télex / Telex: 419000 CER CH
Télégramme / Telegram: CERNLAB GENEVE
Téléphone / Telephone:
Direct: National (022)
International +4122
Central / Exchange: " 836111
Fax direct: "
Fax général/general: " 836655

Votre référence / Your reference

Notre référence / Our reference

Professor Daryl DiBitonto

University of Alabama
College of Arts and Sciences
Department of Physics
206 Gallalee
Tuscaloosa, Alabama 35487-0324
U.S.A.

Geneva, July 18, 1989

Dear Professor DiBitonto,

I am pleased to report to you that in the last L3 General Meeting of July 7, 1989, we discussed your participation and voted to welcome the University of Alabama physics group to join us.

Furthermore, I wish to report to you that on July 14, at 4:20 p.m., the beam has circulated for the first time around LEP exactly according to the plans made years ago.

Your participation at CERN will ensure that the University of Alabama physics department can make a significant contribution to the e^+e^- physics at LEP.

With best regards,

Samuel C.C. Ting

Expression of Interest

to the Superconducting Super Collider Laboratory by the L* Collaboration

May 1990

The University of Alabama, Tuscaloosa, Alabama, USA
L.Baksay, J.Busenitz, D.DiBitonto, L.Jenkins, X.Liu, T.Pennington, M.Timko, D.Whitcomb, L.Wurtz, Y.Yu

The University of South Alabama, Mobile, Alabama, USA
K.Clark, M.Jenkins

The University of Alabama, Huntsville, Alabama, USA
J.Gregory, Y.Takahashi

The University of Alabama, Birmingham, Alabama, USA
J.Harrisson, E.Robinson

Auburn University, Auburn, Alabama, USA
J.Williams

The University of Central Arkansas, Conway, Arkansas, USA
H.Woolverton

Lawrence Livermore National Laboratory, Livermore, California, USA
E.Ables, R.Bionta, H.Britt, A.Chargin, G.Deis, O.Edwards, O.Fackler, J.Heim, C.Henning, D .Makowicki, J.Miller, M.Mugge, W.Neff, H.S.Park, S.Shen, S.Sierskowski, K.Skulina, D.Slack, W.Stoffel, R.Vital

California Institute of Technology, Pasadena, California, USA
M.Chen, G.Gratta, D.Kirkby, R.Mount, H.Newman, R.Y.Zhu

University of California, San Diego, California, USA
J.B.Branson, M.Hebirt, E.Sheer, X.Sopczek

Purdue University, Lafayette, Indiana, USA
A.Bujak, L.Gutay, T.McMahon

Indiana University, Indiana, USA
M.Gebhard, R.Heinz, A.Komives, L.Miller, S.Mufson, J.Musser, G.Spiczak, G.Turner

Johns Hopkins University, Baltimore, Maryland, USA
H.Akbari, J.Bao, C-Y.Chien, G.Feldman, T.Fulton, C.W.Kim, J.F.Krizmanic, J.D.Orndorff, A.Pevsner, W.J.Spangler, C.Spartiotis, A.Szalay

Boston University, Boston, Massachusetts, USA
S.Ahlen, G.Bauer, J.Beatty, J.Brooks, T.Coan, M.Felcini, J.Hu, D.Levin, W.Lu, A.Marin, S.Otwinowski, D.Osborne, J.Rohlf, D.Warner, B.Zhou

Harvard University, Cambridge, Massachusetts, USA
K.Kamar, P.McBride, J.Schuette, K.Strauch

Massachusetts Institute of Technology, Cambridge, Massachusetts, USA
A.L. Anderson, U.Becker, P.Berges J.D.Burger, Y.H.Chang, M.Chen, I.Clare, R.Clare, T.S.Dai, F.J.Eppling, M.Fukushima, M.P.J.Gaudreau, K.Giboni, C.Grinnell, E.S.Hafen, P.Haridas, G.Herten, A.Kerman, T.Kramer, T.Lainus, D.Luckey, P.Marsten, D.B.Montgomery, I.A.Pless, J.M.Qian, M.Sarakinos, S.M.Shotkin, M.Steuer, J.D.Sullivan, K.Sumorok, J.Tang, Samuel C.C. Ting, S.M.Ting, T.J.Wenaus, M.White, S.X.Wu, B.Wysiouch, C.H.Ye

The Charles Stark Draper Laboratory, Cambridge, Massachusetts, USA
R.Araujo, J.Barry, E.Berk, M.Fury, M.Hansberry, T.Hines, G.Holden, F.Nimblett, J.Paradiso, W.Toth, L.Wilk

University of Mississippi, University, Mississippi, USA
L.Cremaldi, J.Furgeson, S.Harper, J.Reidy, J.Zhang

Mississippi State University, Starkville, Mississippi, USA
L.Croft, B.Piercey

Jackson State University, Jackson, Mississippi, USA
F.Lott

Princeton University, Princeton, New Jersey, USA
J.Bakken, M.Convery, P.Denes, D.Lea, P. Piroué, K.Read, H.Sicotte, D.Stickland, R.Sumner, D.Wright

Los Alamos National Laboratory, New Mexico, USA
D.Alde, R.Barber, J.Boissevain, D.Campbell, T.Carey, G.Dransfield, R.Farber, P.Ferguson, V.Gavron, D.Giovanelli, R.Gupta, J.Hanlon, S.Hecker, C.Hosford, J.Kapustinsky, W.W.Kinnison, E.Knapp, B.Korlegaard, R.Kruger, K.Lackner, A.Lapedes, D.M.Lee, M.Leitch, R.Lemons, R.Little, T.Lopez, M.Mattis, M.Merrigan, D.Metzger, W.O.Miller, G.Mills, F.A.Morse, J.M.Moss, E.Mottola, M.Merrigan, S.Newfield, R.Perkins, R.Prael, W.Rodriguez, S.P.Rosen, C.Sadler, V.D.Sandberg, G.H.Sanders, D.Sharp, R.Slansky, B.Smith, W.Sommer, G.Stephenson, D.Strottman, J.Sunier, T.Thompson, G.T.West, D.H.White, J.Williams, W.Wilson, K.Woloshun, H.J.Ziock

University of New Mexico, New Mexico, USA
J.Ellison, D.Finley, S.Humphries, B.H.Wildenthal

Columbia University, New York, USA
E.Aprile, Reshmi Mukherjee

LeCroy Corporation, Chestnut Ridge, New York, USA
M.Gorrics, B.Manor, R.Sumner,

Carnegie Mellon University, Pittsburgh, Pennsylvania, USA
I.Brock, A.Engler, T.Fergusson, R.W.Kraemer, F.Linde, C.Rippich, J.Smith, R.Sutton, H.Vogel

Brown University, Providence Rhode Island, USA
M.Aryal, A.De Silva, D.Rossi, M.Widgoff

University of Tennessee, Knoxville, Tennessee, USA
S.C.Berridge, W.M.Bugg, G.T.Condo, Y.C.Du, T.Handler, H.J.Hargis, E.L.Hart, R.Kroeger, A.Weidemann

Memphis State University, Memphis, Tennessee, USA
D.Franceschetti, S.Jahan, W.Jones

Vanderbilt University, Nashville, Tennessee, USA
S.Csorna

Oak Ridge National Laboratory, Oak Ridge, Tennessee, USA
D.J.Alexander, B.R.Appleton, P.E.Arakawa, J.B.Ball, F.E.Barnes, J.M.Barnes, M.L.Bauer, R.L.Beatty, J.A.Blank, L.A.Boatner, C.Bottcher, H.R.Brashear, C.R.Brinkman, T.J.Burns, J.G.Carter, B.C.Chakoumakos, M.M.Chiles, J.E.Choate, L.G.Christophoruou, F.E.Close, H.O.Cohn, R.I.Crutcher, F.C.Davis, R.E.DePew, J.H.DeVan, T.H.Dunigan, M.S.Emery, H.Faides, T.A.Gabriel, T.A.Herrick, M.J.Hollis, D.T.Ingersoll, J.O.Johnson, J.W.Johnson, H.E.Knee, D.P.Kuban, R.J.Lauf, D.L.McCorkle, S.A.McElhaney, D.L.McElroy, J.W.Moore, F.Plasil, R.T.Primm III, M.J.Rennich, R.T.Santoro, T.E.Shannon, B.H.Singletary, V.K.Sikka, T.P.Sjoreen, M.S.Smith, J.W.Stapleton, M.R.Strayer, R.W.Swindeman, A.W.Trivelpiece, J.R.Tubb, J.F.Wendelken, D.M.Williams, A.C.Williamson, A.Wintenberg, C.Y.Wong, K.G.Young

University of Utah, Salt Lake City, Utah, USA
H.Bergeson, M.Salamon

Howard University, Washington DC, USA
R.M.Catchings, J.Lindesay

University of Geneva, Geneva, Switzerland
M.Bourquin

Swiss Federal Institute of Technology, Zürich, Switzerland
H.Anderhub, J.Behrens, A.Biland, M.Dhina, G.Faber, M.Fabre, R.Fabbretti, K.Freudenreich, M.Haensli, H.Hofer, I.Horvath, E.Isiksal, M.Jongmanns, H.Jung, J.Lettry, P.Lecomte, P.LeCoultre, L.Li, X.Lue, M.MacDermott, M.Maolinbay, D.McNally, M.Pohl, G.Rahal-Callot, P.Razis, H.Rykaczewski, D.Ren, B.Spiess, H.Suter, J.Ulbricht, G.Viertel, H.VonGunten, S.Waldmeier, J.Weber, L.Zehnder

LAPP, Annecy, France
J.J.Blaising, R.Morand, M.Schneegans, M.Vivargent

Physics Institute, RWTH Aachen, Germany
P.Blömeke, M.Buchholz, E.Coulig, H.Haan, K.Hilgers, W.Karpinski, H- H.Kleinmanns, O.Kornadt, W.Krenz, T.Lehmann, K.L.Lübelsmeyer, T.Meinholz, D.Pandoulas, J.Y.Pei, M.Rhöhner, R.Siedling, D.Schmitz, K.Schmiemann, M.Schömag, A.Schultz von Dratzig, J.Schwenke, G.Schwering, M.Toporowsky, W.Wallraff, W.Xiao, Y.Zeng, J.Zhou

Central Research Institute for Physics of the Hungarian Academy of Sciences, Budapest, Hungary
Gy.Bencze, E.Dénes, E.Nagy, J.Tóth, L.Urbán

INFN and University of Florence, Florence, Italy
A.Baldini, M.Bocciolini, M.Bruzzi, A.Cartacci, G Ciancaglini, C.Civinini, R.D'Alessandro, E.Gallo, M.Meschini, M.Pieri, P Spillantini, J.F Wang

INFN and University of Milan, Milan, Italy
E. Borchi, A. Penzo, P. G. Rancoita, L. Riccati, A. Villari, L. Vismara

INFN, Naples and University of Naples, Naples, Italy
A. Aloisio, M. G. Alviggi, E. Brambilla, G. Chiefari, R. De Asmundis, E. Drago, V.Innocente, S Lanzano, L. Merola, M. Napolitano, S. Patricelli, C. Sciacca

University of Rome, Rome, Italy
L. Barone, B. Borgia, F. Cesaroni, F. De Notaristefani, E. Longo, G. Mirabelli, S. Morganti

Tata Institute of Fundamental Research, Bombay, India
T.Aziz, S.Banerjee, S.R.Chendvankar, S.N.Ganguli, S.K.Gupta, A.Gurtu, A.K.Jain, P.K.Malhotra, K.Mazumdar, R.Raghavan, K.Shankar, K.Sudhakar, S.C.Tonwar

Joint Institute for Nuclear Research (JINR), Dubna, USSR
E.Belyakova, A.Cheplakov, A.Cheremukhin, S.Dolya, V.Dunin, Yu.Ershov, N.Fadeev, A.Feshchenko, V.Genchev, I.Geshkov, I.Golutvin, N.Gorbunov, I.Gramenitsky, I.Ivanchenko, M.Kadykov, V.Kalagin, A.Karev, V.Karzhavin, M.Kazarinov, S.Khabarov, V.Khabarov, Yu.Kiryushin, D.Kiss, V.Krivokhizhin, V.Kukhtin, R.Lednicky, I.Lukyanov, V.Lysyakov, A.Makhankov, V.Minashkin, N.Nogaytsev, V.Odintsov, V.Perelygin, D.Peshekhonov, V.Peshekhonov, D.Pose, V.Prikhodko, A.Prokesh, A.Rashevsky, I.Savin, S.Sergeev, M.Shafranov, I.Shpak, A.Skrypnik, G.Smirnov, D.Smolin, V.Sviridov, G.Sultanov, A.Vishnevsky, Yu.Yatsunenko, O.Zaimidoroga, M.Zamyatin, A.Zarubin, V.Zhiltsov, E.Zubarev

Leningrad Nuclear Physics Institute, Leningrad, USSR
V.Andreev, A.Denisov, Y.Dokshitser, V.Ivochkin, V.Janovsky, A.Kaschuk, V.Khoze, A.Krivshich, P.Levtchenko, V.Mayorov, A.Nadtochy, V.Razmyslovich, Y.Ryabov, V.Samsonov, A.Sarantsev, V.Schegelsky, A.Schetkovsky, Y.Sokornov, A.Shevel, N.Smirnov, E.Spiridenkov, V.Suvorov, A.Tsaregorodtsev, G.Velichko, S.Volkov, A.Vorobyov, An.Vorobyov, Y.Zaitte

Institute of Theoretical and Experimental Physics, ITEP, Moscow, USSR
A.Arefiev, A.Artamonov, A.Babaev, V.Bocharov, S.Burov, N.Bystrov, M.Chumakov, A.Dolgolenko, V.Dolgoshein, V.Efremenko, V.Ephstein, A.Epifanzev, A.Fedotov, Yu.Galaktionov, V.Gemanov, P.Gorbunov, A.Gordeev, B.Gordeev, P.Gorichev, Yu.Gorodkov, E.Grigoriev, R.Gurin, Yu.Karnyshkov, V.Khovansky, Yu.Kirilko, A.Klimentov, Yu.Kornetyuk, V.Koutsenko, A.Kovalenko, S.Kruchinin, M.Kubantsev, A.Kuchenkov, A.Kunin, V.Lebedenko, I.Makhlueva, A.Malinin, S.Mamontov, A.Maslennikov, V.Morgunov, A.Nikitin, N.Pankin, V.Plotnikov, V.Plyaskin, V.Pojidaev, A.Rozjkov, M.Ryabinin, I.Satsky, A.Savin, M.Savitsky, A.Selivanov, V.Semetchkin, V.Shamanov, P.Shatalov, S.Shevchenko, V.Shevchenko, K.Shmakov, V.Shoutko, E.Shumilov, A.Smirnov, M.Sokolov, S.Solomentzev, E.Tarkovsky, V.Tchudakov, I.Vetlitsky, V.A.Vinogradov, V.B.Vinogradov, I.Vorobiev, V.Zaitsev, O.Zeldovich, S.Zeldovich, N.Zvetkov

Kurchatov Atomic Institute, Moscow, USSR
S.Barabanov, A.Barkov, S.Belyaev, L.Bragin, N.Chernoplekov, T.Chunyaeva, T.Davlatyan, G.Dorofejev, V.Drozdov, V.Evdokimov, S.Frolov, E.Golubev, E.Grishin, A.Imenitov, V.Karpov, I.Karpushov, E.Klimenko, A.Kochergin, V.Kruglov, V.Kulyasov, Yu.Kurojedov, A.Kuznetsov, S.Lelekhov, O.Lusitenko, Yu.Lusitenko, A.Malofejev, V.Manko, V.Martemyanov, N.Matovetsky, V.Martynenko, A.Matvejev, V.Mokhnotuk, E.Mukhina, A.Myagkov, S. Novikov, A.Ogioblin, I.Ovchinnikov, S.Osetrov, V.Patrikejev, V.Podshibyakin, K.Polulyakh, V.Portugalsky, G.Razorenov, N.Rodina, V.Ryabov, A.Safronov, M.Sedov, V.Selivanov, B.Seregin, E.Shatnyi, M.Solodnev, S.Svertnev, S.Terentjev, E.Velikhov, P.Volkov, A.Voropaev, P.Vorotnikov, T.Vostrikova, M.Vyirodov, E.Vylsotsky, I.Zotov

Institute for High Energy Physics, Serpukhov, USSR
N.Fedyakin, A.Kozelov, R.Krasnokutsky, A.Lebedev, S.Medved, Yu.Mikhailov, E.Razuvaev, R.Shuvalov, E.Slobodyuk, A.Vasiliev

Institute of Nuclear Physics, Novosibirsk, USSR
L.Barkov, A.Skrinsky, E.Solodov

Yerevan Physics Institute, Yerevan, Armenia, USSR
N.Akopov, A.Amatuni, Ts.Amatuni, R.Astabatyan, R.Avakyan, A.Avetesyan, G.Bayatyan, P.Galumyan, A.Hagomeryan, R.Kavoiov, S.Kazaryan, S.Matinyan, G.Mkrtchyan, A.Oganesyan, J.Petrosyan, V.Pogosov, K.Shikhtyarov, A.Sirunyan, S.Taroyan, N.Ter-Isaakyan, G.Vanapetyan

Institute of Physics, Academy of Sciences of the Georgian SSR, Tbilisi
D.Chkareuli, G.Dvali, N.Manjalidze, G.Leptukh, P.Petman, T.Lomtadze, A.Djavrishvili, E.Zadadze, I.Iashvili, K.Ahabadze, M.Svanidze, E.Ioramashvili, N.Roinishvili, L.Gabuniya, L.Hizanishvili

Institute of Physics, Academy of Sciences of the Estonian SSR, Tartu
I.Ots, H.Ulbo

Institute of High Energy Physics, Beijing, China
C.Chen, G.M.Chen, H.S.Chen, S.X.Fang, S.G.Gao, W.X.Gu, Y.F.Gu, Y.N.Guo, Y.Han, J.He, J.T.He, B.N.Jin, H.T.Li, J.Li, P.Q.Li, W.G.Li, X.G.Li, S.Z.Lin, Q.Liu, Y.S.Lu, Z.P.Mao, L.J.Pan, Z.M.Qian, G.Rong, Y.Y.Shuo, X.W.Tang, K.L.Tung, J.H.Wang, L.Z.Wang, R.J.Wu, Y.G.Wu, Z.D.Wu, R.S.Xu, Y.D.Xu, S.T.Xue, C.G.Yang, C.Y.Yang, K.S.Yang, Q.Y.Yang, Z.Q.Yu, B.Y.Zhang, C.C.Zhang, D.H.Zhang, L.S.Zhang, S.Q.Zhang, D.X.Zhao, M.Zhao, Z.P.Zheng, G.Y.Zhu, Q.M.Zhu, Y.C.Zhu, Y.S.Zhu, H.L.Zhuang.

Chinese University of Science and Technology, Hefei, China
H.F.Chen, Z.F.Gong, C.H.Gu, C.Li, Z.Y.Lin, W.G.Ma, C.R.Wang, X.L.Wang, Z.M.Wang, Z.Z.Xu, B.Z.Yang, J.B.Ye, X.Q.Yu, Z.P.Zhang

Shanghai Institute of Ceramics, Shanghai, China
X.L.Fang, P.X.Gu, J.K.Guo, C.F.He, G.Q.Hu, S.K.Hua, H.J.Li, J.L.Li, P.J.Li, Q.Z.Li, Z.L.Pan, D.Z.Shen, G.S.Shen, E.W.Shi, W.T.Su, X.X.Wang, Z.Y.Wei, Y.Y.Xie, L.Xu, Z.L.Xue, D.S.Yan, Z.W.Yin, X.L.Yuan, Y.F.Zhang, G.M.Zhao, Y.L.Zhao, W.Z.Zhong, R.M.Zhou

High Energy Physics Group, Taiwan, China
C.Chang, A.Chen, W.Y.Chen, H.Y.Cheng, Y.C.Gau, S.S.Gau, Y.Y.Lee, W.T.Lin, W.T.Ni, Y.D.Tsai, S.C.Yeh

Waseda University, Science and Engineering Research Laboratory, Tokyo, Japan
T.Doke, J.Kikuchi

Saitama College of Health, Saitama, Japan
K.Matsuda

Kyungpook National University, Taegu, Korea
D.Son, S.K.Cho, J.K.Ko

Gyeongsang National University, Jinju, Korea
J.S.Song, I-G.Park, S-K.Choi, K.S.Chung

Chungnam National University, Daejeon, Korea
H.Y.Lee

Cheonnam National University, Kwangju, Korea
J..Kim

Kangreung National College, Kangreung, Korea
D.W.Kim, G.S.Kang

Korea University, Seoul, Korea
J.S.Kang

Seoul National University, Seoul, Korea
J.Kim

Sangji College, Wonju, Korea
Y.Y.Keum

Taegu University, Taegu, Korea
D.S.Kim

Spokesperson:
Samuel.C.C.Ting
MIT-LNS, Bldg.44
51 Vassar Street
Cambridge, MA02139, USA

A. DESIGN CONSIDERATIONS

A.1. Introduction

The design of the calorimeter derives from the general L* concept: The detector is a precision instrument searching for new physics through, first of all, leptonic and photon channels and second quark channels (the measurement of jets). The calorimeter, therefore, should be multifunctional. It provides identification of electrons, muons, and jets and serves as a tracking device by helping to solve pattern recognition problems. It provides capability to separate electrons from hadrons by measuring shower shape and to separate muons from other particles by total absorption of hadronic components. It must detect muon bremsstrahlung and provide corresponding corrections to muon energy measurements.

The electromagnetic calorimeter is a separate dedicated device for precise measurement of electron and photon energy and is discussed in Chapter VI.

A.2. Energy Measurement by Total Absorption.

Devices used to measure energy by total absorption are of two types: (1) homogeneous, where the same medium is used both for particle detection and absorption, and (2) sampling, where different sampling and absorbing media are used. The electromagnetic energy resolution of a homogeneous calorimeter made of scintillating crystals like BGO or BaF_2 is markedly superior to sampling calorimeters. However, the response to electrons exceeds that of hadrons by a factor of ~1.5. This means that when a homogeneous calorimeter is introduced to ensure very high-precision electromagnetic energy measurements, the pre cision of jet energy measurements is somewhat compromised since in this case compensation is not likely to be achieved.

In the L*, lepton measurements have the highest priority. The L* calorimeter design goals for energy measurement are as follows: The best possible resolution for photons and electrons (better than 1% at 10 GeV); accurate measurement of muon energy losses, in particular due to bremsstrahlung (10% at 10 GeV); and adequate (better than 10% at 100 GeV) jet energy resolution. As can be seen from Fig. V.1, the very high precision of the L* muon detector can only be achieved if one corrects for muon energy losses in the hadron calorimeter.

A.3. Segmentation, Depth, and Time Resolution

Segmentation is determined by hadronic shower size and bremsstrahlung photon measurement and matches that of the electromagnetic calorimeter. Studies (Ref. V.1) show that an average transverse segmentation of $\Delta\eta \times \Delta\varphi = 0.04 \times 0.04$ is adequate. Longitudinal segmentation is needed both for electron identification and for general tracking and pattern recognition (Ref. V.2). We choose the hadron calorimeter to have an average of nine readout segments (about 1 λ each), which ensures the satisfactory measurement of muon bremsstrahlung energy losses.

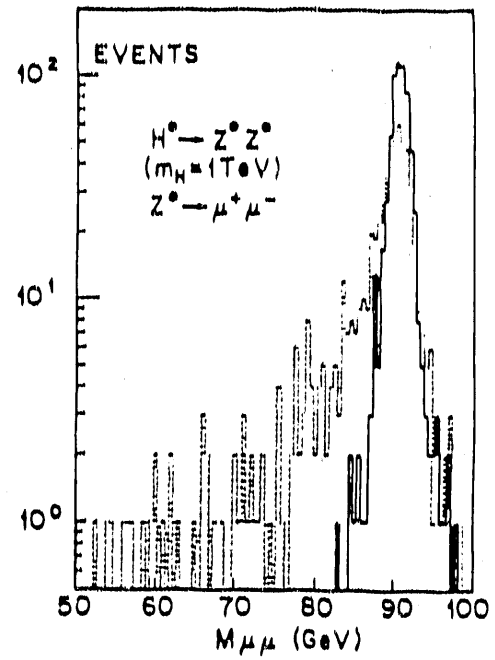

Fig.V.1. An example of deterioration of $Z \rightarrow 2\mu$ mass resolution due to fluctuations of muon energy loss in the 12 λ hadron calorimeter (dotted line). Correction for these fluctuations will be made by calorimeter sampling measurements (solid line). The reaction is $pp \rightarrow H^0$ (1 TeV) $\rightarrow ZZ \rightarrow 4\mu$

According to parameterization (Ref. V.3), 98% of the energy of a 1 TeV hadron is contained in 12 λ. It is necessary to keep the flux resulting from hadronic debris of high energy showers at a level that is acceptable for muon detection. For an incident hadron of several hundred GeV, 12 λ are sufficient to keep this flux below 1%. Good time resolution (~20 ns) is needed to avoid pile-up (Ref. V.4).

A.4. Radiation Hardness Requirements

Studies (Ref. V.5) show that in the rapidity interval from 0 to 3.5 units a Pb-Fe-Si calorimeter with an inner radius of about 1 m should be able to withstand a total yearly neutron fluence of 10^{12} to 10^{13} neutrons/cm^2. The annual dose due to charged particles is less important.

B. SILICON CALORIMETRY

B.1. Introduction

Silicon calorimetry has become an important feature of modern collider and fixed-target experiments with applications ranging from a fraction of one square meter to a few tens of square meters. To date, silicon has been used primarily in electromagnetic calorimeters and to a lesser extent in position-sensitive devices for improved position resolution in hadron calorimeters. The well-understood properties of silicon as an ionization sampling device, its outstanding potential for meeting many of the most stringent requirements of SSC calorimeters, and its

simplicity of structural support have led us to choose it for the L* detector.

B.2. Advantages of Silicon

The intrinsic advantages of silicon are well known. With respect to almost every technical requirement of SSC calorimetry, silicon as a sampling medium is the equal of, or surpasses, other techniques of sampling calorimetry, with the exception of radiation hardness where liquefied rare gases are a clear choice. We briefly summarize here the properties of silicon and compare them to other techniques.

1. With respect to speed, silicon is rivaled only by scintillator systems. It is by far the fastest of the ionization techniques, with transit (or charge collection) time of 15–30 ns, thereby minimizing pile-up problems.

2. Absolute gain for the sampling medium. Like other ionization charge measuring devices, silicon has a fixed gain determined essentially by the thickness of the silicon wafer.

3. Silicon inherently responds linearly to deposited energy. Electron-hole recombination is not important even for fission fragments. There is no loss of energy sensitivity (saturation) for highly ionizing particles similar to that found in both cryogenic and warm liquids.

4. Transverse segmentation. Here silicon is far superior to other techniques and limited only by practical considerations of channel numbers.

5. Longitudinal segmentation. Silicon is similar to other sampling techniques and channel number considerations dominate the choice of segmentation. Sampling thickness of $\sim 1X_0$ and readout segmentation of $\sim 1\lambda$ are feasible.

6. Silicon operates well at room temperature, although operation at −20° C improves radiation damage noise characteristics by 2 orders of magnitude.

7. Silicon is insensitive to magnetic fields and is very likely the technology that gives the most compact device possible.

8. Monitoring of electronics gain by radioactive sources is possible by simple deposition of low-level activity on silicon surfaces.

9. Because the silicon detector arrays can be easily attached to absorber plates, structural frames in calorimeter construction are almost unaffected by the sampling medium and are determined primarily by mechanical and electrical considerations.

10. Another major advantage of silicon is that only low bias voltages are required ($\approx$ 100 V), which markedly simplifies design considerations.

B.3. Disadvantages of Silicon

1. The major disadvantage of silicon is the high cost of finished detectors. This situation is improving with time, but designing silicon calorimeters as compactly as possible remains crucial for economic reasons.

2. Electronics for silicon devices are often perceived to be more expensive than those for other techniques. Where this is true, it results from the attempt to design electronics that make full use of the superior characteristics of silicon – particularly segmentation, speed, and pile-up. For a given set of performance characteristics (such as those achievable with liquid argon or warm liquids), the costs per channel for electronics are essentially identical.

3. While computer simulations indicate that it is possible to achieve $e/\pi = 1$, no full silicon calorimeter has yet been built to demonstrate this property experimentally, although the SICAPO collaboration has such tests under way, and the result on e/π ratio will be available (Ref. V.16).

4. The question of radiation damage to silicon detectors requires attention. A clear understanding of the mechanisms of silicon damage and of their effects on detector performance, and an understanding of the SSC environment and the electronic parameters pertinent to SSC operation, are required to judge the potential effects of radiation on silicon performance.

In summary, if one compares silicon calorimetry with other techniques, the general conclusion is that for the same level of performance – that is, speed, segmentation, etc. – the cost of silicon sampling calorimetry exceeds those of other options only through the cost of the silicon. This may be offset to some extent by simpler mechanical construction requirements for the calorimeter. However, the capability of silicon to improve the calorimeter performance makes silicon an attractive solution.

B.4. Radiation Damage

A brief summary of radiation damage to silicon and its effect on calorimeter performance and parameters is given here.

1. In the hadron calorimeter, the neutron and slow hadron ionization will produce (due to displacement threshold) heavier radiation damage to silicon (approximately by a factor of 100) than the electromagnetic ionization.

2. At radiation levels of 10^{12} to 10^{14} n/cm^2 the major effect of radiation damage is the increase of leakage current in the detector. A secondary but important factor is bulk displacement damage, which results in decreased sensitivity and higher resistivity with increase of bias voltage required to maintain full charge collection. Measurements by Lindstrom (Ref. V.6) have indicated that at room temperature leakage current in 500 μm silicon will increase by 30 μA/cm^2 after a neutron exposure of 10^{13} n/cm^2. We assume here that the radiation dose is derived from the SSC environment and is acquired relatively slowly such that self-annealing takes place.

We wish to emphasize two major points, which have a major impact on the utility of silicon in high radiation environments.

1. Radiation damage in silicon is bulk damage due to trap formation and the leakage current increase due to these traps is highly temperature dependent. The simple expedient of operating the detector at −20°C, which can be done with conventional refrigeration techniques, will reduce leakage current by factors of 30 to 80 and thus give a corresponding increase in radiation hardness.

2. The traditional use of silicon in high-resolution nuclear spectroscopy has of necessity required amplifiers with long shaping times and very low noise. For these amplifiers, noise increase due to radiation-damage-induced leakage current at long shaping times is not tolerable. However, with the 10-ns shaping time used in our design of the SSC preamplifiers, the effect of noise due to leakage currents is nearly negligible. Figure V.2 shows noise vs shaping time for three different values of leakage current.

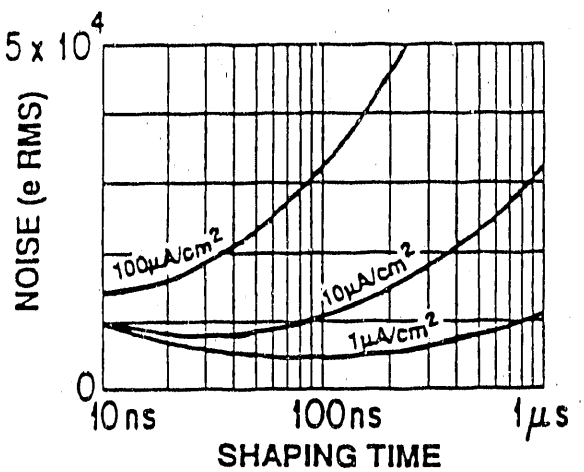

Fig. V.2. Amplifier noise vs shaping time and leakage current for bipolar preamplifier. Calculations are made for 500 μ thick silicon detector with the an area of 3 × 3 cm^2; input capacitance 180 pF at full depletion.

These two factors combine to provide 2 to 3 orders of magnitude improvement in silicon radiation hardness. Extensive calculations indicate neutron doses at the inner face of the L* hadron calorimeter of less than 3×10^{13} neutrons/cm^2/year at $\eta = 3$ for a total 10 years dosage of 3×10^{14} n/cm^2. Without cooling this would lead to a leakage current of 900 μA/cm^2. With cooling to −20°C this is reduced to acceptable level of 12–30 μA/cm^2 with a negligible effect on noise. After 10 years, charge trapping from bulk damage could become important and perhaps require annealing or replacement of a significant fraction of the silicon.

B.5. Silicon Procurement

We are requesting the silicon wafers from the Soviet Union. The Joint Institute of Nuclear Research (Dubna) is coordinating this effort. The total surface required is approximately 5×10^7 cm^2. The Titanium-Magnesium Factory at Zaporozhye, Ukraine, Soviet Union, can produce float-zone refined silicon crystals of either n- or p-type of high resistivity. The monocrystals are currently produced in ingots of up to 76 mm in diameter and more than 10 cm long. Assuming that the wafer thickness will be 0.5 mm and that the waste will be 0.4 mm, the total weight of material required is about 24 tons, including a 20% contingency. The factory can produce 5–6 tons of material annually. Thus, the required amount of silicon can be produced in about 4–5 years.

The required number of wafers is about 3×10^6. This production will be performed primarily in Minsk, Byelorussia, Soviet Union, by the Research Center associated with the University of Byelorussia and by subcontractors. Slicing, lapping, polishing, thermal oxidation, multiple photolithography, ion implantation, and metal (aluminum) deposition will be performed by them. The fabrication of wafers is estimated to be about 7×10^5 wafers per year and can proceed in parallel with silicon ingot production.

The total cost of the raw silicon ingots is estimated to be about 60M Roubles plus 5M$ needed for the purchase of quality control equipment. The estimate of wafer production cost includes cost of labor as well as the purchase of needed equipment. Provided that an R&D program is implemented, the production is estimated to cost 40M Roubles plus 5M$.

C. CENTRAL AND ENDCAP REGIONS

C.1. General Layout and Energy Resolution

Figures V.3 and V.4(a) show the layout for the L* calorimeter hadronic sections. In the hadron calorimeter the passive medium consists of lead and stainless steel layered plates with relative thickness chosen to reduce the electron response of the calorimeter so that e/h remains close to 1 in the hadronic part. There is experimental evidence that particular combinations of calo-

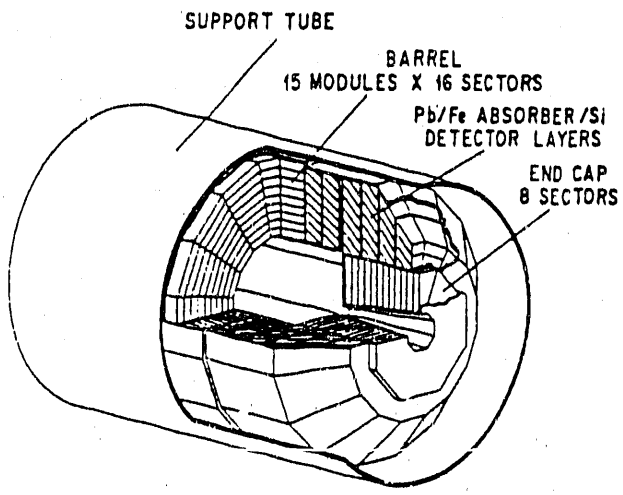

Fig. V.3. The central hadron calorimeter.

rimeter materials will be compensating (Ref. V.7). It is suggested that a Pb-Fe-Si calorimeter should consist of a mixture such that Pb/(Pb + Fe) = 0.25, in length, to ensure that e/h = 1. However, the BaF_2 electromagnetic calorimeter, which is 1.67 λ deep, prevents the entire calorimeter from exhibiting full compensation.

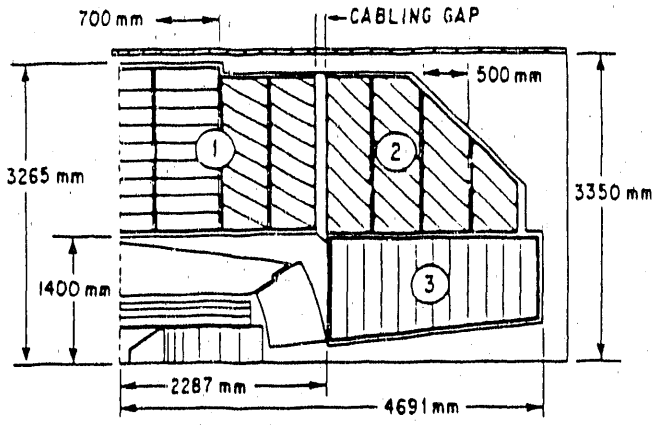

(a) BaF_2 e-m calorimeter in front.

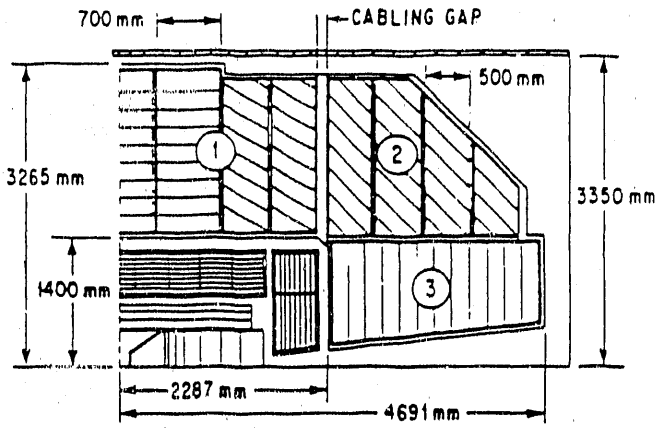

(b) Fine sampling Fe-Pb-Si e-m calorimeter in front.

Fig. V.4. Side quarter section of the central hadron calorimeter. Three out of five assemblies are shown. Absorber layers are shown schematically at correct orientation.

From our experience with the L3 calorimeter, we expect the hadron energy resolution of the BaF_2 (e-m) and Pb-Fe-Si (hadron) calorimeter system to be

$$\frac{\sigma_h}{E} = \frac{50\%}{\sqrt{E}} + 4\%$$

with an e-m resolution of

$$\frac{\sigma_{em}}{E} = \frac{1.3\%}{\sqrt{E}} + 0.5\%$$

Based on indication that liquid xenon is likely to be compensating, the overall resolution involving a liquid xenon e-m section is estimated to be

$$\frac{\sigma_h}{E} = \frac{50\%}{\sqrt{E}} + 2\%$$

As described in Chapter II, the mechanical support for the e-m calorimeter is designed in a way that it can be replaced by a fine sampling (0.5 X_0) silicon section. In this case, the entire calorimeter should be compensating, and the hadron resolution will be

$$\frac{\sigma_h}{E} = \frac{50\%}{\sqrt{E}} + 1\%$$

where the 1% constant term is defined by systematic uncertainties of calibration, uniformity, stability, etc. The e-m resolution for this fine sampling section will be

$$\frac{\sigma_{em}}{E} = \frac{15\%}{\sqrt{E}} + 1\%$$

(1% due to systematics mentioned above). Figure V.4(b) shows the layout of the fine sampling Pb-Fe-Si section. The amount of silicon required for such upgrade is 30% of that required for the central calorimeter.

C.2. Segmentation

A unique requirement of the hadron calorimeter is that it should preserve the excellent muon momentum precision of the L* detector by accurate measurement of the bremsstrahlung photons, as well as other muon energy losses. To achieve the precision of (30–40%)/$\sqrt{E}$ in these measurements, it is necessary to maintain 2 to 4 X_0 sampling throughout the entire calorimeter with good longitudinal segmentation.

The basic silicon pad size will be approximately 3 × 3 cm^2 (or 2.5 × 2.5 cm^2) and 500 μm in thickness. Smaller pad sizes, while feasible, are not required because the L* hadron calorimeter segmentation does not need to exceed the segmentation of the BaF_2 electromagnetic section that precedes it (see Chapter VI). We assume that hadronic towers are constructed by summing preamplifier outputs from the basic 3 × 3 cm^2 units, although some variation in pad size is required to provide full coverage. Towers at small angles at the inner calorimeter edge are 3 × 3 cm^2, whereas at the 90° outer edge they are as large as 12 × 12 cm^2. With the average readout longitudinal segmentation of 9, it leads to a channel count of 180 000 in the hadronic calorimeter.

C.3. Structure

As can be seen in Fig. V.4, the calorimeter begins at r = 1.40 m and extends to r = 3.33 m. In the endcap region, it begins at 2.287 m and extends to 4.691 m from the crossing point along the beam direction. Angular coverage of above 5.7° is provided. The central hadron calorimeter consists of five assemblies weighing between 100 and 800 tons, which in turn are composed of a total of 17 structural modules (15 barrel rings and 2 endcaps). Each of these modules is subdivided into 16 (8 for endcaps) azimuthal segments with 51 to 60 layers of absorber and silicon sense layers. Figure V.5 shows one segment. The mechanical structure of these modules, as well as the assembly procedure, is similar to that of the L3 hadron calorimeter. Structural framing for the modules

consists of two 20-mm-thick stainless-steel membranes between which the absorber plates are installed. Separator/support walls between azimuthal segments run at small angles to radial directions to minimize the dead-region effect. The maximum stress applied to the side membranes is calculated to be ~30 kg/cm^2.

The description of the absorber structure follows (see Fig. V.5). A 2 X_0 layer is 27 mm thick. Absorber plates consist of 18 mm of austenitic stainless steel and 6 mm of lead. A sense layer is bonded to the stainless steel. Thus each layer is a mechanically self-contained unit, and fabrication and testing of the individual layers are performed prior to installation in the modules. The 3-mm space between absorbing plates contains silicon, preamplifiers, and signal-routing circuitry. A 4 X_0 layer consists of a double thickness of lead and stainless steel with a total thickness of 51 mm. The entire calorimeter is 11.7 λ deep at 90 ° and 13.9 λ at 5.7°. At 90° the hadron calorimeter will consist of 35 layers of 2 X_0 thickness and 16 layers of 4 X_0 thickness. Thermal control of the central hadron calorimeter is achieved by liquid cooling of the entire assembly to −20°C. A stainless steel shroud on the exposed surfaces of the calorimeter provides for the containment of both the cooled surfaces and the coolant. Compensation for thermal expansion is provided by the use of similar materials and compliant attachments where necessary. The entire calorimeter weighs 1710 tons.

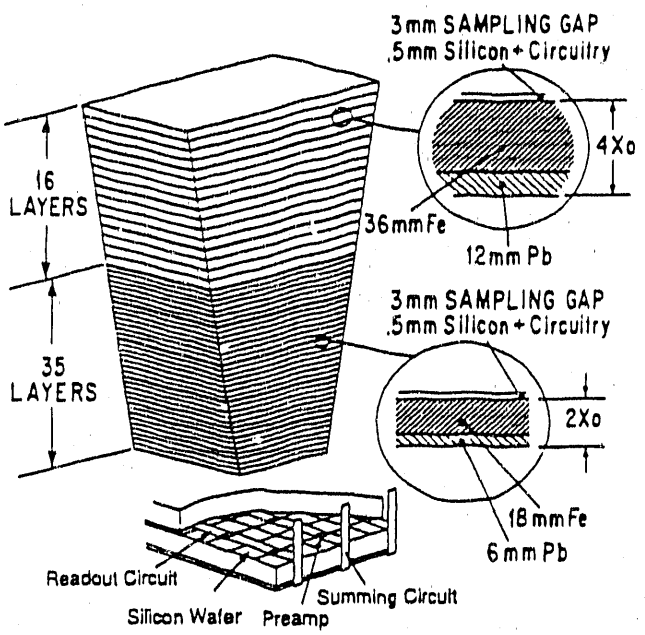

Fig. V.5. The calorimeter absorber/detector structure at 90°.

C.4. Electronics

Preamplifiers

The estimated total area of silicon required is 5200 m^2, yielding approximately 5.8 million 3 ×3 cm^2 detector elements. For 500 μm silicon, the pad capacitance will be approximately 180 pF. Larger pad sizes will be formed by area summing these pads within layers. This minimizes signal-to-noise problems and simplifies the system by requiring only a single ASIC (application-specific integrated circuits) preamplifier design throughout. Oak Ridge National Laboratory (ORNL) has produced a preamplifier under generic R&D funding for a detector capacitance of 100 pF with a power dissipation of 2.5 mW, a rise time of 14 ns, and a signal-to-noise ratio of 6:1 for minimum ionizing particles. Studies indicate that at 180 pF we can achieve a signal-to-noise ratio of 4:1. Power dissipation could be traded off for more speed and lower noise. A conservative power dissipation of 10 mW per channel is assumed. The ASIC preamplifier will be configured into quad preamplifiers and located at the intersection of silicon pads. Packaged amplifiers of this type can be produced at a cost of about 1.15$ per amplifier in the quantities needed for this detector. The ability to design and produce these elements cheaply is an essential factor in favor of using silicon.

Signal Routing

Within a given layer, signals from individual preamplifiers are combined to form larger-area layer signals which are then routed to the edge of the absorber where summing amplifiers are located (Fig. V.5). Signals from several consecutive layers are then summed together to create a signal for an individual channel. On average, nine longitudinal segments will be formed in this way. All the signals are routed to the outer rim of the calorimeter assembly, where pipelined storage and digitization, as well as trigger-formation circuitry, are housed.

Trigger Considerations

It is clear that the major responsibility for the first level trigger will fall to the electromagnetic and hadron calorimeters. Not only will tower sums provide an energy trigger, but it also seems feasible to provide a very fast isolated muon trigger. With an average longitudinal segmentation of 9, tracking of isolated muons is certainly achievable and highly desirable. Such segmentation also improves the bremsstrahlung corrections to the muon momentum measurements.

Additional summing amplifiers for triggering purposes will be located at the perimeter of the calorimeter, where appropriate segment sums can be made and sent to the trigger electronics. Coarser sums may be developed for the first level trigger and finer sums for the second level trigger. While the first level trigger is likely to be formed from thresholds on analog sums, the data may be digitized, with flash ADCs, for computing second level triggers. The digitization rate depends heavily on the design of the triggering system. After the first level trigger, the rate should be below 1 MHz. After the second level

trigger, the rate should be below 10 kHz. In any case, pipelined storage will be required to hold the data for trigger decision. While data acquisition will involve all 180 000 channels, the first and second level trigger will work with coarser resolution by summing together many segments.

Power Dissipation and Cooling

Heat generated within the calorimeter is primarily from two sources: electronics and detector leakage current. The predominant source of heat for the electronics comes from the preamplifiers. A conservative estimate yields electronic power consumption within the calorimeter of 67 kW, where 10 kW is due to detector dark current. Dark current will be increased with radiation exposure. We estimate conservatively a maximum leakage current of 40 μA/cm^2, which would be localized to high-radiation areas. If we assume that the entire calorimeter exhibits such a high current, the maximum power generated is 200 kW at the end of 10 years, leading to a power load for the entire calorimeter of less than 300 kW.

C.5. Specifications and Performance

Central Calorimeter	
Inner radius	140.0 cm
Outer radius	333.0 cm
Support tube inner radius	335.0 cm
Ring modules	15
Azimuthal segmentation	16
Total weight	1506 tons
Endcaps	
Length along beam	230.0 cm
Azimuthal segmentation	8
Inner radius (minimum)	20.3 cm
Outer radius	138 cm
Total weight (two modules)	204 tons
Absorber	
Material	Pb + Fe (stainless steel)
$2X_0$ layer	0.6 cm Pb + 1.8 cm Fe
Layers ($2X_0$)	35
$4X_0$ layer	1.2 cm Pb + 3.6 cm Fe
Layers ($4X_0$)	16 at 90°; 25 at 5.7°
Depth	
With BaF_2 and support tube	11.7λ at 90°
With BaF_2	13.9λ at 5.7°
Segmentation	
$\Delta\eta \times \Delta\varphi$(average)	0.04 × 0.04
Longitudinal (average)	9
Number of channels	180,000
Readout and Performance	
High resistivity silicon pads:	
Area	3 × 3 cm^2
Thickness	500 μm
Charge collection time	15 ns
MIP signal (mean)	54K electrons
Preamplifier noise (at 180 pF, 10 ns shaping)	13K electrons
Estimated e-m energy res.:	
In $2X_0$ section	28%/$\sqrt{E}$
In $4X_0$ section	40%/$\sqrt{E}$
Estimated hadron energy res.:	
With BaF_2 e-m calorimeter	50%/$\sqrt{E}$ + 4%
With fine sampling silicon e-m calorimeter	50%/$\sqrt{E}$ + 1%

D. FORWARD CALORIMETER SYSTEMS

D.1. Forward Acceptance

The forward electromagnetic and hadronic calorimetry covers the angular region from 6.7° down to 0.3°.

D.2. Choice of Detector Technology

The anticipated high-radiation environment in the forward region places severe constraints on the choice of detector technology. At a distance of 10.5 m from the primary interaction vertex, the expected neutron fluency at 2.0° (η = 4.05) is 10^{14} neutrons/cm^2/year while the corresponding gamma ray dose at the same position is 10 Mrad (Ref. V.5). This ensures operation at radiation levels comparable or less than in the endcap region of the central calorimeter. Below this angle the radiation levels rise rapidly and can seriously reduce the operational lifetime of most detector technologies.

For the angular region above 2.0° BaF_2 is chosen as the electromagnetic detector medium, followed by a silicon sampling medium for the hadron calorimeter. Below 2.0°, we choose a radiation-hardened warm liquid technology both for electromagnetic and hadronic sections, which will go down as far as 0.3° (η = 5.95). To maintain better hermeticity over the transition region at 2°, we prefer warm liquid technology over cryogenic technology (LAr). As a backup solution for the choice of BaF_2 and silicon, we propose a warm liquid technology for the total forward calorimeter.

D.3. Forward Calorimeter Layout

The forward calorimeter shown in Fig. II.1 covers the angular region from 6.7° (η = 2.84) down to 0.3° (η = 5.95) and extends between 10.5 and 13.5 m from the interaction point. The detector is divided into an inner and outer sections, separated at 2.0° (Fig. V.6).

The outer forward calorimeter consists of a (25 X_0, 1.7λ) BaF_2 electromagnetic section followed by a 12 λ lead-stainless steel hadron calorimeter with silicon sampling media. This outer silicon hadron calorimeter consists of a 6 λ front section composed of 42 layers of 6 mm of lead, 18 mm of stainless steel, a 3-mm detector gap,

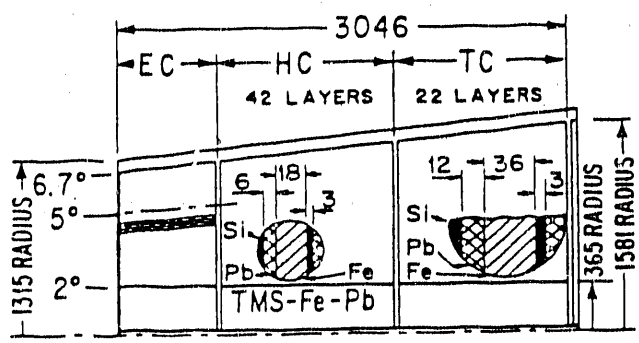

Fig. V.6. Longitudinal view of the forward calorimeter system showing the outer electromagnetic calorimeter (BaF2), the outer hadron calorimeter (SI), and the inner calorimeter (TMS) below $\phi = 2°$.

and a 6-λ tail section composed of 22 layers of double-thickness absorber layers and 3-mm gap. The expected energy resolution for this device is $\sigma/E = 0.013/\sqrt{(E)} + 0.5\%$ (electromagnetic) and $50\%/\sqrt{(E)} + 4\%$ (hadronic).

The inner forward calorimeter (plug) consists of a sampling TMS calorimeter. The two back sections have the similar absorber structure as the outer forward calorimeter with dual 3-mm-gap TMS ionization chambers. The front section consists of 25 absorber layers (each of 1 X_0) providing a total of 1.8 λ.

The total weight of the forward calorimeter unit is 260 tons for the hadronic section and 20 tons for the electromagnetic section.

D.4. Outer Forward Electromagnetic Calorimeter

For the outer forward electromagnetic calorimeter we choose a similar transverse segmentation of $\Delta\eta = \Delta\phi \leq 0.04$ (on average) as in the central calorimeter. There are in total 7610 crystals in the outer forward electromagnetic calorimeter.

The photosensors and the DAQ chain for the BaF_2 crystals are identical to those used in the central electromagnetic calorimeter (see Chapter VI). Also, the mechanical support of the crystals will use similar techniques as in the central region.

The BaF_2 calorimeter forms a ring mounted against the forward hadron calorimeter sitting in the support tube (see Figs. II.1 and V.6).

D.5. Outer Forward Hadron Calorimeter

The outer forward hadron calorimeter uses for ease of fabrication and hermeticity two sizes of silicon detectors providing a segmentation of $\Delta\eta = \Delta\phi \leq 0.04$ (on average) thus matching the BaF_2 crystals. The detector sizes (see Fig. V.7) for two regions are 20×20 mm^2 ($2° \leq \theta < 4°$) and 40×40 mm^2 ($4° \leq \theta \leq 6.7°$).

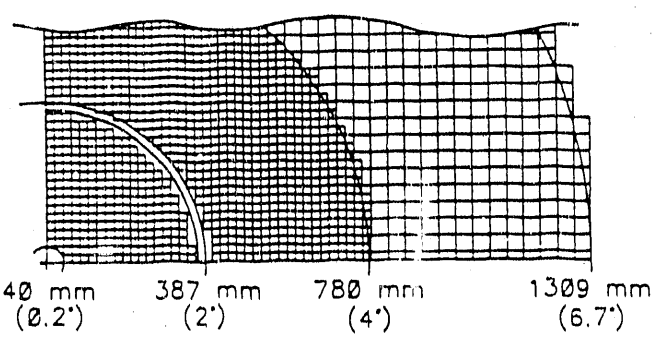

Fig. V.7. Cross section of the outer hadron calorimeter showing the Si detector arrangement (above 2°) and the inner calorimeter (TMS) with its subdivision of the electrodes.

The corresponding number of silicon detector elements in these two regions is 3544 and 2228 per layer, respectively. Detector elements are grouped into tower segments.

The silicon detectors will be mounted against the absorber slices, which form rings around the beam tube. For installation and service reasons the rings are grouped into two longitudinally separated assemblies. Radiation-hard variants of the central calorimeter electronics will be used for the front end electronics of this detector. Later stages of the DAQ chain will be modified for the much larger occupancy in the forward direction.

D.6. Inner Forward Calorimeter

Below 2.0°, the choice of technology for the inner (plug) forward calorimeter is warm liquid [tetramethylsilane (TMS)] with Pb-Fe radiator material. Equal detector response (compensation) for the measurement of electromagnetic and hadronic energy can be expected (Ref. V.8). Warm liquid hydrocarbon and silane media such as TMS and tetramethylpentane (TMP) can satisfy the detector requirements for radiation hardness (Ref. V.9). The TMS ionization chambers will be mounted in containers allowing for the pressure build-up due to chemical disintegration.

The electrodes of the ionization chambers are segmented in the following way: each of the 89 planes is subdivided into 940 cells of 20×20 mm^2. By summing five consecutive layers 33464 tower segments are formed (see Fig. V.7).

With the development of fast, radiation-hard charge preamplifiers for warm liquid calorimetry (Refs. V.10 and V.11), fast detector response is possible despite the relatively slow drift velocities in these liquids. In response to the repetition rate of the SSC only the very front spike (16 ns) of the ionization signal will be used. Under these conditions only moderately severe purity requirements need to be met: Free electron lifetimes of $\geq 1\ \mu$s are more than sufficient for adequate charge collection efficiency.

To maintain the intrinsically fast response of the front-end electronics (less than 10 ns), the preamplifier must be mounted directly on the detector. Detector capacitance, in turn, must be kept as low as possible, either by the choice of small electrode size or by series connection of larger electrodes. For the pad size of 20×20 mm^2 and 3-mm gap proposed for this calorimeter, the corresponding source capacitance will easily guarantee an amplifier risetime between 5 ns and 10 ns on the basis of previous design considerations for fast, front-end electronics (Ref. V.10).

D.7. Electronics

A monolithic front-end charge preamplifier manufactured in an industrial radiation-hardened (D-I) BiFET technology has recently been developed for warm liquid calorimetry (Ref. V.11) with < 500 rms electrons of noise.

This same design can also be applied to a silicon ionization medium which meets and exceeds the corresponding requirements for speed, sensitivity, and radiation hardness. Fast output rise times can be achieved for the pad size of 20 × 20 mm^2 and 3-mm gap foreseen in the TMS calorimeter from the low input source capacitance (3 pF). For the larger pads of 40 × 40-mm^2 (340 pF), the same amplifier rise time can be maintained by raising the noise specifications from this preamplifier (see Sect. C.4). In a recent design upgrade, the rise time of this device is now faster than 10 ns with typically < 10 mW of power dissipation. The radiation hardness measured for this new polysilicon technology is 4×10^{14} neutrons/cm^2 and roughly an order of magnitude higher in radiation hardness to γ ray exposure than previous BIFET technologies. This latter design compensates for changes in transistor β values and the corresponding increase in low-frequency noise that would otherwise occur after exposure to radiation (Ref. V.12).

E. ALTERNATIVE TECHNOLOGY

Our alternative for the central and endcap regions uses liquid scintillator sampling. ITEP, Moscow, together with ORNL will be responsible for this option. Sampling calorimeters with plastic scintillator readout are well developed and are not risky from technological point of view. By introducing liquid scintillator (which is also a well-established technique), we can avoid any potential difficulties with respect to radiation hardness of a scintillator since it can be exchanged.

An alternative technique for the forward calorimeter system was discussed above in Sect. D.2 of this chapter.

E.1. Liquid Scintillator Calorimeter

The mechanical design and readout segmentation for a liquid scintillator calorimeter are the same as for the silicon option, except for the detector gap (5 mm) and optimization of absorber/detector thickness.

The liquid scintillator detectors are placed between the absorber plates in sealed leak-tight stainless steel containers, with the possibility to exchange the liquid in the entire calorimeter. The inside surfaces of the containers are painted with a reflecting paint, and the inside volume is divided internally by thin reflecting separators into cells with typical size of 6 × 6 cm^2, with a thickness of 5 mm. The light readout of each cell is made through a wavelength shifting (WLS) fiber that spirals inside the liquid scintillator cell (shown in Fig. V.8). The fibers pass through container walls and run along the module sides, reaching photodetectors mounted at the back of the modules. Several fibers are connected to each photodetector.

Mineral-oil-based liquid scintillator will be used because of its high hydrogen content. Physical properties of a typical scintillator are light yield 66% of anthracene, light attenuation length 4 m, decay time 2 ns, and maximum emission wavelength 423 nm.

The fiber has a diameter of 1 mm and consists of a WLS core and of a cladding of about 30 μm thickness, with refractive index lower than that in the core. The scintillation light is absorbed by the WLS in the fiber core and is then reemitted with the longer wavelength. A fraction of reemitted light (6–7%) is trapped inside the fiber and travels to the photodetectors. Only the part of the fiber contained inside the liquid scintillator cell has the WLS in its core. Outside the cell, the fiber core is clear. This improves the light transmission and reduces Cherenkov light conversion in the fibers. Modern scintillating fibers are known to be radiation resistant up to 10 Mrad. Radiation resistance of WLS fibers should be better. Monte Carlo simulation of the light collection efficiency for a minimum ionizing particle in the cell of 6 × 6 cm^2 with liquid scintillator thickness of 5 mm with realistic geometry and absorption/reflection coefficients shows that the number of photons at the photodetector input is 80/MIP/detector layer. A photodector with a gain of 1000 will allow the detection of minimum ionizing particles above the noise level of room temperature electronics. A possible candidate for such a photodetector is a hybrid photodiode with a silicon anode, which is presently being developed by Hamamatsu. In this device photoelectrons are accelerated in vacuum by applying a voltage of 10–15 kV before entering the silicon anode where a few thousand electron-hole pairs are created. This device can be segmented with cathode-anode pads of 3 × 3 mm^2, and a vacuum tube can house as many as 100 of these segments. The signals are fast, with a rise and fall time of 3 and 8 ns, respectively.

The R&D issues for this technique are the following. The light collection system clearly needs optimization and careful experimental study. The type of scintillator should be optimized for the optical fiber used. It should match the absorption spectrum of the fiber and it should not attack the fiber chemically. Fiber gluing and sealing tech-

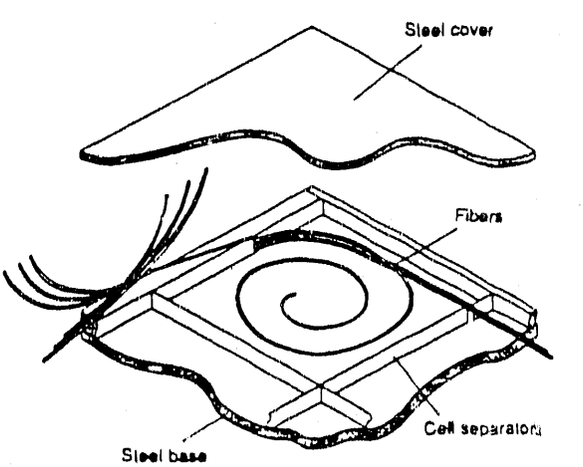

Fig. V.8. A cell of liquid scintillating calorimeter with WLS fiber readout.

niques should also be developed as well as corresponding photodetectors. They have to be fast, compact, stable, tolerant to magnetic field and cost-effective. Radiation damage tests on WLS fibers should be performed, as well.

F. SIMULATION

A major simulation effort is needed during the design phase to optimize detector performances and cost. It is imperative that during this phase computer models be continually checked with test beam data at each step.

The initial studies will focus on a BaF_2 electromagnetic, Pb-Fe-Si and Pb-Fe-TMS hadron calorimeters, as well as on the alternative choices. Presently, CALOR89 contains the most detailed representation of the physics necessary for good simulation and is used for this work. GEANT will be used for ray tracing.

Simulation studies will include studies of resolution and compensation, including time-dependent effects due to neutron moderation time or radiation damage; position-sensitive effects; determination of the best particle separation (i.e., discrimination between electrons and hadrons) as a function of longitudinal sampling frequency, transverse cell size and tower structures; investigation of hermeticity based on realistic engineering; investigation of albedo corrections to the e/π ratio; and radiation field mapping. In addition, handling of muon bremsstrahlung in CALOR89 will be improved, and remaining discrepancies between experimental results and simulation calculations will be reconciled.

This work will be jointly carried out by ITEP, IHEP (Serpukhov), Dubna from the Soviet Union, RWTH (Aachen) in Germany and by the University of Mississippi (UMiss), Los Alamos National Laboratory (LANL), ORNL, and the University of Tennessee (UTenn), with ITEP, UMiss, and RWTH (Aachen) being the coordinating centers in each country. To ensure adequate computing resources, a program to adapt CALOR89 to the parallel computing environment of a Unix-based microprocessor farm has been initiated by UMiss. To facilitate the use of geometry profiles which can be extracted from engineering design studies ORNL and UMiss are participating in a program to incorporate certain CAD/CAM packages into the geometry package of CALOR89.

The UMiss-ORNL-UTenn group presently is benchmarking CALOR89 using experimental results reported by the ZEUS, HELIOS, and SICAPO collaborations.

G. RESEARCH AND DEVELOPMENT

G.1. Past and Ongoing Projects

The L* hadron calorimeter R&D program includes the following detector techniques: Si detectors, liquid scintillator, planar gas proportional counters (PPC), and warm liquid TMS. The relative merits of these techniques are compared in Table V.1. The program is the joint effort of the following institutes and research centers:

- Silicon Detector Project: Dubna, ORNL, ITEP (Moscow), UTenn, UMiss, University of Alabama (UAlabama), University and INFN of Milano and Florence, and RWTH Aachen 1 Physics Institute (FRG).
- Liquid Scintillator Project: ITEP, ORNL, LANL, UMiss, and TIFR (Bombay).
- Planar Proportional Chamber PPC Project: ITEP, IHEP (Serpukhov), and IHEP (Beijing, China).
- TMS Project: ITEP, RWTH Aachen 1, and UAlabama.
- Radiation Damage Studies: IAE (Kurchatov Institute, Moscow), ORNL, RWTH Aachen 1, UAlabama, UTenn, and TIFR (Bombay).
- Simulation Studies: ITEP, IHEP (Serpuhkov), Dubna, ORNL, LANL, UMiss, UTenn, RWTH Aachen 1 Physics Institute, and TIFR (Bombay).

The L* R&D program at ITEP (Moscow) was started in 1988. The work is performed by a group of 40 physicists, engineers, and technicians who for the last few years worked on the construction and testing of the L3 hadron calorimeter. Test beam facilities at the ITEP 10-GeV proton synchrotron are used and test beam facilities at Serpukhov 70-GeV proton synchrotron can also be made available.

The liquid scintillator project described in Sect. E is the result of this R&D effort. Other projects are described below.

Silicon Detector Project

Within the USSR the program is being undertaken by JINR Dubna in collaboration with the TMF at Zaporozhye and the University of Byelorussia (Minsk), USSR to

Table V.1. Comparison of Hadron Calorimeter Detector Techniques

Detector technique	Fast response (ns)	Radiation longevity per year	Signal/noise for m.i.p. per cell	R&D issues
Silicon pads (3 × 3 cm²)	20	10^6 rad, 10^{13} n/cm²	4	Cost, electronics, compensation
Liquid scintillator	10	10^7 rad, 10^{14} n/cm²	10	Readout, mechanical design
Gas PPC	10	High	> 10	Mechanical tolerances, compensation
TMS (readout pads 2 × 2 cm²)	100	10^7 rad, 10^{14} n/cm²	5	Low signals, purity, and electronics

develop a cost-effective technology for large scale production of radiation-hard silicon pad detectors. A specialized research laboratory is being constructed to carry out this research. It will include clean areas and detector tooling facilities.

In addition, a joint silicon detector project will be undertaken by the collaboration of ITEP, Dubna, ORNL, and the UTenn to build a plane of silicon detectors with a total area of 50 × 50 cm^2 in order to perform a test-beam scan of hadron and electron showers and to measure the pion to electron response ratio for various absorbers and absorber compositions. The silicon pads used by ITEP have an area of 5 × 5 cm^2, have a thickness of 400 μm, and are made by the planar process from 5 Kohm-cm n-type silicon (Ref. V.14). The detectors have a small leakage current (average 10 nA/cm^2) and a capacitance of 600–800 pF at a total depletion voltage of 100 V. Few pads have been tested recently to check the quality of the detectors and to find an appropriate match to the multichannel slow readout electronics existing at ITEP. Two detector planes will be produced soon. Beam tests of a silicon detector plane, with fast electronic readout (now being developed by ORNL and UTenn), are scheduled for the end of 1990.

The SICAPO collaboration started the development of silicon calorimetry in 1983 at CERN, building and testing silicon-tungsten and silicon-uranium electromagnetic calorimeters between 4 and 50 GeV (Ref. V.15). In previous years the SICAPO collaboration showed that a silicon hadron calorimeter for both silicon-uranium (Ref. V.16) and silicon (iron and lead) (Ref. V.7) can be made compensating by reducing its response to the electromagnetic component of the hadronic shower. At present SICAPO is building the first prototype of a Si/(Fe + Pb) hadron calorimeter, about 5 λ deep, equipped with about 20 000 silicon detectors; measurements on the lateral hadronic shower development are being carried out currently at CERN. The Si/(Fe + Pb) hadron calorimeter will be tested at CERN by summer 1991. To date the first two mosaics, each made of 480 silicon detectors with a total area of 0.2 m^2, have been put into operation. The use of these mosaics as active medium of a calorimeter with both Fe and Fe + Pb (thicknesses of Pb = 0.25 thickness of Fe) as absorber has allowed the measurements of lateral and longitudinal shower development for 12-GeV protons. A BiCMOS preamplifier with a rise time of 7.5 ns and a maximum voltage swing of 7 V, optimized for the operation of a detector capacitance of 150 pF, has been developed (Ref. V.17).

The Aachen research work on silicon detectors will be carried out together with other German physics institutes and industry. The goal is to develop ultra radiation-hard large-area silicon detectors particularly suited for the forward region. Radiation damage tests will be carried out and annealing procedures will be developed. As an intermediate prototype test, a calorimeter system consisting of 10 layers of a 5 × 5 matrix of 50 × 50 mm^2 silicon pad detectors together with a radiation-hard ASIC electronics system will be built and tested in 1991.

UTenn and ORNL have been heavily involved in silicon calorimetry. Tennessee has built a set of four silicon tungsten electromagnetic calorimeters for the SLD detector with a total area of 2 m^2 (Refs. V.3 and V.13). A beam test of these modules was conducted in April 1989 and the results were in agreement with design specifications. Tennessee also has received SSC generic R&D funds to develop low cost sources of silicon detectors and to participate in the SICAPO collaboration study of silicon hadron calorimetry. ORNL received similar funds to design ASIC fast amplifiers for silicon detectors. Along with UMiss both participate in the Silicon Electromagnetic Calorimeter Collaboration to construct a 3-m^2 electromagnetic calorimeter to SSC specifications.

Planar Proportional Chamber (PPC) Project

Planar Proportional Chambers and their application to the fast radiation resistant calorimetry are being studied by ITEP (Moscow), IHEP (Serpukhov), and IHEP (Beijing). PPC is a gaseous detector with planar metallic electrodes. The gap between the electrodes is small (1 mm) and is maintained with high precision (10 μm). At a sufficiently high voltage, the electric field is sufficiently large for avalanches to occur. The gain of about 10 000 – 100 000 at 55–60 kV/cm was measured with a 5 × 5 cm^2 prototype detector (see Fig. V.9) filled with isobutane gas. The response is very fast (7 ns). The high-voltage dependence of the PPC response is shown in Fig. V.10.

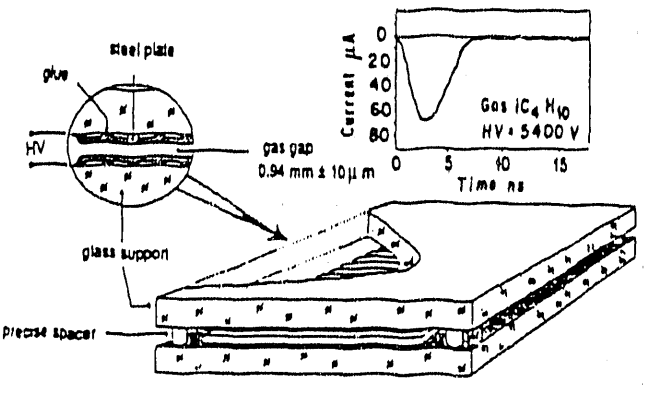

Fig. V.9. Planar proportional chamber (PPC) prototype and typical chamber response to MIP.

PPCs can work with intense particle beams because the space-charge effects normally causing saturation and aging effects are minimal for planar electrodes. The working gas for PPCs should not be transparent to its own UV light to prevent the development of secondary avalanches. Beam tests with a larger prototype of 50 × 50 cm^2 made of 64 PPC cells are scheduled for

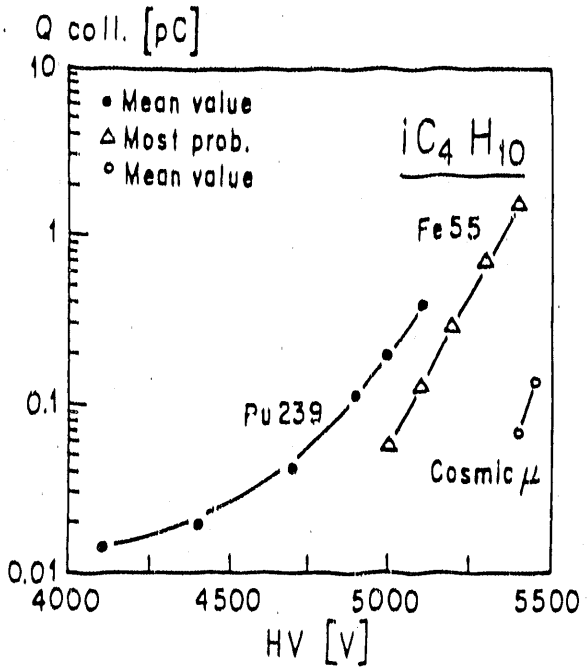

Fig. V.10. HV dependence of the PPC response to different radiation sources.

1990. R&D issues to be addressed include the rate dependence of PPC efficiency and aging effects. Nonflammable gas mixtures with the same properties as isobutane need to be identified. In the beam tests the pion-to-electron ratio has to be measured. Mass production technology of large-area PPCs is being studied.

TMS Project

The Aachen group has instrumented the forward regions of the L3 and TASSO detectors. A major effort has been invested in the simulation of these detectors using the GHEISHA package now being widely used at major laboratories. The current activities focus on warm liquid ionization chambers and silicon detector research work. Special programs have been set up to investigate the radioaction damage to TMP and TMS. Two stainless steel containers housing the ionization media and an electrode system have been built in Aachen. They will be exposed during the next months at a high radiation area of the SPS and will allow detailed measurements of the drift velocity, lifetime, pressure build-up, and gas decomposition as a function of the radiation dose. Together with industry the Aachen group has set up a program to develop ultra clean stainless steel containers for TMS particularly in view of mass fabrication. Several techniques like laser welding and high temperature soldering will be pursued.

After these investigations the activities will be focused in designing and building a radiation-hard prototype calorimeter, where a system engineering approach to the construction of a large calorimeter will play a dominant role. Beam tests which will be carried out in early 1992, will allow the absorber structure to be finalized in order to obtain full compensation.

A total of 100 TMS chambers of 50 × 50 cm^2 will be built in ITEP. About 30 are operational now. These chambers have a liquid gap size of 3 + 3 mm and 4 + 4 mm. The readout electrodes have an area of 6 × 50 cm^2. A purification/filling system for the TMS liquid has been built. Techniques for cleaning and degassing the chamber surfaces have been developed. Free electron life times as large as 8 μs were obtained in a fully operational chamber. (Electron drift time is about 300 ns at 10 kV/cm). Multiple measurements confirmed that the purity of TMS inside the sealed chamber does not change over the period of six months. The scan of hadron and electron showers inside the uranium and lead absorbers with a single TMS chamber was performed in the ITEP test beam. A typical result is shown in Fig. V.11. Another set of measurements was performed with 11 TMS chambers behind uranium and iron absorbers. Electromagnetic resolution of 25%/√E was measured with 5 mm uranium and with 25 mm iron absorbers in the energy range of 2–6 GeV.

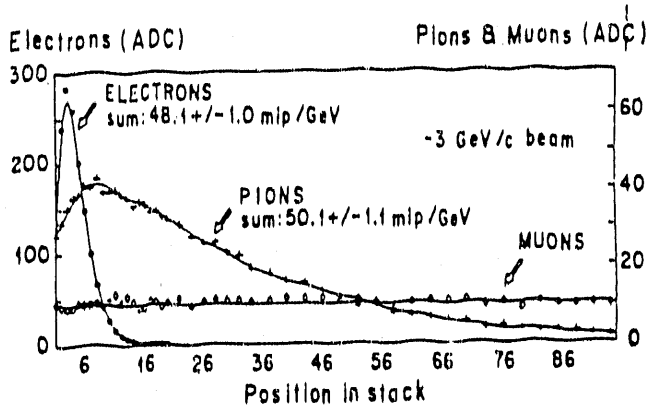

Fig. V.11. Shower curves for 3-GeV electrons, pions, and muons measured with a single TMS chamber inside a stack of 5-mm uranium plates.

The Warm Liquid Calorimetry Collaboration is presently investigating fundamental properties of warm liquid technology for calorimetry at the SSC. UAlabama, which is a member of this collaboration, is presently funded by the SSC Laboratory for research on this warm liquid sybsystem. Test beam measurements are presently under way at Fermilab to measure compensation of electromagnetic and hadronic energy response expected with this technology, the feasibility of integrated swimming pool detector configurations, and general materials compatibility issues. UAlabama began work in warm liquid calorimetry through the SSC generic detector R&D program with the development of fast forward calorimetry for the SSC and is now developing fast, ultra-sensitive, radiation-hardened electronics for this

technology. A distinguishing feature of this approach is the ability to extract a fast detector signal, despite the relatively long drift times in these fluids. The UAlabama group has already designed and built fast, radiation-hard charge preamplifiers for this technology and is now developing and testing faster designs with high radiation hardness.

The UAlabama group is also working closely with United States industry to develop warm liquid vessels with highly integrated electrode designs. In collaboration with Coors Ceramics and other ceramic manufacturers, this group is developing an integrated ceramic electrode with a flexible metallized anode pattern, similar to printed circuit board technology. Feedthrough connections in this scheme are then routed through a common multichannel tab on the same ceramic substrate. A laser welded outer stainless steel vessel for this electrode is presently being developed by Hutchinson Technologies.

For the TMS option the Tata Institute in Bombay is fabricating steel containers made by electron/laser welding thin steel plates on both sides of steel spacer bars. Performance tests will be carried out.

Simulation

To carry out simulations for the detector design and physics studies, as a part of the R&D program, the CALOR89 code package must be adapted to run on a parallel processing computing system. This system will be based on a series of RISC processors, following L3's extensive experience. The UMiss, ORNL, and LANL will be actively involved in this work. Close collaboration with SSCL will be maintained.

At the RWTH Aachen the successfully used GHEISHA code is continuously improved and speeded up.

At TIFR (Bombay), a GEANT has been set up with a segmented BaF_2 in front of an absorber/scintillator hadron calorimeter. A dual processor Apollo DN1000 (25 MIPs) will be used for detailed simulation studies.

G.2. R&D Requirements to the SSC

There are 40 physicists and engineers from ITEP and 30 physicists and engineers from Dubna working on the R&D effort for the L* collaboration supported by the Soviet government. In this section we list our requests to SSC for FY 1991 and FY 1992.

Silicon Procurement in the Soviet Union

The issue of silicon supply in the quantities required and on the time scale necessary is one of crucial importance. The main considerations have been addressed in Chapter V, Sect. B.1. A considerable R&D effort in the Soviet Union is required and is described below.

At Dubna, R&D will be aimed at developing the cost-optimized technology required for the large-scale production of radiation-hard silicon detectors. In efforts related directly to an interface with industry, Dubna will develop technology that will be applicable to industrial mass production and involve quality control at each production step. The collaboration between Dubna and USSR industry should result in cost-reducing measures. R&D associated with this activity is needed. Specific steps include the definition of specifications for silicon monocrystals; production of test samples and test evaluations; definition of final specifications for production steps by the end of 1992; and design of equipment for quality control. Institutions involved in this integrated effort are JINR (Dubna), the University of Byelorussia, ZTMF (Zaporozhye), ITEP (Moscow), ORNL, UTenn, and RWTH Aachen.

The work at Dubna will be carried out from 1991 on. It will involve facilities having a total area of 350 m^2 and a clean area of 70 m^2. A deionized water installation will be available together with slicing, lapping, and polishing machines. Thermodiffusion, thermal oxidation growth, photolithography, and metal deposition will be carried out. In the second phase, additional tools will be installed for the examination and evaluation of silicon properties, together with equipment needed for the design and fabrication of photolithography masks. The total anticipated cost is 6900K roubles and 1150K$.

Silicon Calorimetry in the United States

The Silicon Electromagnetic Calorimeter Collaboration subsystem proposal to the SSC laboratory will be expanded to include hadron calorimeter elements. Presently, the proposal has partial funding for the first year. In the following discussion, it is assumed that the SECC proposal will be fully funded. The L* collaboration proposed to build a full azimuthal segment ($2\pi/16$) of a 90° L* calorimeter module including cabling, signal routing, mounting boards, coiling, and full electronics through tower sums for the first level trigger with pipeline storage and digitization. We envision a 2-year program beginning in January 1991. A few planes of the calorimeter will be instrumented with silicon obtained from commercial suppliers; and the remainder, with detectors from the production facilities in the Soviet Union as the silicon becomes available.

A program of radiation damage studies will be initiated immediately to study effects of radiation-induced energy resolution and rise-time characteristics. These effects are expected to be very dependent on the particular silicon used. Therefore, tests will be performed with detectors made from TopSil, Wacker, Hamamatsu, and Soviet material, as well as from high-resistivity silicon produced by technologies other than float zone. A matter of particular significance that must be studied is that low temperatures introduced to reduce effects of leakage current may well increase the signal degradation effects by inhibiting self annealing of cluster vacancies.

Design and production of radiation hardened electronics (both bipolar and CMOS) will be pursued, including preamplifiers suitable for hadronic pads, summing amplifiers, pipeline storage elements and digitization circuitry.

A silicon plane with an area of 0.5 × 0.5 m^2 is under construction for tests at ITEP to establish parameters necessary for compensation and verify the SICAPO results on compensation. Preamplifiers developed at ORNL for the SECC system will be used in these tests.

Milestones are June 1992 for the final decision on radiation hardness and June 1993 for the final decision on Soviet capability to provide finished detectors. Our requests for silicon hadron calorimetry R&D are presented in Table V.2.

Table. V.2. Budget Request for Silicon Calorimetry R&D

		FY 91 (K$)	FY 92 (K$)
Electronics	Design	200	100
	ASIC rad-hardened bipolar run	100	
	ASIC rad-hardened CMOS run	100	100
	Packaging, cables	20	150
	Fast DAQ system		75
Mechanical design, construction, and refrigeration		75	
Radiation damage studies		50	50
Silicon purchase		60	
Silicon Calorimetry R&D Total		605	475

Liquid Scintillating Calorimeter

ORNL will proceed with the development of a liquid scintillator technique as the main backup option of the L* hadron calorimeter. The hadron calorimeter prototype 6λ long module with 60 liquid scintillator readout planes is to be constructed and tested by ORNL in collaboration with ITEP (Moscow).

Lawrence Livermore National Laboratory (LLNL) will construct a prototype liquid scintillator cell containing a spiral of wavelength shifting fiber for characterizing its performance using fast readout electronic schemes and new photodetectors.

We are requesting 350K$ for these activities in FY 1991 and FY 1992.

Simulation Studies

The simulation studies will be intense during the design phase of the L* calorimeter construction and prototype beam tests. The engineering simulation studies required to support the design, construction, and testing of the L* calorimeter are estimated to cost 575K$ per year.

Warm Liquid Calorimeter for the Forward Region

We propose to build the prototype warm liquid calorimeter for the L* forward region. Requested funds are to support an engineering design of the calorimeter prototype to cover travel expenses to meet with collaborators in Europe and Asia and to purchase prototype vessels, the fluid purification system, and electronics. We are requesting support from home institutes (e.g.,the annual request from UAlabama is 200K$ for operational funds and 200$K for capital equipment).

R&D Budget Request

Our requests to SSC for R&D of hadron calorimeter detector techniques and simulation are presented in Table V.3.

As stated in this chapter, there have been many efforts at Dubna, ITEP, and other USSR laboratories on R&D for hadron calorimeter. We request the SSC to invite 10 Soviet physicists and engineers to integrate the ideas and experience to the SSC standards. We request travel and per diem support per person of 32K$, or 320K$ total per year.

Table V.3. L* Hadron Calorimeter R&D Budget Request (K$)

Activity	FY 1991	FY 1992
Silicon procurement in the U.S.S.R.	750	400
Support of Soviet scientists at SSCL	320	320
Silicon calorimetry R&D in the U.S.	605	475
Liquid scintillator project R&D	350	350
TMS R&D for forward region	400	400
Simulation studies	575	575
Hadron Calorimeter R&D Total	3000	2520

References

V.1. G. Brandenburg et al., Proc. of the 1986 Snowmass Study, p.420; R. Partridge,, Proc. of the 1984 Snowmass Study, p. 567; T. Akesson et al., Proc. at the Workshop on Physics at Future Accelerators, CERN 87-07 vol. 1, p. 174.

V.2. B. Adeva et al., "The Construction of the L3 Experiment," NIM A289 (1990), 35.

V.3. Yu Galaktionov et al., to be published.

V.4. Proc. of the Workshop on Calorimetry for the SSC, Tuscaloosa, Alabama, March 13–17, 1989.

V.5. D. Groom, Proc. of the Snowmass Study ,1988, p. 711.

V.6. G. Lindstrom et al., in Proc of Tuscaloosa Workshop on Calorimetry, 1989, C. Bertrand et al., Silicon Calorimetry for SSC, Summary Report of the Silicon Calorimetry Working Group, OREXP-89-0902.

V.7. SICAPO Collaboration, E. Borchi et al., Phys. Lett. B222 (1989), 525.

V.8. R. Wigmans, NIM A259 (1987), 389; M. G. Albrow et al., NIM A265 (1988), 303; K. Ankoviak et al., NIM A279 (1989), 83.

V.9. R. Holroyd, "Effects of Radiation Damage to TMP, TMS, and Liquid Argon Solutions," SSC-SR-1035 (June 1988), p. 335,; R. Holroyd and D. Anderson, NIM A236 (1985), 294.

V.10. D. DiBitonto et al., NIM A279 (1989), 100.

V.11. D. DiBitonto et al., "Fast, Radiation-Hard Charge Preamplifier for Warm Liquid Calorimetry," Proc. of the Workshop on Calorimetry for the SSC, Tuscaloosa, Alabama, March 13–17, 1989.

V.12. P. M. Van Peteghem et al., Proc. of the ESSCIRC, San Francisco, September 1989.

V.13. S. Berridge et al., "The Small Angle E-M Calorimeter at SLD: A 2 m^2 Application of Silicon Detector Diodes. Trans. on Nuc. Sci, vol. 36, No.1 (1988), 339.

V.14. E. Fretwurst, G. Lindstrom et al., Technical Progress Report for the Development of the Plug Calorimeter, H1-TR110, Sept. 1987; E. Fretwurst et al., and R. Wunstorf et al., in ECFA Study Week on Instrumentation Technology for High-Luminosity Hadron Colliders, CERN 89-10, vol. (1989), 319 and 321.

V.15. SICAPO Collaboration, G. Barbiellini et al., NIM A235 (1985), 55.

V.16. SICAPO Collaboration, F. Lemeilleur et al., Phys. Lett. B222 (1989), 518; A. L. Angelis et al., to be published in Phys. Lett. B.

V.17. A. Gola, G. Pessina, and P. G. Rancoita, "Fast Front-End Electronics for Experiments Using Silicon Calorimeters at SSC/LHC Colliders," to be published in NIM (1990).

END

DATE FILMED

11 / 1 / 90